QATAR UNIVERSITY

COLLEGE OF ENGINEERING

DEVELOPMENT OF MULTI-PHASE VARIABLE FREQUENCY DRIVES FOR THE OIL & GAS INDUSTRY

BY

IZZEDDIN SHEHADA

A Thesis Submitted to

the Faculty of the College of Engineering

in Partial Fulfillment of the Requirements for the Degree of

Masters of Science in Electrical Engineering

June 2019

COMMITTEE PAGE

The members of the Committee approve the Thesis of Izzeddin Shehada defended on 18/04/2019.

_____

Adel Gastli
Thesis Supervisor

_____

Lazhar Ben-Brahim
Thesis Supervisor

Approved:

_____

Abdel Magid Hamouda , Dean, College of Engineering

ABSTRACT

SHEHADA, IZZEDDIN, A.H., Masters: April : 2019,

Masters of Science in Electrical Engineering

Title: Development of Multi-Phase Variable Frequency Drives for the Oil & Gas Industry

Supervisors of Thesis: Adel Gastli and Lazhar Ben-Brahim.

Liquefied Natural Gas (LNG) plants rely heavily on LNG compressors exceeding 100 MW power range. These compressors are mainly driven by gas turbines and high power helper motors operated via Variable Frequency Drives (VFDs). The VFDs offer a wide range of control and flexibility to the typically large motors allowing the driven system to meet desired process operation requirements in the LNG plants. Such motor drive systems have the capability to meet the power demand required for starting very large LNG compressors and provide additional power (helper) when necessary. High performance VFDs contribute to a great extent in enhancing the performance of LNG compressors and their reliability. Various types of VFDs are available in the oil and gas industry. Their performance and reliability depend on the topology of the VFD system. To satisfy the requirement of oil and gas applications and obtain the highest dynamic performance of the drive, special considerations are taken in choosing the appropriate drive topology.

This thesis presents and discusses the design of a high power multilevel and multi-phase motor drive system suitable for LNG compressor applications. Specifically, a 5-phase 5-level Neutral Point Clamped (NPC) based high power motor drive system is proposed. The proposed system was designed for a 33 MW 6.3 kV induction motor and its performances were tested and simulated under different operating conditions. It showed

superior results compared to the widely and commonly used 3-phase 3-level NCP inverter. The produced phase voltage has five levels, which had reduced the voltage and current Total Harmonics Distortion (THD) significantly and provided smoother output torque with minimized torque ripples.

DEDICATION

To my wife Leena and my children Abdullah and Omar without whom this thesis would have been completed two years ago.

ACKNOWLEDGMENTS

I would like to gratefully express my acknowledgement to my supervisors Prof. Adel Gastli and Prof. Lazhar Ben-Brahim for their trust, time, and guidance which helped me to complete my thesis. Also, I would like to express my appreciation to my two managers Lucas and Justin for being understanding which helped me balance between my work and study. Last but not least, I express gratitude to my family and friends for supporting and encouraging me to complete my master studies through rough times.

TABLE OF CONTENTS

LIST OF TABLES

LIST OF FIGURES

Chapter 1: Introduction

1.1 Background

Natural gas is the cleanest fossil fuel [1] and it has found its way to various applications mainly in power generation and industry. It is estimated that demand of natural gas will increase by around 40% by 2040 with approximately 26% share of world's energy supply [2]. Transporting natural gas by pipelines is inefficient for distances longer than 3500 km [1] thus the natural gas is being liquefied into Liquefied Natural Gas (LNG) by cooling it down to -162°C for easier storing and transportation. LNG has 600 times less volume than natural gas which make it cheaper to transport and store. Regasification plants transformers LNG transformed back to gas for the commercial use [3]. The process of gas liquefaction takes place in LNG trains. Figure 1-1 shows schematic of typical LNG train.

The state of Qatar is the largest LNG producer with 14 LNG trains producing approximately 77 Million Tons Per Annum (MTPA) of LNG. Recently Qatar petroleum has announced its intention to increase LNG production from 77 MTPA to 110 MTPA within the next 5-7 years by adding additional four up scaled trains with a capacity reaching up to 8 MTPA [4].

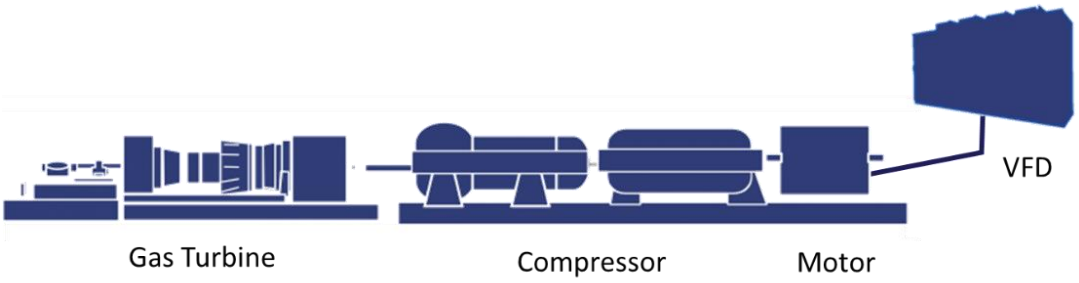

Figure 1-1 LNG train refrigeration configuration

1.2 LNG Compressors

The most important process in natural gas liquefaction is the refrigeration process where the gas is cooled in stages to reach the desired temperature. The cooling is achieved in series of heat exchangers where fluids like propane (C3) or nitrogen are used as refrigerants as displayed in Figure 1-2. The refrigerants are circulated using very large compressors that are traditionally drive by gas turbines [5]. The compressor size depends on train size. In the past, the LNG trains were designed to produce between 3 to 5 MTPA as shown in Figure 1-3 [6] however recently large LNG trains with 8 MTPA capacity exists [7]**Error! Reference source not found.**.

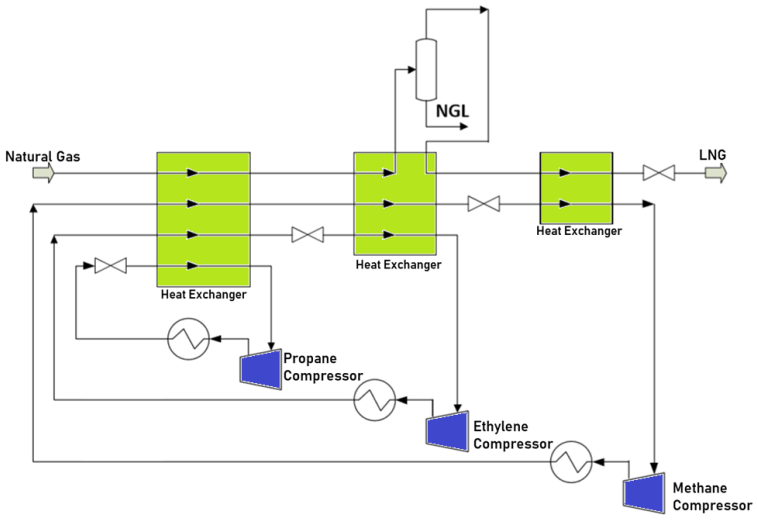

Figure 1-2 Optimized cascade liquefaction process

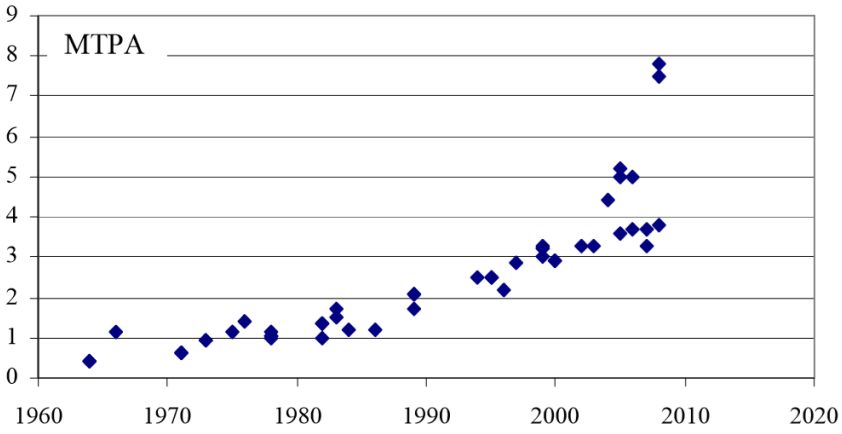

Figure 1-3 LNG train capacity trend

The up scaled LNG trains require larger compressors for the refrigeration processes and larger turbines have to be used to drive them. However with demands exceeding 110 MW, gas turbines alone are not enough to deliver the required power especially during overloads [8]. In addition, as it can be seen in Figure 1-4 the turbine efficiency is sensitive to ambient temperature and the performance degrades during the hot seasons [9]. Hence a high power VFD driven motor is used along the turbine to cover the shortage of power demand and compensate for the gas turbine deficiency during summer.

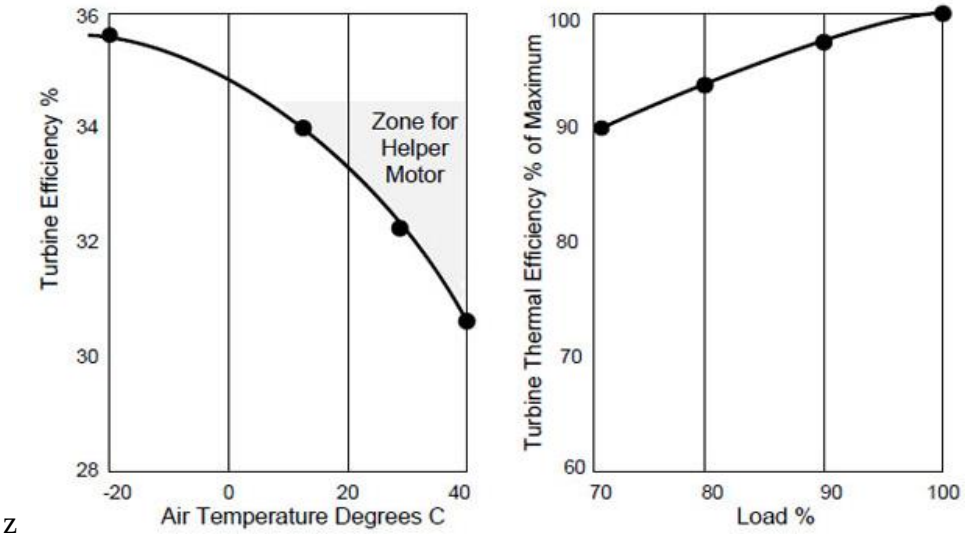

z

Figure 1-4 Turbine efficiency with respect to ambient temperature

1.3 Variable Frequency Drives

Production, distribution, refining processes and applications in the oil and gas industry depends heavily on electric motor-driven pumps and pumping systems. Designing and maintaining efficient and reliable electric motor drive systems is very vital for ensuring maximum productivity and profitability especially for operations at peak performance. For continuous optimum drive system performance, researchers are focusing on VFD to regulate the electric motor speed and effectively controlling its energy use.

VFD changes the output voltage to have full control of speed and torque of the motor to optimize operational cost and enhance efficiency [14]. A generalized VFD schematic is shown in Figure 1-5. The VFD usually have integrated input multi-winding phase shift transformer that draw AC power from electrical utility and step it down to suitable voltage matching the rectifiers ratings that it feeds. Rectification stage in medium voltage VFDs is

often done using parallel multi-pulse diode rectifiers. A combination of two or more sets of identical six pulse rectifiers are powered by one of the secondary windings of the input transformers. These rectifiers arrangement comply with line harmonics standards and requirements. The basic principle is that the harmonics generated by one rectifier is being cancelled by the harmonics generated by another rectifier. This achieved by proper design of the phase shift input transformer so the harmonics will not appear on the primary side [8] [15].

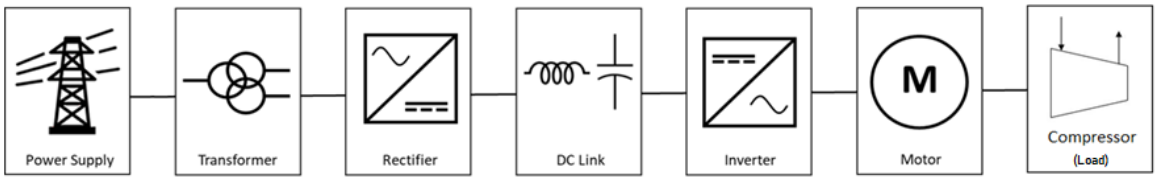

Figure 1-5 General Schematic of VFD

In order to have rigid DC voltage supply for the voltage source inverters or a smooth DC current for current source inverter, a DC link is required. The DC link is an intermediate circuit that consist of capacitors or inductors that temporary stores energy for next section, which is the inverter. The basic function of inverter is to convert the fixed DC voltage to AC voltage with variable magnitude and frequency. The medium voltage inverters have been designed in variety of topologies to produce the best possible waveform with highest reliability and efficiency [8] [15]. The inverter feeds a motor to drive the load to meet the required demand.

VFDs provide two main functions in LNG applications. The first is to accelerate the compressor train till the speed reaches the turbine firing speed (turbine self-sustain speed).

The second is compensate for the gas turbine output fluctuation due to ambient temperature variation during the day and different seasons. They also help during process overloading conditions [16]. Using the VFDs to gradually ramping the motor up to speed and by automatically controlling the motor torque, the drive allows the motor to run at full horsepower only when necessary [17]. This results in reduced power peaks, lower energy costs and higher operating efficiency. In addition, the motor is protected against starting inrush currents which reduces the thermal effect on the motor and subsequently minimizing downtime and maintenance cost.

VFD driven motors are essential part of the existing LNG trains in Qatar. The trains have been built over a period stretching from 1993 till 2010 [10]. This resulted in various types and topologies of VFD to be installed in the different LNG trains to drive the helper motors on the liquefaction processes. The first trains with capacity of 4.7 MTPA are fitted with 8MW and 12MW ABB VFDs which utilities the Load Commutated Inverters (LCI) a type of Current Source Inverters (CSI) [10] [11]**Error! Reference source not found.** . The newer larger LNG trains of 7.8 MTPA capacity utilized the voltage source inverters. They are equipped with 15MW Siemens EVFD which is based on multi-cell inverter topology where the medium voltage is achieved by connecting a series of low voltage inverters. The VFDs are connected in a unique way to a four-winding motor to supply a total power of 45MW [9] [12].

In addition, 3-level inverters based on Neutral-Point-Clamped (NPC) topology are used by Ansaldo and TMEIC to drive helper motors up to 13MW in multiple processes [13].

1.4 Problem Statement and Thesis Objectives

Up scaled LNG trains with large compressors require larger inverter fed motors. Oversizing typical inverters leads to several problems such as the high harmonics and torque pulsation and has several limitations such as cooling requirement and increased components ratings and size. To keep up with the increased power size, these issues should be taken into account. LNG applications require high power VFD driven motors with high reliability, fault tolerance capability, low torque ripples and low line side harmonics to ensure a reliable and sustainable production.

The main objective of this project is to conduct a comprehensive study of current multi-phase VFD topologies for oil and gas applications, then propose and develop a new VFD topology suitable for LNG applications.

1.5 Thesis Outline

The thesis consists of five chapters. Background of LNG industry in the state of Qatar and the importance of VFDs to LNG trains as presented in chapter 1. Chapter 2 presents a literature review and theoretical background for the different motor types available and their selection criteria for LNG application. It also reviews the common types of high power medium voltage inverters used in oil & gas industry. Chapter 3 shows the mathematical modeling of 5-phase induction motor in the *dq* domain and a general modeling of multi-phase machines as well. Chapter 4 describes the proposed design of 5-phase 5-level inverter for LNG plants and explains its principle of operation. Chapter 5 investigates the performance of the proposed drive system and compares it with other common VFDs

topologies using MATLAB SIMULINK. Chapter 6 concludes the thesis and suggests future work.

Chapter 2: Literature Review

2.1 AC Motor Types

The most two common AC types of electric motors in natural gas compressor system drives are AC synchronous motors and asynchronous motors or as more commonly referred to as induction motors. Direct current (DC) motors of the brushless type may also be used in combination with speed control and AC to DC power converters, but these are typically not found in gas compressor installations [21].

The squirrel-cage and the slip-ring are the most used induction motors and from synchronous motors the salient-pole and the cylindrical rotor.

2.1.1 Induction Motors

Induction motors are often the choice for various industrial production processes. The two primary induction motors are the squirrel-cage and wound-rotor type. The wound type motors have stator core constructed of laminated sheets and set of insulated electrical windings wounded inside the slots of the laminated stator connected in either star or delta. The rotor of this type compromise of cylindrical laminated core and sets of insulated windings star connected at one end and the other windings ends are connected on slip rings mounted on at the end of the shaft. An external varying resistance can be connected to the wound type rotor through the brushes and slip rings. With this configuration, the total rotor resistance can be changed and hence it can be utilized for speed control of the motor and high starting torque can be obtained. Subsequently, wound type induction motors are commonly used in high starting torque and low starting current applications. However, due

to the nature of these motor, the slip-ring type motors are not commonly used for natural gas compressor drives are avoided due their higher hazard risk and higher cost consequences. Therefore, this type of motors will not be considered in this thesis.

The most widely used induction motor is the squirrel cage. It is often used for driving blowers, compressors and pumps. The construction is simple due to the absence of slip rings and brushes. A major difference between with the wound-rotor type is the rotor winding. The rotor winding is constructed of a series of longitudinal conductors bars arranged to form a cylinder mounted in steel rings. The rotor conductors are shorted electrically with the help of end rings called. The squirrel cage motors are known to have simple yet rugged construction. The rotor is not connected to any external power source. Compared to synchronous machine, the initial cost is cheaper.

2.1.2 Synchronous Motors

The stator of synchronous machine is identical to that stator of the induction. The rotors of these machines classified into salient pole and non-salient pole (cylindrical) rotors. In salient pole synchronous motors type, the rotor consist number of projected poles (salient poles) made up from steel laminations. The windings are mounted on these poles supported by pole-cap and winding supports. The shape of the salient rotor result in an air gap that is not constant. However, the salient type is suitable for lower speed electrical machines typically less than 1500RPM where in LNG compressor a speed of 3000 or 3600RPM is required. Generally salient pole construction for such application is impossible because of limitation of mechanical strength fixation for the poles and the field winding. For such applications where higher speed is required, cylindrical rotors type is used [19].

In the cylindrical rotor, the field winding coils are slide in multiple slots around the rotor periphery and arranged to produce constant radial air gap and weight distribution around the rotor. This design is capable of providing larger overload capacity and will reduce the harmonic components. In addition, it contributes to the motor's superior starting characteristics which sufficiently withstanding the load large moment of inertia [22].

DC current flows in the field coils setting up a magnetic field on the rotor that will synchronize with that of the stator and the motor will then spin at the synchronous speed. DC current is supplied by commonly via brushless excitation system. On the other hand, brushed excitation needs require periodic preventive maintenance and these requirements become more frequent and difficult with machine of higher speed and higher capacity.

2.1.3 Comparison of induction motors and synchronous

Synchronous motors can have larger air gap compared to the induction motors. This due to the fact that the synchronous motors obtain their magnetic field by direct excitation current whereas in the induction machines it is obtained through the air gap. Larger air gap makes it feasible for the manufacture to build a physically smaller motor and cheaper than the equivalent horsepower squirrel-cage induction motors [23].

Figure 2-1 shows the tradeoff between machine ratings vs. speed and it highlights the area of each machine. It also shows the physical limitation of motors that can be realized. The higher the rotational speed, the higher the centrifugal force it is applied to rotor which increases the rotor radius. The rotor has limited stiffness thus the magnitude of centrifugal force is can withstand is limited. Thus as the rotating speed is higher, the motor capacity

will be lower. The synchronous machines are often selected for high capacity application [24].

Figure 2-2 provides generalized chart for sizing synchronous and induction motors. Even though the induction motor rating range goes up to 25MW, the synchronous motors are applied for power levels higher than 15 MW [25]. A rough rule of thumb states in [23] that the initial cost of synchronous motors is less expensive compared to squirrel-cage induction motors once the rating exceeds 1 HP per rpm.

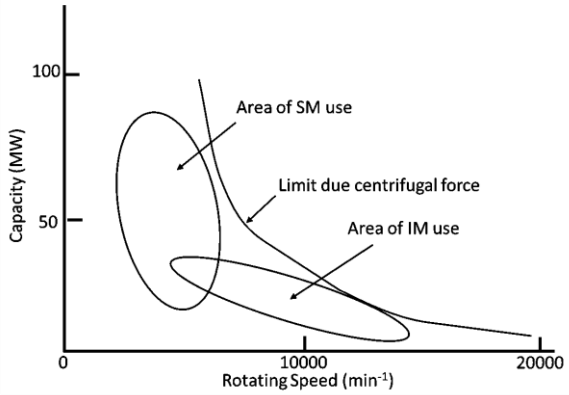

Figure 2-1 Area of use of induction and synchronous motors.

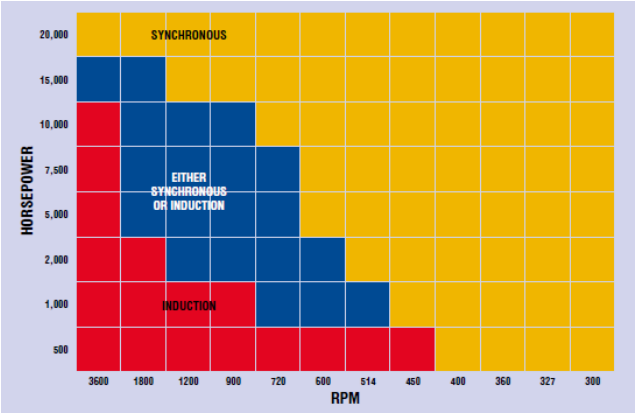

Figure 2-2 Generalized chart for motor type selection.

The LNG compressors are of high inertia and run at 3000 RPM and the synchronous motor has been the choice in the up-scaled LNG trains.

However, recently the induction motor is taking over higher power range as there has been a leapfrogging in induction motor design from 22 MW to 80 MW with rotation speed up to 4,000 (rpm). This is the equivalent to the traditional largest synchronous motor used in LNG plants; the 75-MW synchronous machine. The new induction motor has higher reliability since it has much less rotating parts and smaller footprint (Figure 2-3) [21]. This up scaled motor size was possible by the use of multi-phase motors.

Since the up time and the operational reliability is the most important in LNG plants and since the induction motors is catching up to the current trend of up-scaled LNG trains, the induction motors has been selected for the proposed topology in this thesis.

Figure 2-3 Largest 80MW induction motor during no-load test.

2.1.4 Multi-phase Motors

The increased size of motors capacity required equaled sized converters to meet their load demand. This resulted in oversized power electronics devices of the drives and the use of larger transformers. Oversized devices generate excessive heat, which requires bigger spaces and cooling systems; which in turns result in excessive cost and eventually leads to an impractical motor drive system [26]. In addition, oversized machine such as squirrel cage induction motors result operates in poor power factor and efficiency [27]. Multi-level inverter is one obvious solution to this problem. Multi-level inverters utilize lower rated switching devices to build high power level converters. However, there are some limitations factor such as the insulation level and rated power of semiconductor switches [28].

The advancement of power electronics technology allowed additional degree of freedom in variable speed drives by providing multi-phase supply options. Traditionally, the choice of three-phase stator comes from the three-phase power supply that is already available. With the help variable frequency drives, it is possible to supply motors with a phase count higher than three. A machine with more than three phases or has multiple three phases windings sets that share the same rotor, each contribute to produce the overall electromagnetic torque is considered a multi-phase motor.

In the last years, the multi-phase motors interest in medium and high power application has been growing especially in where high torque, high power and higher reliability is required. Multi-phase motor design offers many advantages such as lower torque pulsation, less current per phase, reduced DC link voltage, lesser harmonics and higher reliability [29] [30], which in turns reduces the voltage, and current rating requirement of converters and

increases their fault tolerance capability [28] [33]. It worth mentioning that the multi-phase design is independent of type of machines; it applied to both synchronous and induction machines.

Using multilevel inverter, multi-phase machine or both is debatable but it depends on the application and some limitation factors such as the insulation level and rated power.

2.1.5 Multi-phase Arrangement

There are various multi-phase motor winding schemes. It depends on the number *N* of stator phases and on the spatial displacement between the phases. Two typical phase arrangement are used; Symmetrical distribution of phases around the stator circumference with 360/*N* electrical degrees phase shift as in the design of the five-phase and seven-phase motors. The other arrangement is when the number of phases is multiple of three where the windings are grouped into *n* sets of three phase windings have 60/*n* electrical degrees shift. This arrangement is called split-phase [34]. Examples of symmetrical and split phase arrangement are shown in Figure 2-4.

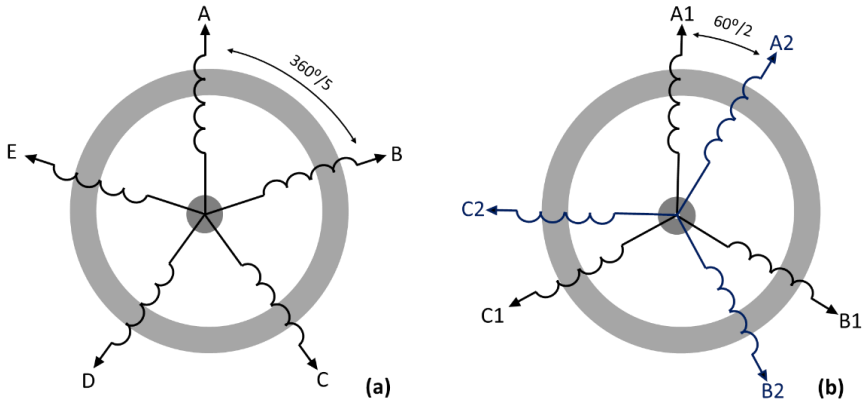

Figure 2-4 Example of multiple phase winding scheme: (a) symmetrical 5-phase (b) split phase double star.

Split Phase Motor with six phases composes of two similar stator windings that share the same magnetic circuit. With such arrangement, it is possible to divide total power requirement between two drives. Typically six-phase split-phase motor is built by dividing the phase belt of a typical three-phase motor into two equal parts with spatial phase separation of 30 electrical degrees as shown in Figure 2-4. With this, a split phase motor will have two independent stator windings sharing the magnetic structure [29]. Dual stator is another multi-phase configuration where it is not necessary to have two similar winding groups. The two windings can have different number of poles, phases or ratings [35].

The split phase arrangement may has the advantage of using proven three phase technology, however, faults in one of winding will be greatly de-rate of the motor power whereas in symmetrical arrangement the de-rating is less. The multi-phase motor arrangement selected for the proposed topology is the symmetrical arrangement.

2.2 VFD Inverter Topologies

Motors speed depend on the network supply frequency. Regardless of the driven load changes, the motor speed remains constant. Variable frequency drives are being employed to efficiently match load speed and torque demand. The advancement in power converters and the progress semiconductor technology has allowed for the development of many various types of drive topologies[31]. The topologies are usually classified based on main power section components types, numbers and way of arrangement.

To satisfy the requirement of oil and gas applications and obtain the highest dynamic performance of the drive, special considerations are taken in choosing the appropriate drive topology.

2.2.1 Introduction

There are different ways to categorize VFD inverters; the most common is by the characteristic of their DC link; current-source inverter (CSI) and voltage-source inverter (VSI). In three phase system, CSI converts the DC current to variable three phase alternating current often with a large series inductor in the DC link whereas in VSI the DC voltage converts to three phase AC voltage with variable magnitude and frequency often with shut capacitors in the DC link [32]. The most common type of CSI in medium voltage application is the LCI. It is undoubtedly that the LCI is a matured, well established and economical solution, however, the LCI based drives have some inherit drawbacks such as high low-harmonic torque ripples, input filter requirements and complex starting techniques[36]. This makes the LCI based drives lose their dominance in the developing market for medium voltage applications[37].

In high power medium voltage applications, Voltage Source Inverters (VSI) are commonly used due to their superior performance; especially in multilevel topologies. Industrial equipment power demands are in the level of tens of megawatt and almost reaching hundred megawatt rated power[38]. In Free Port LNG facility in Texas, GE is supplying six 75MW motors and 80MW motor in Nice France. Drives of this size are usually connected to medium voltage grid (2.3~6.9 kV) and due to limitation of the semiconductor switches, it is difficult to connect to single switch directly to the grid[39].

To overcome this problem, various series and parallel arrangements are needed to withstand the voltage and provide the required power.

Generally, the VSI is classified into the classical inverters and the multilevel inverters. Multilevel inverters are the obvious solution to reduce the voltage stress on the semiconductor switch. Smaller voltage steps than voltage supply (VDC) would lead to waveform closer to the sinusoidal, improve the power quality and reduce the voltage requirement on the semiconductor switch. Multilevel inverter basic concept is to synthesizing a staircase voltage waveform by using series of semiconductor switches with multiple lower voltage sources to achieve the power conversion. There is variety of high power configuration proposed for multilevel VSI. Among these, the most common ones are the Cascaded H-Bridge (CHB), flying capacitors and diode Neutral Point Clamped (NPC) topologies[31]. There are many other hybrid topologies developed over the last decade however these are based on the common inverters.

2.2.2 Classical VSI Inverter

The simplest inverter is the classical two-level inverter, which can produce line to ground output voltage of either the DC supply voltage (VDC) or zero. A standard two level inverter has six switches (Figure 2-5). The switches in one leg cannot be switched on simultaneously because it will cause a short in the DC link. The output waveform would be a square wave, which has a large differential voltage (dv/dt) and high harmonic content. The require output waveform should be close to sinusoidal for effective operation.

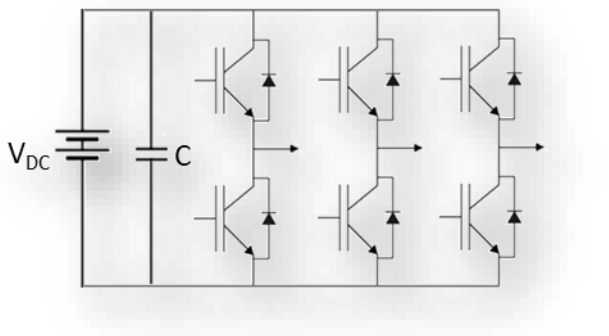

Figure 2-5 Two-level three phase inverter.

In order to have higher rated inverters, the voltage and current capability of the semiconductors switches should be increased. The increase of the voltage results in increased price and drop of the performance. Such limitation of the two-level inverter makes them not suitable for high power application.

2.2.3 Cascaded H-bridge Inverter

The H-bridge is a power conversion cells that is composed of two legs each with a pair of switching devices for each phase (Figure 2-6). The cell is able to produce output voltage of either the full DC supply voltage (VDC) or zero.

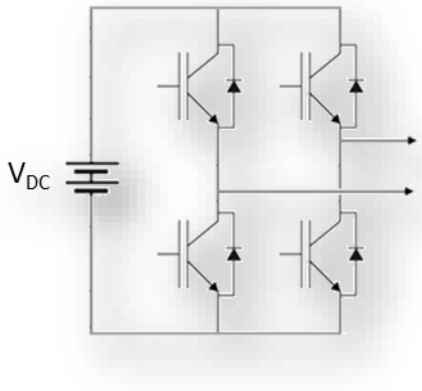

Figure 2-6 Single phase H-bridge inverter.

H-bridge cells can be connected in series in their AC side forming multi-level inverter that is able to produce higher voltage. Hence the Cascaded H-Bridge (CHB) name came. The CHB makes it possible to have medium voltage out using low voltage power module each with its own isolated DC supply[40]. The number of cells required in cascaded H-Bridge multilevel inverters is determined by the required voltage output. For n cells, the number of levels is (2*n*+1). The number of levels is odd in this topology. A nine-level CHB configuration is shown in Figure 2-7 where each phase leg has four H-bridge each with its own separated DC source.

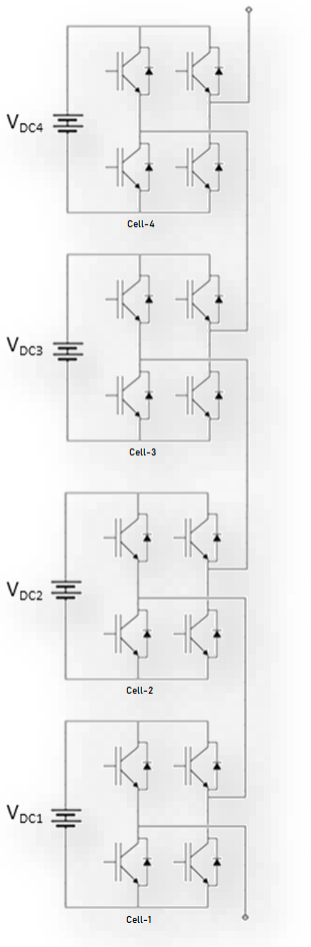

Figure 2-7 Five-level CHB for one phase.

In medium voltage application where higher voltage is required, higher number of cells is used. For 7.2kV motor application, up to 7 cells are used per phase to obtain the required voltage[46]. Even though the use of low voltage components has its economical advantages but it results in huge number of components being used which could compromise the reliability and increase the complexity. By-pass function are often provided with this arrangement to enhance the reliability, however it adds in to the system complexity.

2.2.4 Flying Capacitor Inverter

This topology is also known as the capacitor clamped inverter. The voltage clamping is done using capacitors in ladder form. For n level inverter, (n-1)*(n-2)/2 auxiliary capacitors are required. By changing the switches states the output voltage can be produced with various steps. Figure 2-8 shows five-level flying capacitor inverter for one phase. The advantages of this topology are that it provides redundancy as two or more valid switching states are possible [43] and the use of filter is unnecessary. This arrangement requires huge number of capacitors which make it bulky, costly and complex [47]. However, this topology is very challenging for inverter fed motor applications where machine back EMF and high inductance resistance ration of motor must be considered [39].

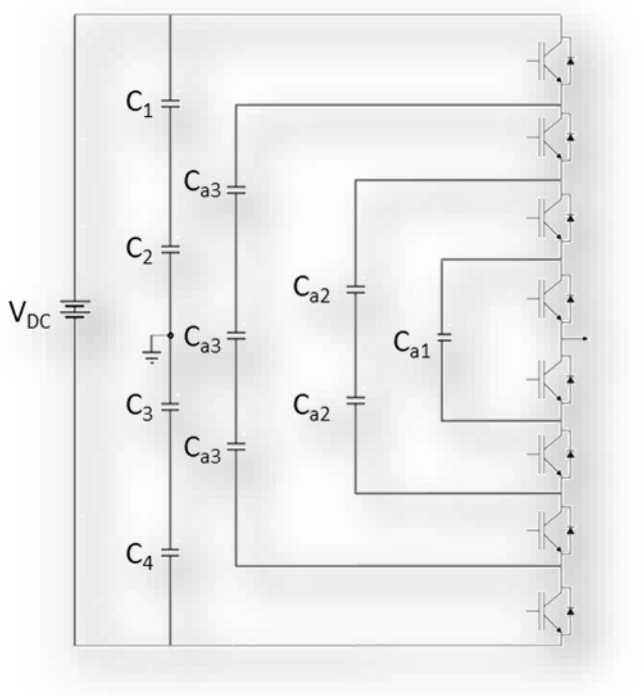

Figure 2-8 Five-level flying capacitor inverter of one phase.

2.2.5 Diode NPC Inverter

The diode NPC inverters started with three level inverters. In this topology, two capacitors are connected in series across the DC voltage supply forming a neutral point in the middle and in each leg two pairs of semiconductors are used. The center of each pair is clamped to the neutral using clamping diodes rather than capacitors as shown in Figure 2-9. This arrangement will make it possible to produce line voltage of half of the full DC supply as well as the half of the DC supply in addition to zero (VDC, 0.5VDC and 0). The resulted output waveform is three level square waves (figure-2-10), however, compared to two-level inverter it is closer to the sinusoidal form and it has less harmonics. The advantages of this scheme other than lower harmonics are allowing the use of switches of

lower voltage and power rating and lower voltage stress because of the reduction dv/dt at the output. Unlike the H-bridge cells, isolated DC supply is not always required and a common DC bus can be used for all phase legs. The three level diode NPC inverters are commonly used in the medium voltage applications [25] [41].

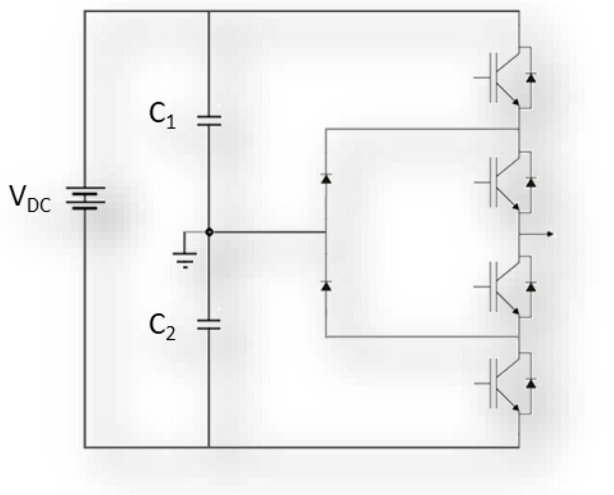

Figure 2-9 Three-level diode neutral point clamped inverter of one phase.

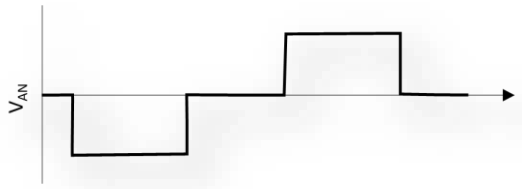

Figure 2-10 Three-level diode NPC inverter voltage waveform of one phase.

The neutral clamping method can be extended to make five-level inverter. Increasing the levels will result in better waveform closer to the sinusoidal form. As a result, less harmonic distortion is obtained. An inverter of n levels requires (*n*-1)*(*n*-2) clamping diodes

for each phase leg [42]. The five-level NPC utilizes four capacitor series along the voltage supply in each phase. The switches are connected to capacitors through clamping diodes. Figure 2-11 shows the schematic for five level diode NPC inverter. This arrangement will cause one quarter of the voltage supply to appear across each capacitor and result of voltage levels VDC, 0.25VDC, 0.5VDC, 0.75VDC and 0 as depicted in Figure 2-12.

However, the increased number of capacitors increases the complexity of balancing the voltage and the cost increase much further compared to the three-level inverter.

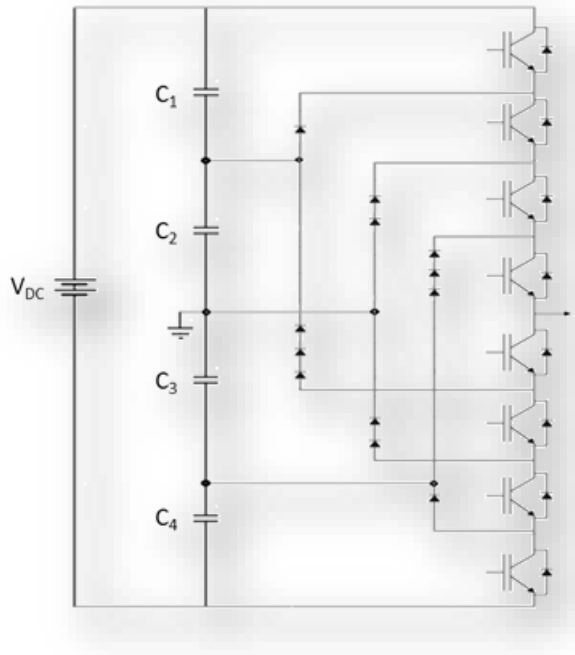

Figure 2-11 Five-level diode neutral point clamped inverter of one phase.

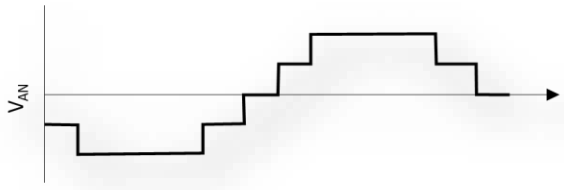

Figure 2-12 Five-level diode NPC inverter voltage waveform of one phase.

Higher level inverter can be realized using neutral clamping method. Adding more steps will synthesize sinusoidal waveform. Zero harmonics can be achieved by infinite number of levels [39] however this causes this topology to be too bulky, impractical and too complex for control for higher number of levels [43].

In NPC topology, each of the diodes must have a rating similar to the semiconductor switches, so for an inverter of n levels, (*n*-1) (*n*-2) clamping diodes are required for each of phases legs. For a multiphase machine, this results in huge increment of inverter components count. Figure 2-13 shows a chart of the components number as function of voltage levels for a five phase machine.

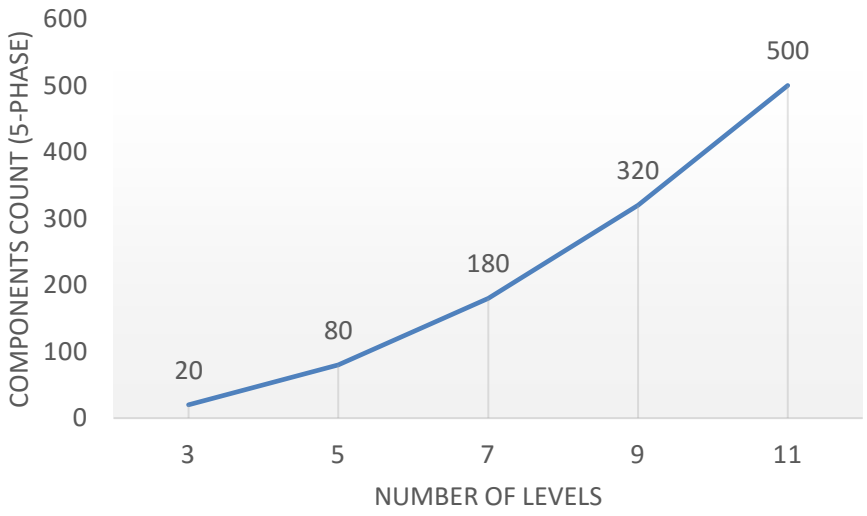

Figure 2-13 Five-level diode NPC inverter voltage waveform of one phase.

2.2.6 Topology Selection Consideration

LNG compressor drive application requires drives with highest reliability. Even though there is no comparable mean time between failures for the different drive topologies [44],

however the number of components in a system and its complexity can be used to reflect its reliability. The cascaded H-bridge topology with DC link voltage of ~600 VDC requires high number of cells to achieve medium voltage output level. Although no extra clamping diodes and capacitors are not required to increase the level but component counts is massive. The flying capacitors topology will require (n-1)(n-2)/2 capacitor in each phase which increase the requirement of voltage sensing and balancing of its capacitors making it impractical and more challenging than it is. On the other hand, the diode NPC has reached a mature state of development and has reliable operating conditions at the required power rating. Enhancing the out voltage waveform by increasing the number of levels will increase the components counts and may introduce some issues such as capacitors imbalance. However, the use of decentralized DC link in modularized layout will prevent the voltage imbalance from occurring[37]. In this thesis, diode NPC topology will be utilized in the proposed topology. A five-level voltage output will be targeted to ensure a better system performance without compromising its reliability.

Chapter 3: Multi-Phase Motor Modeling

3.1 Mathematical Model of Five-Phase Induction Motor

The mathematical derivation is considered for symmetrical distribution of multi-phase motors. The first phase count after the 3-phase motor is the 5-phase motor where the spatial displacement between a phase and the next one is $\alpha=2\pi/5$. A General assumption that the stator and rotor are of same phase construction is made for the sake of simplicity. The 5-phase machine, the stator has ten phase belts with spatial displacement of 36^o, thus having a phase displacement α of 72^o. The model of the induction machine is made with the assumptions that all phases are balanced and mutual inductances are equal.

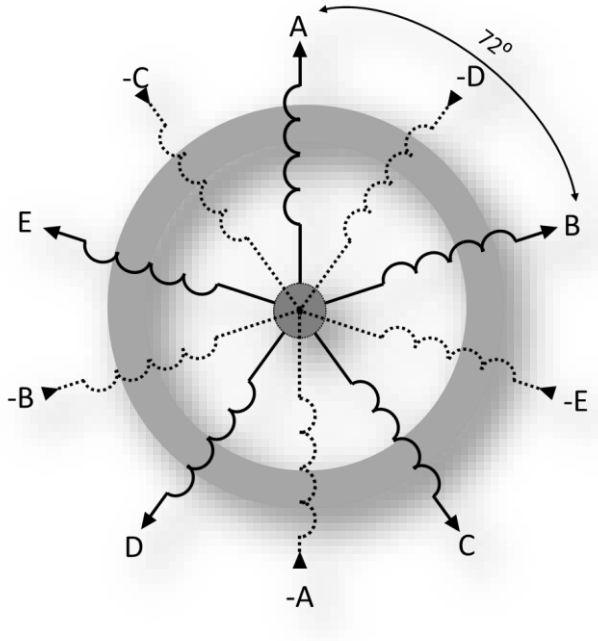

Figure 3-1 Schematic of multi-phase induction motor (5-phase example).

Using all standard assumptions of electrical machine theory, the voltage equilibrium and flux linkage equations can be written as:

$$v_s = R_s i_s + \frac{d}{dt}\Psi_s \tag{3.1}$$

$$v_r = R_r i_r + \frac{d}{dt}\Psi_r \tag{3.2}$$

$$\Psi_s = L_s i_s + L_{sr} i_r \tag{3.3}$$

$$\Psi_r = L_r i_r + L_{rs} i_r \tag{3.4}$$

Where,

$v_s = [v_{as}, v_{bs}, v_{cs}, v_{ds}, v_{es}]^T$ is the stator voltage vector

$v_r = [v_{ar}, v_{br}, v_{cr}, v_{dr}, v_{er}]^T$ is the rotor voltage vector

$i_s = [i_{as}, i_{bs}, i_{cs}, i_{ds}, i_{es}]^T$ is the stator current vector

$i_r = [i_{ar}, i_{br}, i_{cr}, i_{dr}, i_{er}]^T$ is the rotor current vector

$\Psi_s = [\Psi_{as}, \Psi_{bs}, \Psi_{cs}, \Psi_{ds}, \Psi_{es}]$ is the statpr flux linkages vector

$\Psi_r = [\Psi_{ar}, \Psi_{br}, \Psi_{cr}, \Psi_{dr}, \Psi_{er}]$ is the rotor flux linkages vector

$L_s = \begin{bmatrix} L_{ls}+M & M\cos(\alpha) & M\cos(2\alpha) & M\cos(2\alpha) & M\cos(\alpha) \\ M\cos(\alpha) & L_{ls}+M & M\cos(\alpha) & M\cos(2\alpha) & M\cos(2\alpha) \\ M\cos(2\alpha) & M\cos(\alpha) & L_{ls}+M & M\cos(\alpha) & M\cos(2\alpha) \\ M\cos(2\alpha) & M\cos(2\alpha) & M\cos(\alpha) & L_{ls}+M & M\cos(\alpha) \\ M\cos(\alpha) & M\cos(2\alpha) & M\cos(2\alpha) & M\cos(\alpha) & L_{ls}+M \end{bmatrix}$ is the stator inductance matrix, L_{ls} is the self-inductance of the stator and M the magnetizing inductance

$$L_r = \begin{bmatrix} L_{lr}+M & M\cos(\alpha) & M\cos(2\alpha) & M\cos(2\alpha) & M\cos(\alpha) \\ M\cos(\alpha) & L_{lr}+M & M\cos(\alpha) & M\cos(2\alpha) & M\cos(2\alpha) \\ M\cos(2\alpha) & M\cos(\alpha) & L_{lr}+M & M\cos(\alpha) & M\cos(2\alpha) \\ M\cos(2\alpha) & M\cos(2\alpha) & M\cos(\alpha) & L_{lr}+M & M\cos(\alpha) \\ M\cos(\alpha) & M\cos(2\alpha) & M\cos(2\alpha) & M\cos(\alpha) & L_{lr}+M \end{bmatrix}$$ is the rotor inductance matrix and L_{lr} is the self-inductance of the rotor.

$$L_{sr} = \mathrm{M}\begin{bmatrix} \cos(\theta) & \cos(\theta+\alpha) & \cos(\theta+2\alpha) & \cos(\theta-2\alpha) & \cos(\theta-\alpha) \\ \cos(\theta-\alpha) & \cos(\theta) & \cos(\theta+\alpha) & \cos(\theta+2\alpha) & \cos(\theta-2\alpha) \\ \cos(\theta-2\alpha) & \cos(\theta-\alpha) & \cos(\theta) & \cos(\theta+\alpha) & \cos(\theta+2\alpha) \\ \cos(\theta+2\alpha) & \cos(\theta-2\alpha) & \cos(\theta-\alpha) & \cos(\theta) & \cos(\theta+\alpha) \\ \cos(\theta+\alpha) & \cos(\theta+2\alpha) & \cos(\theta-2\alpha) & \cos(\theta-\alpha) & \cos(\theta) \end{bmatrix}$$ is the mutual inductances matrix between stator and rotor windings and θ is the angle between phase 'a' axis of the rotor with respect to the stator.

$L_{rs} = {L_{sr}}^T$ is the mutual inductances matrix between rotor and stator windings

R_s=diag(R_s R_s R_s R_s R_s) is diagonal matrices of stator resistance

R_r=diag(R_r R_r R_r R_r R_r) is diagonal matrices of stator resistance

The delivered torque can be expressed by:

$$T_e = P i_s^T \frac{dL_{sr}}{d\theta} i_r \qquad (3.5)$$

3.2 Five-Phase Induction Motor Model in DQ Reference Frame

The induction motor analysis is commonly done in rotor d-q reference domain that is associated with motor rotor. This will result in time-invariant coefficient for the voltage, current and flux linkages equations. The transformation of the motor equations will reduce the complexity mathematical equations [45].

The first frame is the static frame from the stator winding at $2\pi/5$ degrees to each other for the case of the five phase. The second is the frame $\alpha\beta$, which is orthogonal reference frame where angle between the two axes is 90^o. The angle between a-axis for static reference frame and α-axis from the orthogonal reference frame is zero. The last one is the rotor frame dq. In this frame the d-axis is along the north and South Pole of the rotor and the q-axis is at 90^o from the d-axis. The d-axis of this frame is shifted by angle θ with respect to stator static frame a-axis. The transformation relations between the three frames are shown by Figure 3-2 and Figure 3-3.

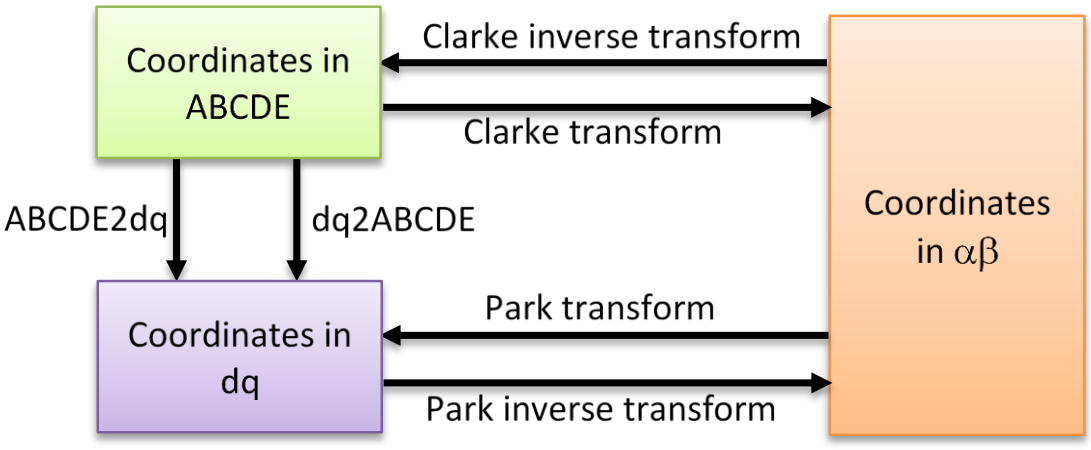

Figure 3-2 Relation between ABCDE, dq and αβ.

For a 5-phase equally distributed machine, the transformation from *abcdq* to *dqxy*0 and their inverse equaion are given in equation (3.6) and (3.7) [48].

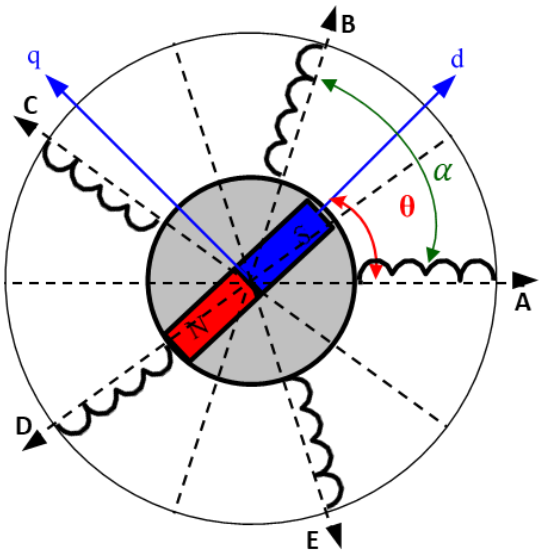

Figure 3-3 Schematic of 5-phase induction machine frame transformation.

$$\begin{bmatrix} v_{ds} \\ v_{qs} \\ v_{xs} \\ v_{ys} \\ v_{0s} \end{bmatrix} = \sqrt{\frac{2}{5}} \begin{bmatrix} 1 & \cos(\theta - \frac{2\pi}{5}) & \cos(\theta - \frac{4\pi}{5}) & \cos(\theta - \frac{6\pi}{5}) & \cos(\theta - \frac{8\pi}{5}) \\ 0 & \sin(\theta - \frac{2\pi}{5}) & \sin(\theta - \frac{4\pi}{5}) & \sin(\theta - \frac{6\pi}{5}) & \sin(\theta - \frac{8\pi}{5}) \\ 1 & \cos(\theta - \frac{4\pi}{5}) & \cos(\theta - \frac{8\pi}{5}) & \cos(\theta - \frac{12\pi}{5}) & \cos(\theta - \frac{16\pi}{5}) \\ 0 & \sin(\theta - \frac{4\pi}{5}) & \sin(\theta - \frac{8\pi}{5}) & \sin(\theta - \frac{12\pi}{5}) & \sin(\theta - \frac{16\pi}{5}) \\ \sqrt{2}^{-1} & \sqrt{2}^{-1} & \sqrt{2}^{-1} & \sqrt{2}^{-1} & \sqrt{2}^{-1} \end{bmatrix} \begin{bmatrix} v_a \\ v_b \\ v_c \\ v_d \\ v_e \end{bmatrix} \tag{3.6}$$

$$\begin{bmatrix} v_{dr} \\ v_{qr} \\ v_{xr} \\ v_{yr} \\ v_{0r} \end{bmatrix} = \sqrt{\frac{2}{5}} \begin{bmatrix} 1 & \cos(\delta - \frac{2\pi}{5}) & \cos(\delta - \frac{4\pi}{5}) & \cos(\delta - \frac{6\pi}{5}) & \cos(\delta - \frac{8\pi}{5}) \\ 0 & \sin(\delta - \frac{2\pi}{5}) & \sin(\delta - \frac{4\pi}{5}) & \sin(\delta - \frac{6\pi}{5}) & \sin(\delta - \frac{8\pi}{5}) \\ 1 & \cos(\delta - \frac{4\pi}{5}) & \cos(\delta - \frac{8\pi}{5}) & \cos(\delta - \frac{12\pi}{5}) & \cos(\delta - \frac{16\pi}{5}) \\ 0 & \sin(\delta - \frac{4\pi}{5}) & \sin(\delta - \frac{8\pi}{5}) & \sin(\delta - \frac{12\pi}{5}) & \sin(\delta - \frac{16\pi}{5}) \\ \sqrt{2}^{-1} & \sqrt{2}^{-1} & \sqrt{2}^{-1} & \sqrt{2}^{-1} & \sqrt{2}^{-1} \end{bmatrix} \begin{bmatrix} v_a \\ v_b \\ v_c \\ v_d \\ v_e \end{bmatrix} \tag{3.7}$$

θ is the angle between phase a axis of the stator and d axis, δ is the angle between phase a axis of the rotor and d axis where $\delta = \theta_s - \theta$. Applying the transformation matrix, the stator and rotor equations are referred to rotor domain. This yield to the following equations for voltage:

$$v_{ds} = R_s i_{ds} + \frac{d}{dt}\psi_{ds} - \omega_e \psi_{qs} \tag{3.8}$$

$$v_{qs} = R_s i_{qs} + \frac{d}{dt}\psi_{qs} - \omega_e \psi_{ds} \tag{3.9}$$

$$v_{xs} = R_s i_{xs} + \frac{d}{dt}\psi_{dx} \tag{3.10}$$

$$v_{ys} = R_s i_{ys} + \frac{d}{dt}\psi_{dy} \tag{3.11}$$

$$v_{0s} = R_s i_{0s} + \frac{d}{dt}\psi_{0y} \tag{3.12}$$

$$v_{dr} = R_r i_{dr} + \frac{d}{dt}\psi_{dr} - (\omega_e - \omega_r)\psi_{qs} \tag{3.13}$$

$$v_{qr} = R_r i_{qr} + \frac{d}{dt}\psi_{qr} - (\omega_e - \omega_r)\psi_{qr} \tag{3.14}$$

$$v_{xr} = R_r i_{xr} + \frac{d}{dt}\psi_{xr} \tag{3.15}$$

$$v_{yr} = R_r i_{yr} + \frac{d}{dt}\psi_{yr} \tag{3.16}$$

$$v_{0r} = R_r i_{0r} + \frac{d}{dt}\psi_{0r} \tag{3.17}$$

The stator & rotor linkage equations are given by:

$$\psi_{ds} = L_{ls} i_{ds} + L_m (i_{ds} + i_{dr}) \tag{3.18}$$

$$\psi_{qs} = L_{ls} i_{ds} + L_m \left(i_{qs} + i_{qr}\right) \tag{3.19}$$

$$\psi_{xs} = L_{ls} i_{xs} \tag{3.20}$$

$$\psi_{ys} = L_{ls} i_{ys} \tag{3.21}$$

$$\psi_{0s} = L_{ls} i_{0s} \tag{3.22}$$

$$\psi_{dr} = L_{lr} i_{dr} + L_m (i_{ds} + i_{dr}) \tag{3.23}$$

$$\psi_{qr} = L_{lr} i_{dr} + L_m (i_{qs} + i_{qr}) \tag{3.24}$$

$$\psi_{xr} = L_{lr} i_{xr} \tag{3.25}$$

$$\psi_{yr} = L_{lr} i_{yr} \tag{3.26}$$

$$\psi_{0r} = L_{lr} i_{0r} \tag{3.27}$$

$$i_{ds} = \frac{\psi_{ds}(L_{lr}+L_m) - L_m \psi_{dr}}{(L_{ls}L_{lr}+L_{ls}L_m+L_{lr}L_m)} \tag{3.28}$$

$$i_{qs} = \frac{\psi_{qs}(L_{lr} + L_m) - L_m \psi_{qr}}{(L_{ls}L_{lr}+L_{ls}L_m + L_{lr}L_m)} \tag{3.29}$$

$$i_{dr} = \frac{\psi_{dr}(L_{ls} + L_m) - L_m \psi_{ds}}{(L_{ls}L_{lr}+L_{ls}L_m + L_{lr}L_m)} \tag{3.30}$$

$$i_{qr} = \frac{\psi_{qr}(L_{ls} + L_m) - L_m \psi_{qs}}{(L_{ls}L_{lr}+L_{ls}L_m + L_{lr}L_m)} \tag{3.31}$$

v_{ds}, v_{qs}, v_{xs}, v_{ys}, v_{0s}, v_{dr}, v_{qr}, v_{xr}, v_{yr}, v_{0r}, i_{ds}, i_{qs}, i_{xs}, i_{ys}, i_{0s}, i_{dr}, i_{qr}, i_{xr}, i_{yr}, i_{0r} , are the d-q axis stator & rotor's voltage and current, Ψ_{ds},Ψ_{qs},Ψ_{dr},Ψ_{qr} are d-q axis flux linkage.

The mechanical dynamics of the motor is studied by the electromagnetic torque of the motor. The developed electromagnetic torque expressed in dq-domain is given by:

$$T_e = P L_m (\Psi_d i_d + \Psi_q i_q) \tag{3.32}$$

Equation (3.33) is used to relate the load torque to the electromagnetic torque:

$$T_e - T_L = \frac{J}{P}\frac{d}{dt}\omega_m \tag{3.33}$$

Rotor electrical speed and angle are given by (3.34) and (3.35)

$$\omega_m = \frac{2}{P}\omega_r \tag{3.34}$$

$$\theta_r = \int \omega_r \tag{3.35}$$

T_e is electromagnetic torque, T_L is load torque, J is moment of inertia, P is number of pole pairs, $L_m = \frac{2}{5}M$ is mutual inductance of the stator to the rotor and ω_r rotor electrical speed [49].

3.3 Multi-Phase Induction Motor Modeling

The d−q models of induction machine can be extended to any number of phases. Considering symmetrical design of multiphase motor with phase displacement $\alpha = 2\pi/n$ with all phases connect to one neutral point and the induction machine equations already transformed into the rotating frame at angular speed ω_e, the generalized transformation matrix shown in 3.36 can be applied[50].

$$\begin{bmatrix} v_d \\ v_q \\ v_x \\ v_y \\ \vdots \\ 0_+ \\ 0_- \end{bmatrix} = \sqrt{\frac{2}{n}} \begin{bmatrix} 1 & \cos(\theta-\alpha) & \cos(\theta-2\alpha) & \cos(\theta-3\alpha) & \cdots & \cos(\theta-n\alpha) \\ 0 & \sin(\theta-\alpha) & \sin(\theta-2\alpha) & \sin(\theta-3\alpha) & \cdots & \sin(\theta-n\alpha) \\ 1 & \cos(\theta-2\alpha) & \cos(\theta-4\alpha) & \cos(\theta-6\alpha) & \cdots & \cos(\theta-n\alpha) \\ 0 & \sin(\theta-2\alpha) & \sin(\theta-4\alpha) & \sin(\theta-6\alpha) & \cdots & \sin(\theta-n\alpha) \\ \sqrt{2}^{-1} & \sqrt{2}^{-1} & \sqrt{2}^{-1} & \sqrt{2}^{-1} & \cdots & \sqrt{2}^{-1} \\ \sqrt{2}^{-1} & -\sqrt{2}^{-1} & \sqrt{2}^{-1} & -\sqrt{2}^{-1} & \cdots & \sqrt{2}^{-1} \end{bmatrix} \begin{bmatrix} v_a \\ v_b \\ v_c \\ v_d \\ v_e \\ \vdots \\ v_n \end{bmatrix} \quad (3.36)$$

The first and second rows state the variables that will lead to production of the flux and torque. The two zero sequence components are in the last rows of the matrix where the last is used only when the phase number is even. The zero sequence doesn't exist for odd phase number star connected multiphase motor without grounding the neutral. The x–y components are in between and they do not contribute to the produced torque. Thus equations 3.8 till 3.35 can be applied with the exception that $L_m = \frac{2}{n}M$ where n is the number of phases of the multiphase machine.

3.4 Comparison of Multi-Phase Induction Motor

As established in the previous chapter, increasing the phase count of multi-phase machine has many advantages but on the other hand, it impacts the power electronics requirement on the inverter side. In order to determine the optimum phase number for proposed scheme, a simulation comparison was conducted for multiphase machines of similar coil design but with different phase count number. The details of the simulation are in Chapter 5. Two indicators have been defined, the current total harmonic distortion and the torque ripple. The result of the comparison is shown in Figure 3-4. It shows that both current harmonics and torque ripples don't improve much when phase count increased beyond five. Thus, the five phase machine has been selected for the proposed topology.

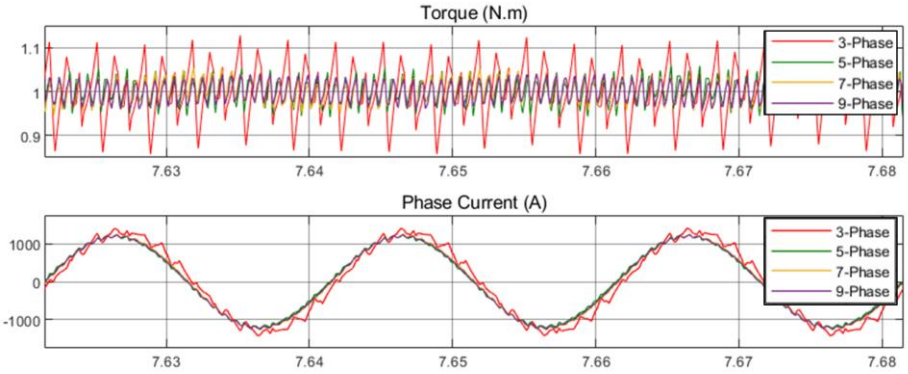

Figure 3-4 Torque and current waveform of different phase count machines.

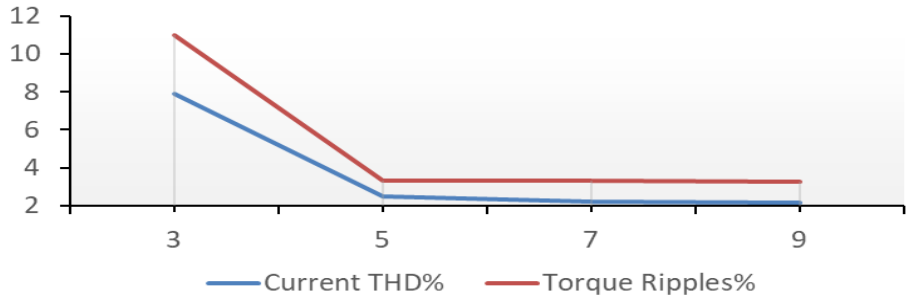

Figure 3-5 Schematic of 5-phase induction machine frame transformation.

Chapter 4: Development of a New High Power 5-Phase-5-Level Electric Drive System for LNG Plants

4.1 Introduction

As established earlier the up scaled LNG compressors requires high power starter and helper inverter fed motors. To satisfy the reliability as well as high power requirements, a high power drive system using multi-phase machine (5-phase) is proposed instead of a three-phase machine and multilevel inverter topology connected in an innovative way.

The 5-phase machines have lower torque ripples, greater efficiency, higher torque density, and reduced required rating per inverter leg [41] [51] [52][42]. To design the proposed 5-phase drive system, an appropriate power electronics converter such as Voltage Source Inverter (VSI) is selected. The VSI based on Insulated Gate Controlled Thyristor (IGCT) has inherent advantages regarding power factor, torque ripples and grid harmonics. To cope with the LNG plants requirement such as high power, efficiency and reliability, a topology based on 5-level Neutral-Point-Clamped (NPC) inverter is used for the proposed electric drive. NPC inverters are widely used in high power applications and have the highest converter efficiency among the available topologies and are thus the most preferred choice for many industrial MV applications, such as in oil/gas [29] [36]. Also, this type of inverter has reached a mature state of development. Most drive manufacturers have these inverters readily available as modules in reliable operating conditions, and at the required power rating. In the proposed drive system, a special topology for the selected 5-phase

machine drive is proposed. Each of the 5-phase of the induction machine is fed by a special Full-Bridge NPC (two NPC legs) as shown in Figure 4-1. This NPC-Cell based configuration uses IGCT devices to achieve high power drive system operating at low switching frequency, low loss, and high voltage handling. A high reliability is achieved using the proposed simple circuit topology using a small number of devices. The proposed topology can drive a motor with 6.6 kV with a power up to 50 MW.

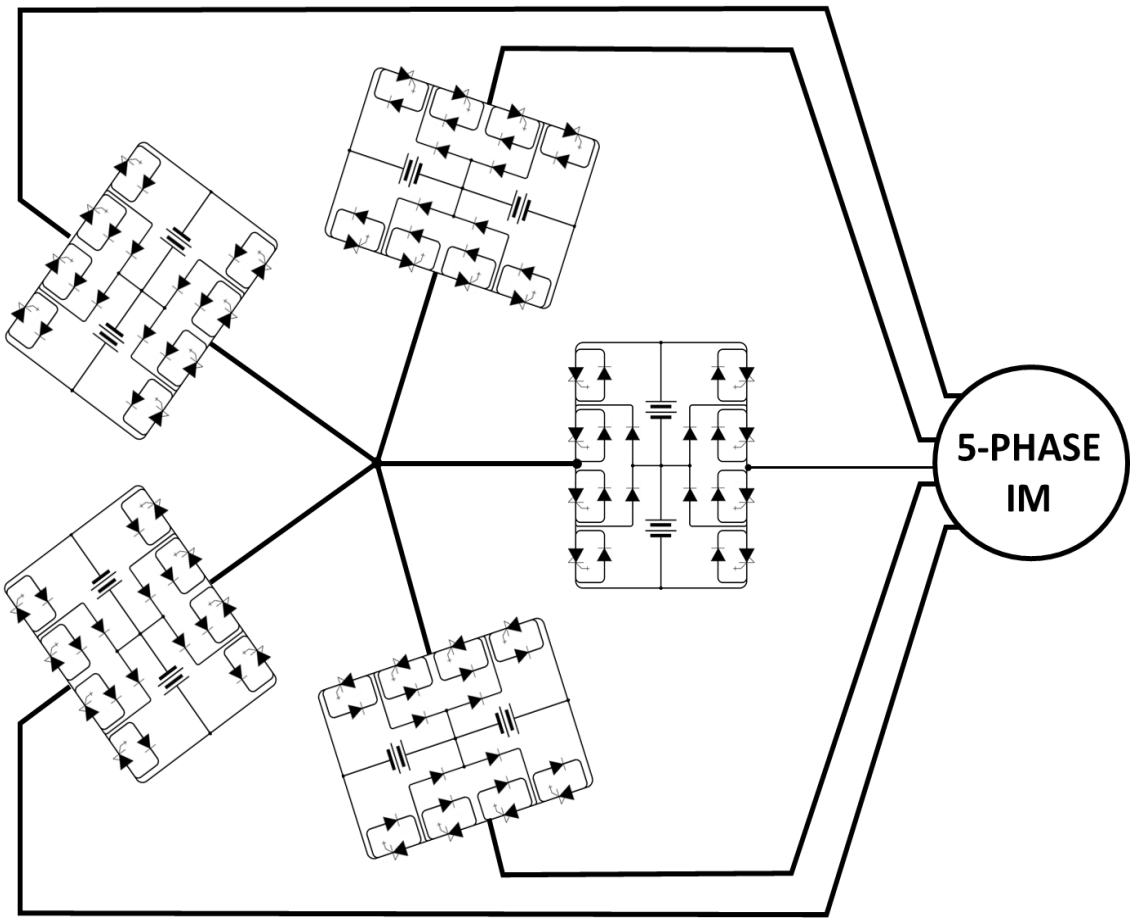

Figure 4-1 Proposed inverter fed motor topology.

4.2 One Cell Five Level NPC Operation

The principle of operation of the 5-level one-cell of NPC is depicted in Figure 4-2. A single phase inverter consists of two legs of a 3-level inverter. The batteries represent a common DC bus structure of the inverter with a positive, negative and a neutral connection. Each bus contributes to half of the voltage *E*/2 and combined they produce the full voltage *E*. This circuit topology can output different voltage levels by changing the voltage produced by each of the inverter legs.

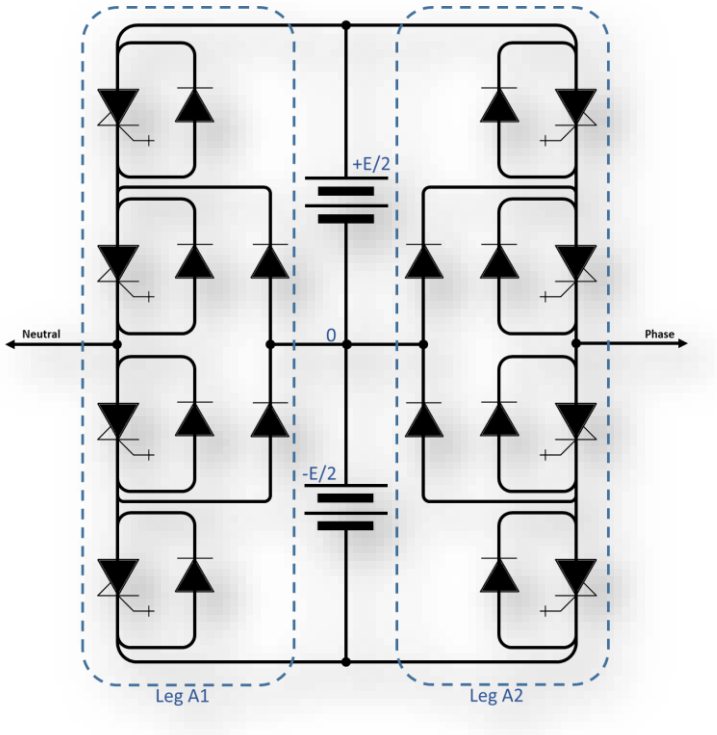

Figure 4-2 Schematic of one cell five level NPC cell.

The reference point of these levels is the neutral bus and is obtained by combination of output voltages from the two legs of single phase inverter as shown in Figure 4-3.

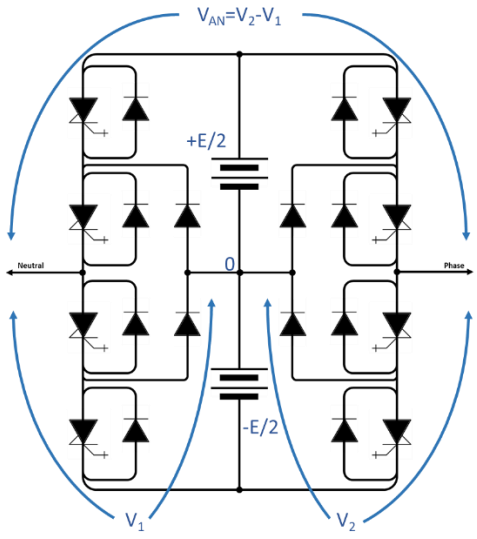

Figure 4-3 Operation principle one cell five level NPC cell.

Each leg is capable of producing three levels; +*E*/2, zero, -*E*/2. Then with the proposed configuration, it possible to output the following five voltage levels or steps: +*E*, +*E*/2, zero, -*E*/2 and –*E*.

Starting with the full negative output –*E*, it requires *E*/2 voltage on leg A_1 by and -*E*/2 voltage on leg A_2. This is achieved by turning on Q_1 and Q_2 on leg A_1 and Q_7 and Q_8 on leg A_2 while all other IGCTs are off. Figure 4-4 illustrates cell condition at V_{AN}=-*E*. The second level is –*E*/2. It can be achieved by two different combinations. Either by having the *E*/2 on leg A_1 and 0 on leg A_2 or by having 0 of leg A_1 and –*E*/2 on leg A_2. Figure 4-5 illustrates the two different combination for –*E*/2 level; by turning on Q_1 and Q_2 on leg A_1 and Q_6 and

Q_7 on leg A_2 while keeping the rest in off condition (Figure 4-5A) or by turning on Q_2 and Q_3 on leg A_1 and Q_5 and Q_6 on leg A_2 whereas the rest in off condition (Figure 4-5B).

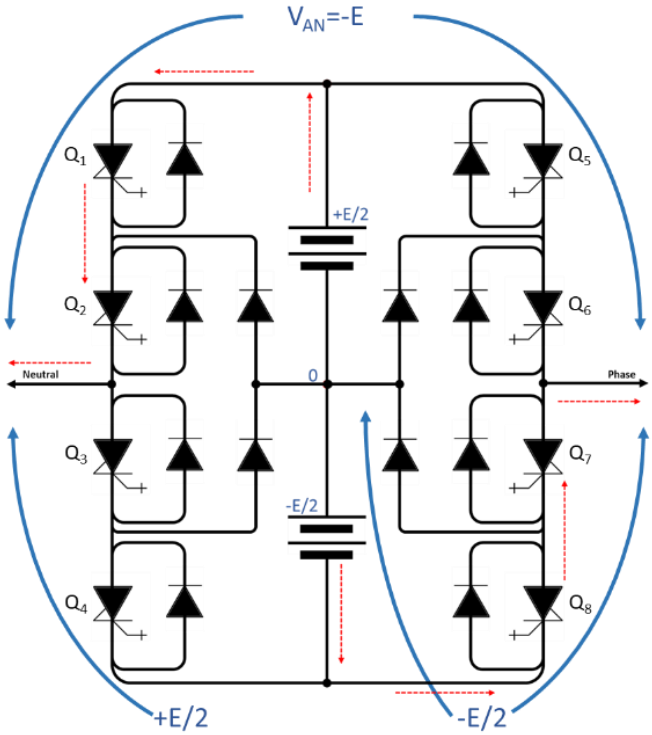

Figure 4-4 Cell illustration for V_{AN}=-E.

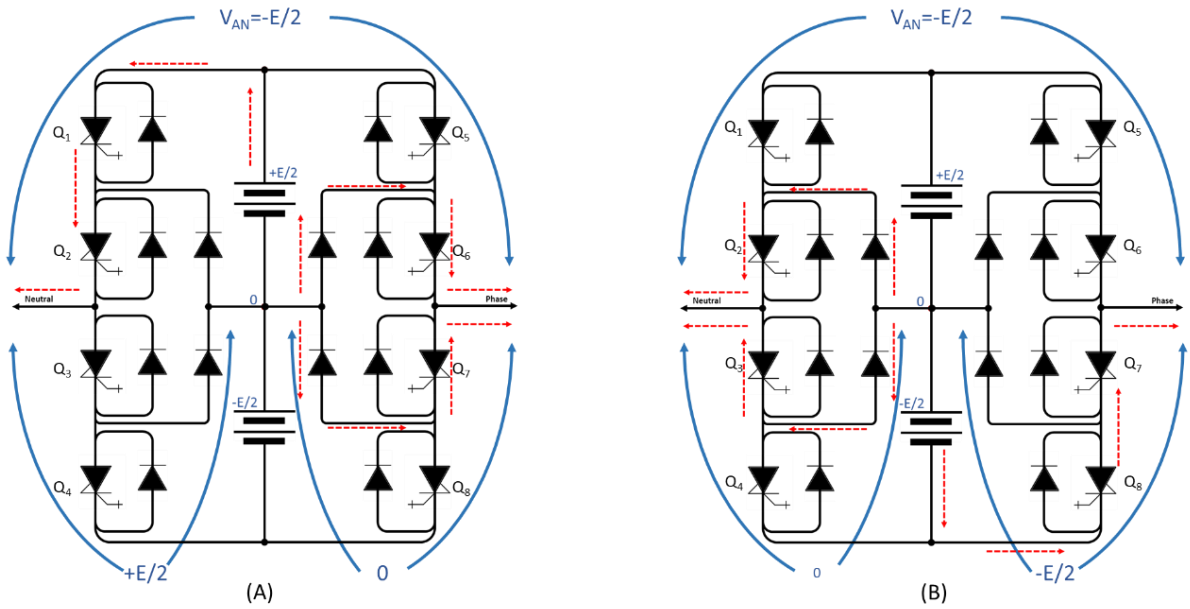

Figure 4-5 Cell illustration for V_{AN}=-E.

The third level is the zero voltage level, it can be achieved by three different combinations; zero voltage in each of the inverter legs or by having similar voltages on both of the cell legs. Figure 4-6A shows the case of zero voltage obtained by turning of Q_2 and Q_3 in leg one and Q_6 and Q_7 in leg 2 while all other IGCTs are off. In this case each of leg produces zero voltages and thus the resultant is zero.

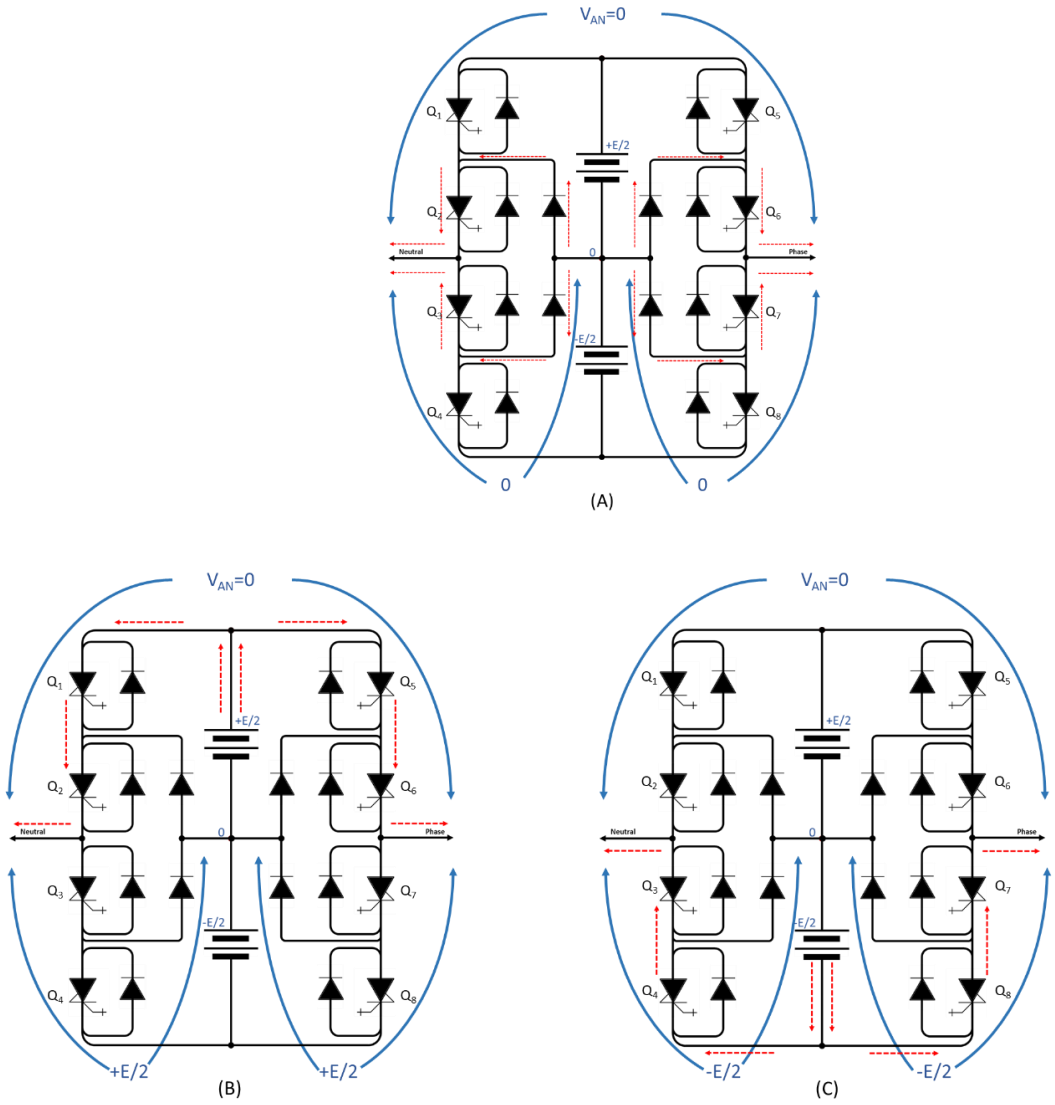

Figure 4-6 Cell illustration for V_{AN}=0.

The other case of zero voltage output is shown in Figure 4-6B & Figure 4-6C. By turning on Q_1 and Q_2 on leg one and Q_5 and Q_6 on leg 2 while the rest are off, both legs will have +E/2 voltage and resultant will be zero. Similarly it can be achieved by having –*E*/2 output in each leg by turning on Q_3 and Q_4 on leg one and Q_7 and Q_8 on leg 2 whereas the rest are off.

The next level is +*E*/2. Similar to –*E*/2 level, it can be achieved by two different switching combinations. Either by having the 0 on leg A_1 and -*E*/2 on leg A_2 or by having *E*/2 of leg A_1 and 0 on leg A_2. Figure 4-7 illustrates the two combination for *E*/2 level; by turning on Q_1 and Q_2 on leg A1 and Q_6 and Q_7 on leg A_2 whereas other switches are off (Figure 4-7A) or by turning on Q_2 and Q_3 on leg A_1 and Q_5 and Q_6 on leg A_2 while keeping the other switches in off condition (Figure 4-7B).

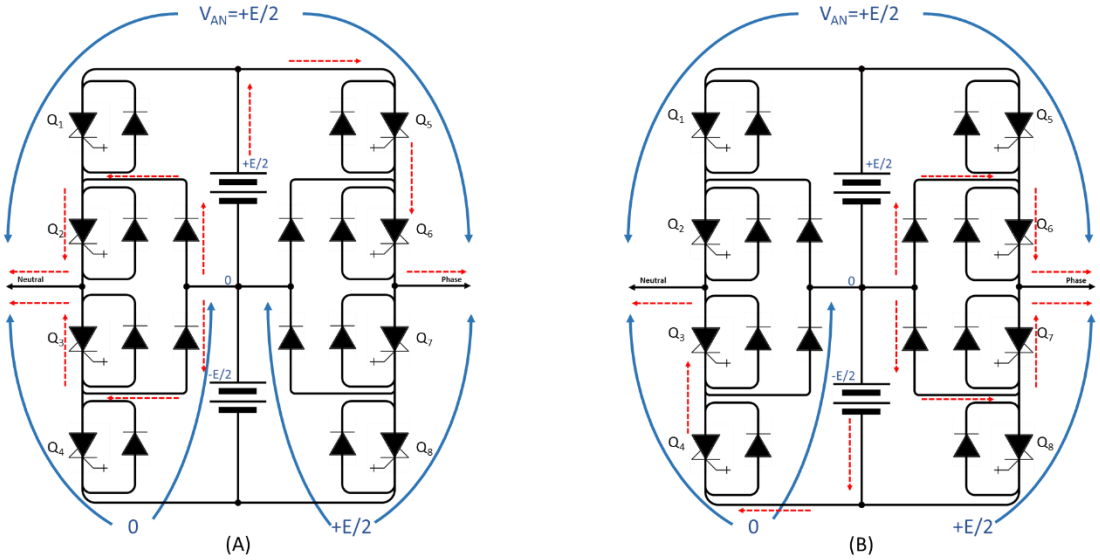

Figure 4-7 Cell illustration for V_{AN}=+*E*/2.

The final level is the full voltage level +*E*. It is realized by having the –*E*/2 on leg A_1 and *E*/2 on leg A_2. This is accomplished by turning on Q_3 and Q_4 on leg A_1 and Q_5 and Q_6 on leg A_2 while the other IGCTs are off as illustrated in Figure 4-8.

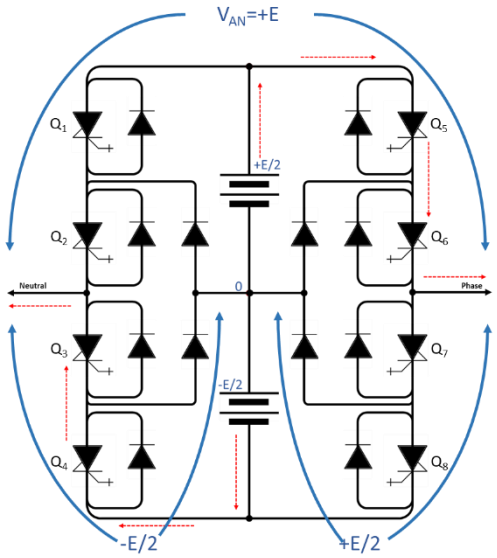

Figure 4-8 Cell illustration for V_{AN}=+E.

Table 4-1 summarizes the different voltage levels and the possible combinations to achieve the required voltage level. Figure 4-9 shows the output voltage levels of the proposed 5-level NPC cell.

Table 4-1 Combination of voltage levels of star-connected circuit

Voltage Level#		**1**	**2**		**3**			**4**		**5**
V ***1***	*0 to phase A*	*-E/2*	*-E/2*	*0*	*-E/2*	*0*	*+E/2*	*0*	*+E/2*	*+E/2*
V ***2***	*0 to Neutral*	*+E/2*	*0*	*+E/2*	*-E/2*	*0*	*+E/2*	*-E/2*	*0*	*-E/2*
$V_{AN}=V_2-V_1$:		*-E*	*-E/2*			*0*			*+E/2*	*+E*

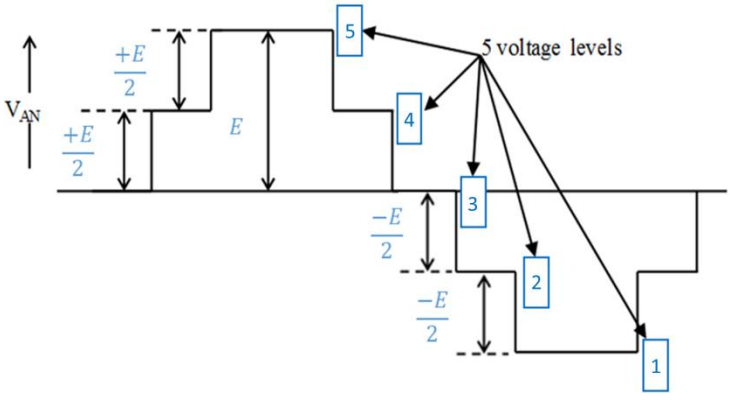

Figure 4-9 Voltage levels of one cell five level NPC inverter

4.3 Five Phase Five Level NPC Operation

As the name implies, five inverters are required for a five level inverter. The inverters are connected in start formation by linking the neutral connection of each inverter together as shown in Figure 4-10. Modular design with isolated DC source is selected to ensure continuity of operation even if one leg is lost in addition to avoiding voltage unbalance issues.

Similar to single cell operation, the other four phases' inverters operate in the same manner but with a phase shift of $2\pi/5$ of each other. This will result in two different values for line-to-line voltage; one for the consecutive phases and one for nonconsecutive phases.

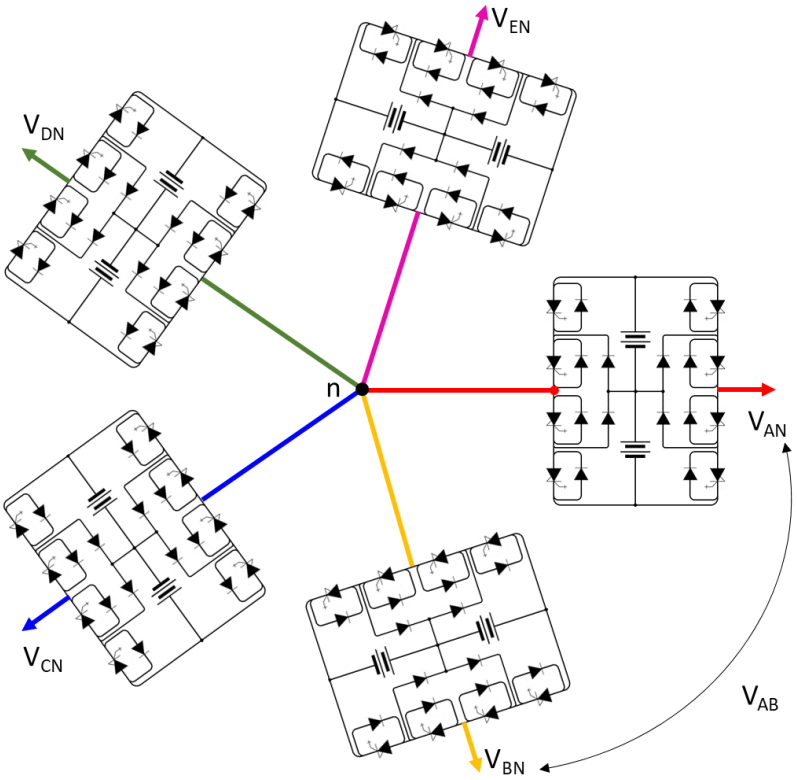

Figure 4-10 Five level five phases NPC inverter schematic

Figure 4-11 shows the phase's voltage waveform of phase A, phase B and the line voltage V_{AB} (V_{AN}-V_{BN}). The produced consecutive line to line voltages has 7 levels; +3E/2, +E, +E/2, zero, -E/2, –E and -3E/2.

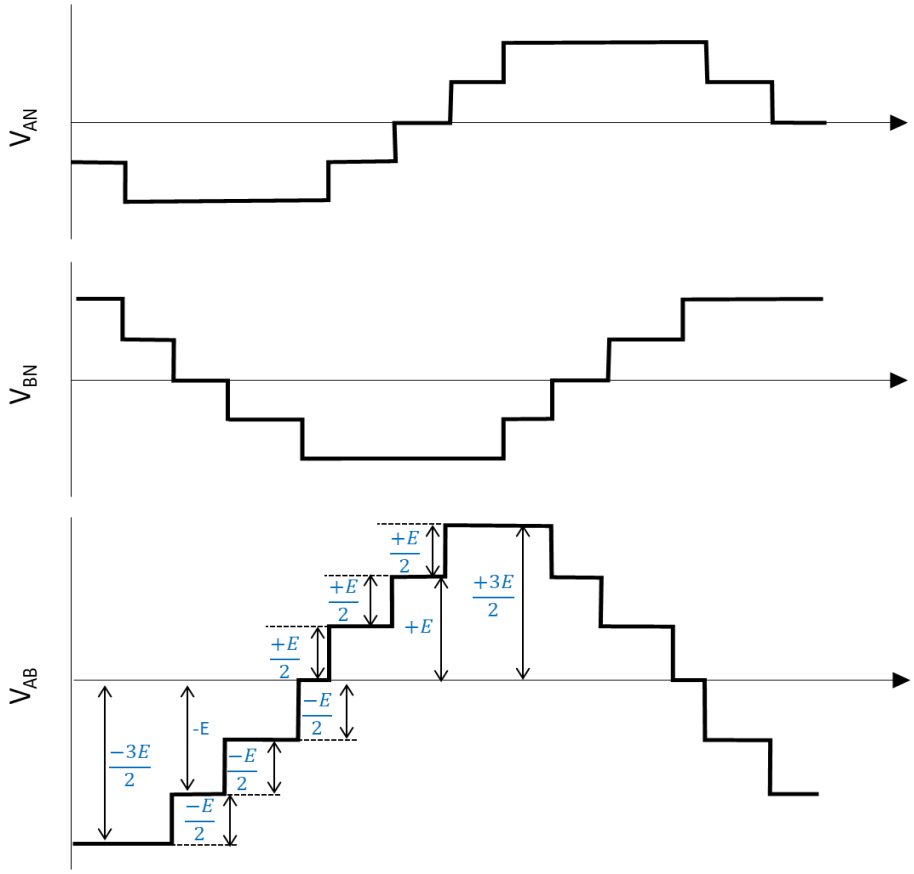

Figure 4-11 Line voltage levels of five level five phase NPC inverter

Compared to the 3-level NPC inverters, the expected number of levels is nine. The 8th and 9th voltage levels do not appear in the consecutive phases as the peaks of V_{AN} and V_{BN} do not overlap because of the smaller phase shift. Table 4-2 shows the voltage levels of two consecutive phases and the resultant line voltage over one complete cycle.

Table 4-2 Phase and line voltage of consecutive phases in five phase inverter topology

V_{AN}	**-E/2**	**-E**	**-E**	**-E**	**-E**	**-E/2**	**0**	**E/2**	**E**	**E**	**E**	**E**	**E/2**	**0**
V_{BN}	E	E/2	0	-E/2	-E	-E	-E	-E	-E/2	0	E/2	E	E	E
$V_{AB} = V_{AN}$- V_{BN}	-3E/2	-3E/2	-E	-E/2	0	E/2	E	3E/2	3E/2	E	E/2	0	-E/2	-E

The performance of the 5-level 5-phase inverter is investigated in the next chapter.

Chapter 5: Modeling and Simulation of 5-Phase-5-Level Inverter fed Motor

5.1 Introduction

To study the performance of the proposed system, the model of the drive system has been built in MATLAB/SIMULINK software platform. The simulated model comprises three main parts: 5-level inverter, 5-phase indication motor and controller. This chapter describes the details of the modeling of these 3 parts of the drive system.

5.2 Parts' Modeling

5.2.1 Controller Block

The open-loop volt-per-hertz (V/f) control is used for the simulation of the 5-level 5-phase inverter. The control is defined by voltage and frequency base point for the motor. As the motor speed rises, the stator voltage rises proportionally to maintain the voltage to frequency ratio constant, which leads to approximately constant flux operation. The motor operates at optimum point below the base point because of the constant ratio and hence the maximum torque is constant (Figure 5-1).

MATLAB/SIMULINK functions are used to generate five voltage reference signals with V/f concept. The reference signals are input to the PWM generator. The five level PWM generator is realized by four high frequency triangular carrier waves generator and comparators (Figure 5-2). This will generates the pulses for each of the inverters' IGBTs.

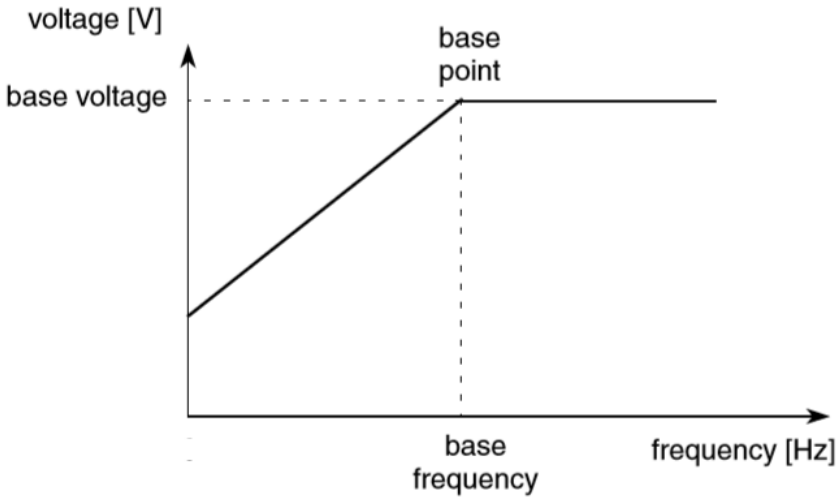

Figure 5-1 V/F controller curve.

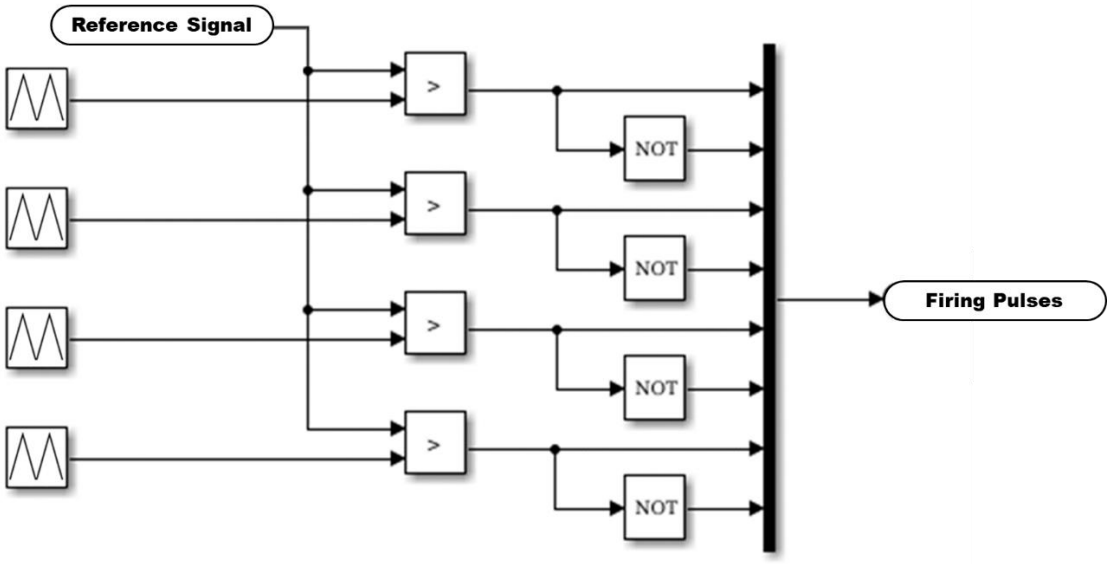

Figure 5-2 PWM firing signals.

Different types of PWM are possible. Level shifted phase disposition PWM (PDPWM) is first used. In this scheme four carriers in phase are used. The selected carrier frequency

is 750Hz, which is common for large power inverters. The carriers are compared with five refernce signals; one for each phase to generate the firing pulses (Figure 5-3).

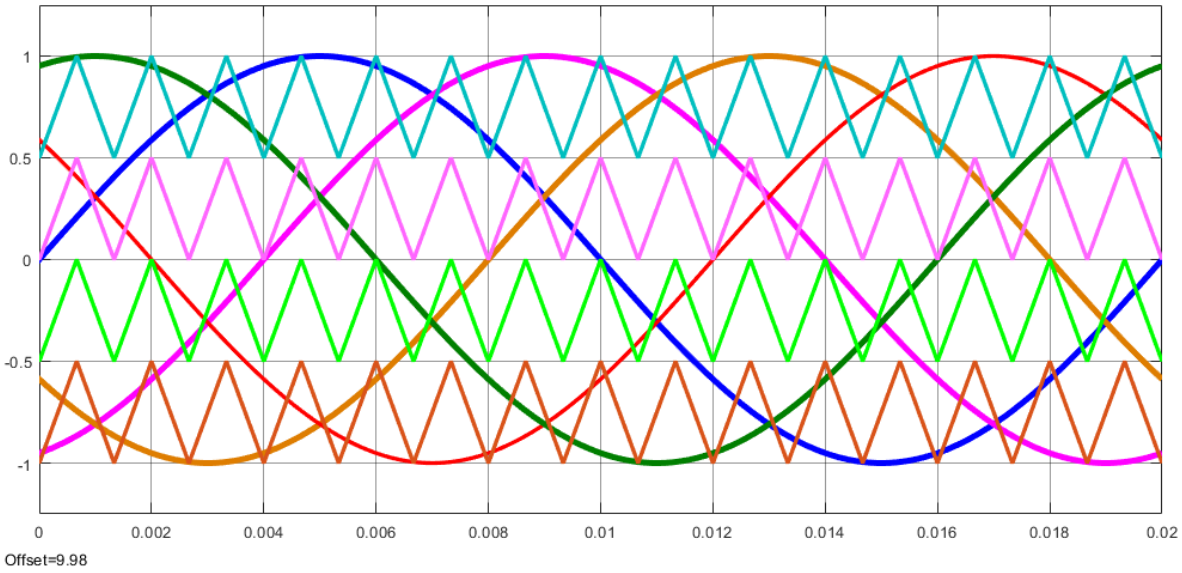

Figure 5-3 Phase disposition PWM for five phases.

5.2.2 Inverter Model

MATLAB/SIMULINK uses ideal power electronic components. Thus, in terms of operation the IGCT can be built using ideal IGBT model component (simplified mode of an IGBT /Diode pair where the forward voltages of the forced-commutated device and diode are ignored with default values for internal resistance and snubber resistance & capacitance). Figure 5-4 shows the equivalent IGBT schematic of one cell of the 5-level inverter.

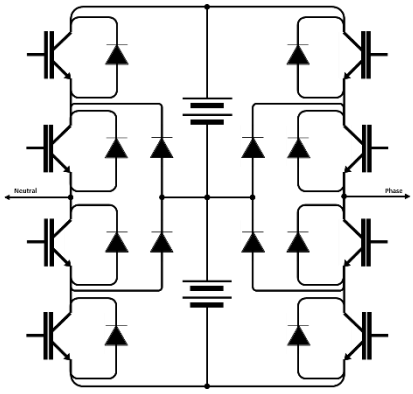

Figure 5-4 IGBT based 5-level inverter used in MATLAB/SIMULINK.

5.2.3 Induction Motor Model

The mathematical model equations for the multi-phase induction motor presented in chapter 3 are used to build the SIMULINK model. The motor model blocks are shown in Figure 5-5 and the selected motor parameters are listed in Table 5-1.

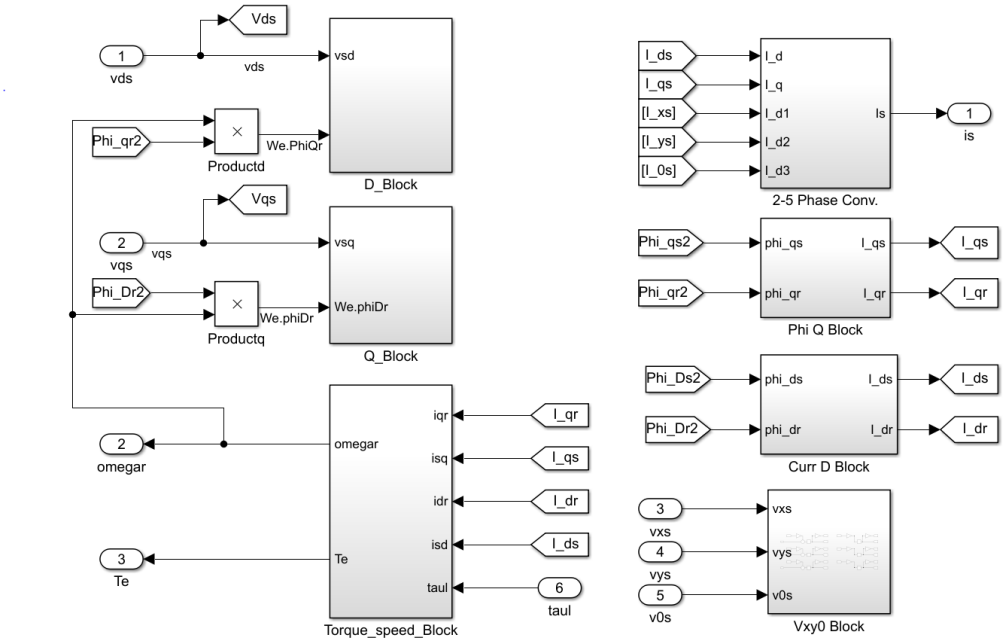

Figure 5-5 SIMULINK model of 5-phase induction motor

Table 5-1 Motor Parameters

Parameter	Value
Rated Power	33 MW
Rated Voltage	6.3kV
Rated Speed	3000
Stator Resistance	9.9m Ω
Rotor Resistance	6.9m Ω
Stator Self-Inductance	0.632m Ω
Rotor Self-Inductance	0.442m Ω
Mutual inductance	47.4m Ω
Number of Poles	2

5.2.4 Five Level Five Phase Inverter Fed Motor Model

By integrating the controller, the five-level inverters and the motor, the system is complete and ready for simulation. A schematic diagram of the integrated system is shown in Figure 5-6.

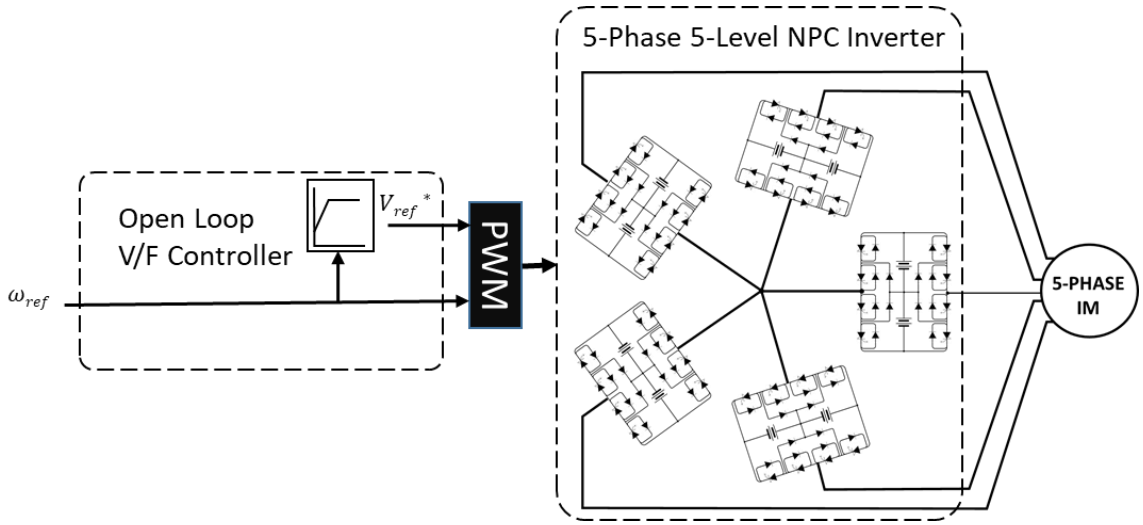

Figure 5-6 Schematic of 5-level 5-phase inverter fed induction motor

5.3 Performance Measure

At each simulation case, the system performance has been measured against the below defined key indicators.

5.3.1 Voltage Total Harmonic Distortion (THD)

The inverter output voltage is non-sinusoidal thus the sum of all phases' voltages is not zero at any instant. The nonlinearity is caused by the PWM process. The modulation technique has influence on the over the voltage. Voltage harmonics have negative effect on the motor as they cause further core losses in motor.

5.3.2 Current THD

The non-sinusoidal current waveform results in increased current harmonics that adds to the heating losses in motor windings. Similar to the voltage harmonics, the current harmonics are greatly related to the modulation technique.

5.3.3 Torque Ripples

Because of the switching nature of the inverter, torque ripples always exist. It is as a result of the non-sinusoidal voltage and current waveform. Larger torque ripples magnitude raise the concern for torsional excitation of train string.

5.3.4 Pulsating Torque Frequency

Pulsating torques refers to the set of torque harmonics of the motor. By neglecting the torque pulsation associated to the machine construction, the frequencies of pulsating torques are entirely dependent on the inverter topology and control, but the machine parameters contribute to their magnitudes. The shaft Eigen mode excitation is impacted to great extent

by the pulsating torque frequencies rather than their magnitudes. Knowing the pulsating torque is convenient for torsional analysis.

5.4 Simulation Results of 5-Level 5-Phase Inverter Fed Motor

The developed SIMULINK model has been simulated with parameters in Table 5-1. Different operating conditions and controller parameters have been considered to study the dynamic performance of the 5-level 5-phase inverter fed induction motor.

5.4.1 Inverter Performance

Figure 5-7 shows the phase voltages and Figure 5-8 shows phase voltages V_A and V_B and their resultant line voltage V_{AB}. It is observed that each phase voltage exhibits 5 levels as expected while the line voltage has 7 levels only. The line voltage total harmonic distortion at full speed is measured to be 25.88%.

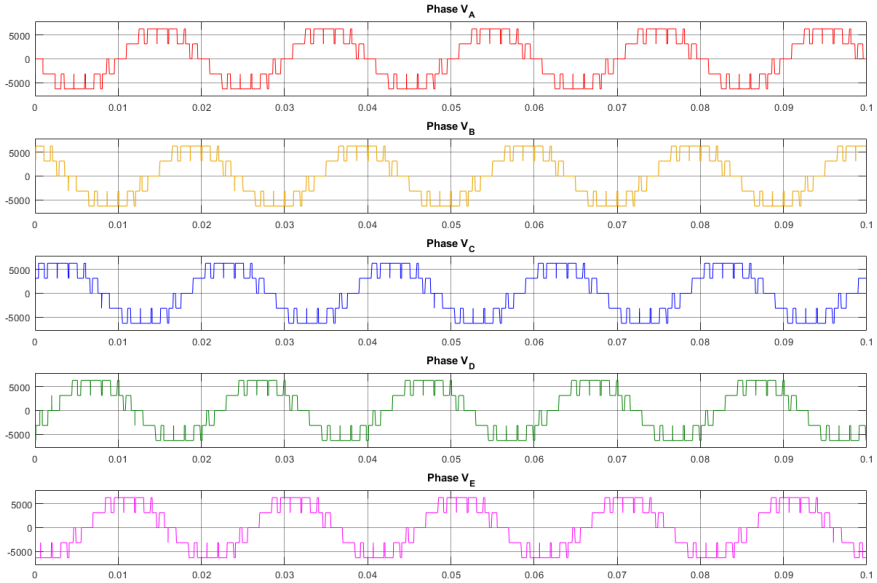

Figure 5-7 5-level 5-phases' inverter phase voltage

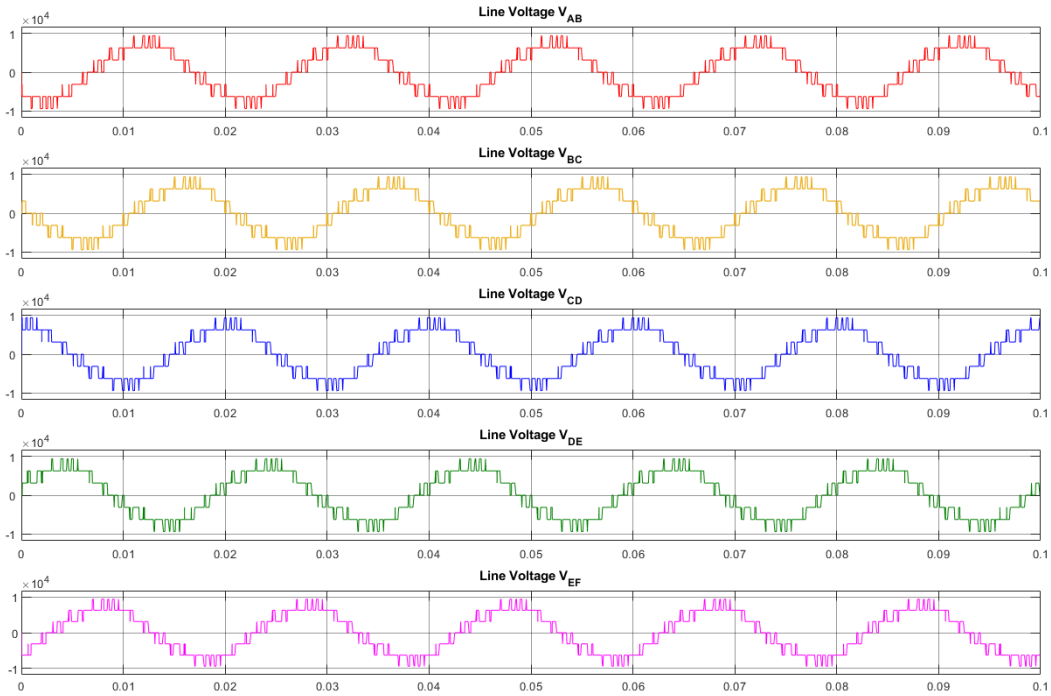

Figure 5-8 5-level 5-phases' inverter line voltage

5.4.2 Motor Starting Characteristics

Direct motor start up by applying rated voltage and frequency without loading the motor was simulated first. As can be seen in Figure 5-9, the motor exhibits very high transients during starting because of the uncontrolled start. The motor starting took more than 6 sec due to the huge inertia of the motor. At steady state, the average torque went down to zero when the speed reached 3000 rpm (synchronous speed).

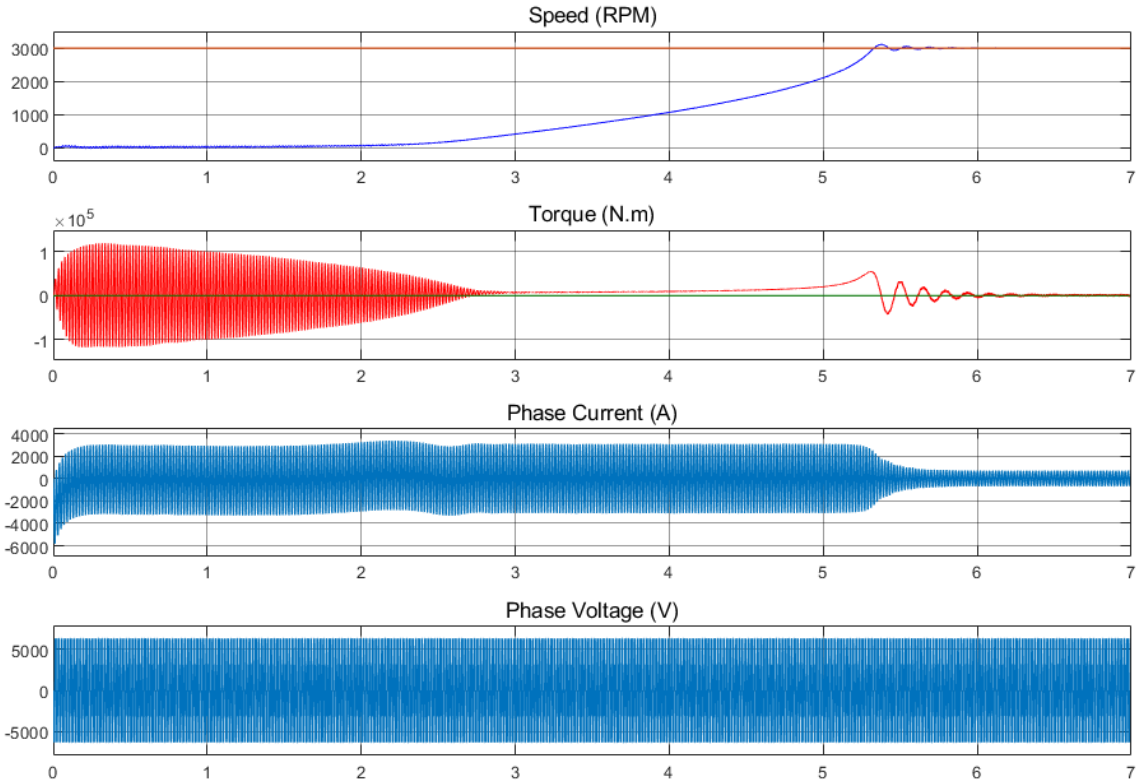

Figure 5-9 Dynamic of direct motor start

Figure 5-10 shows the speed and voltage responses of the system. The speed reference was increased in steps and the motor speed followed the speed reference very closely. The voltage level and switching increase as per the reference speed. At very load speed, using this control scheme, the inverter behaves like 3-level inverter.

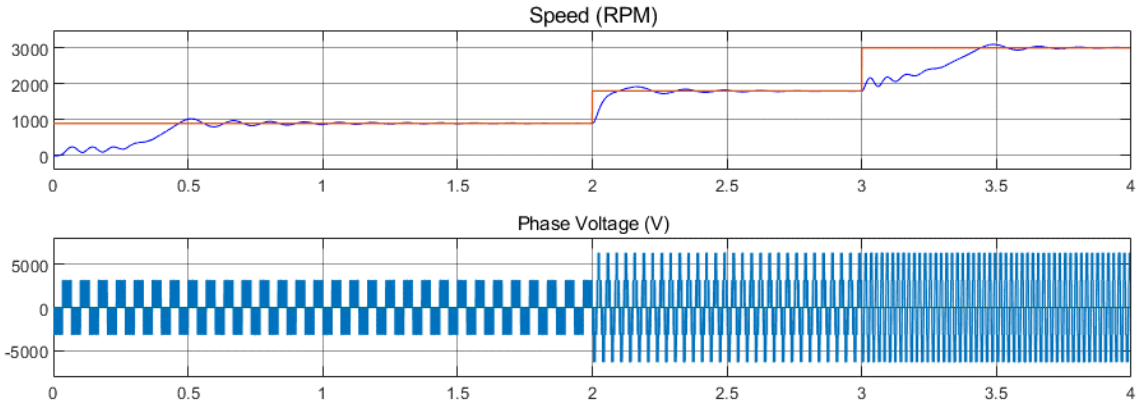

Figure 5-10 Speed and phase voltage plots

5.4.3 Motor Loading Characteristics

The model was simulated at full speed at no load then the load was gradually increased at constant rate up to rated value over three seconds. The dynamic response of the motor is shown in Figure 5-11.

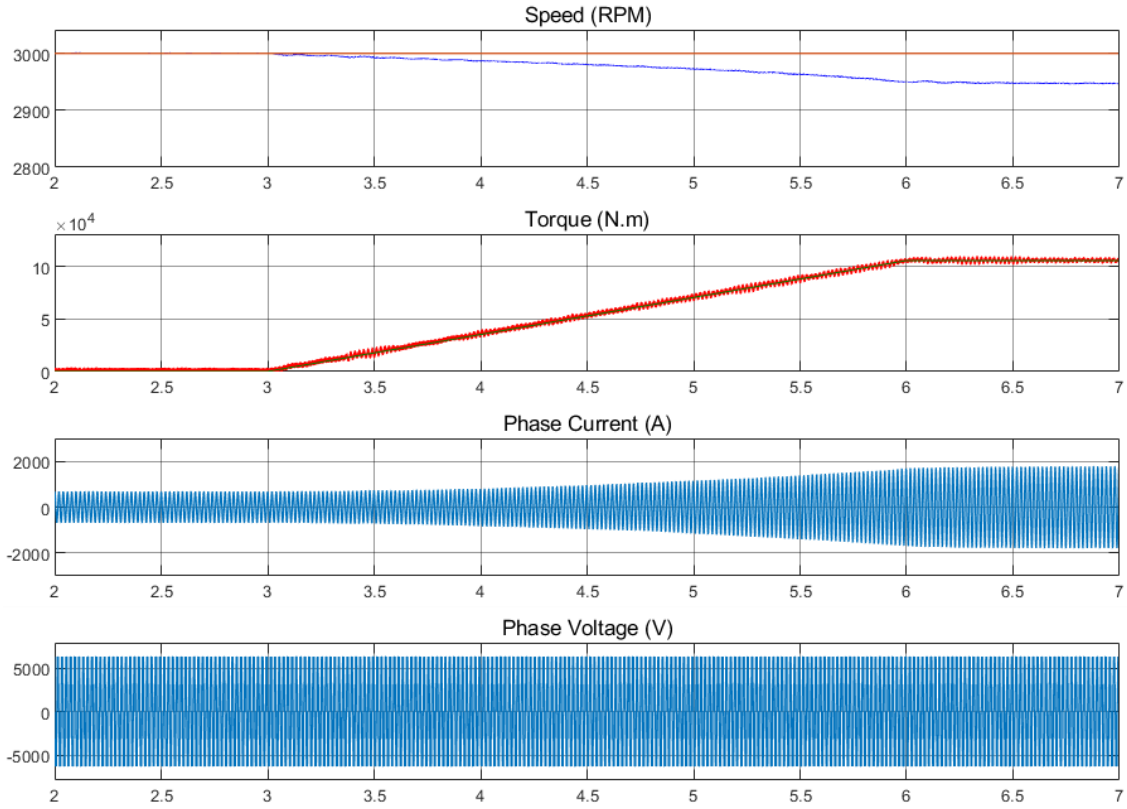

Figure 5-11 Dynamic response of motor loading

The no load current is 700 A, which accounts for 40% of the rated current. At full load, the speed drops to 2947 rpm (98.2% speed) and the current increases to 1750 A. The five phases' output currents are shown in Figure 5-12. The THD percentage at full load steady state operation is 1.09% (Figure 5-13).

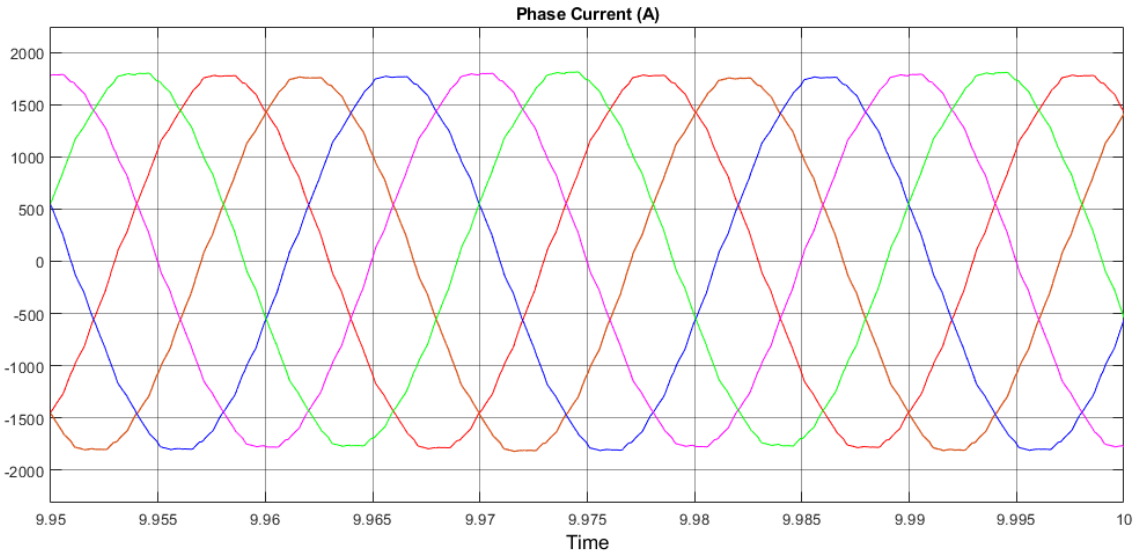

Figure 5-12 Steady state current of five level five phase inverter fed motor

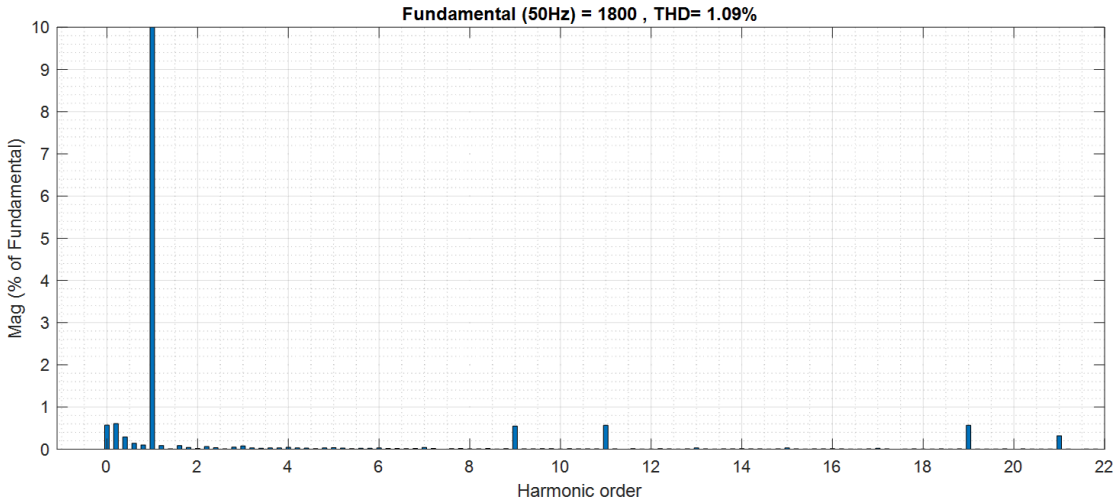

Figure 5-13 Harmonic spectrum of torque waveform

5.4.4 Torque Characteristics

The steady-state motor torque characteristic at full load operation is shown in Figure 5-14.

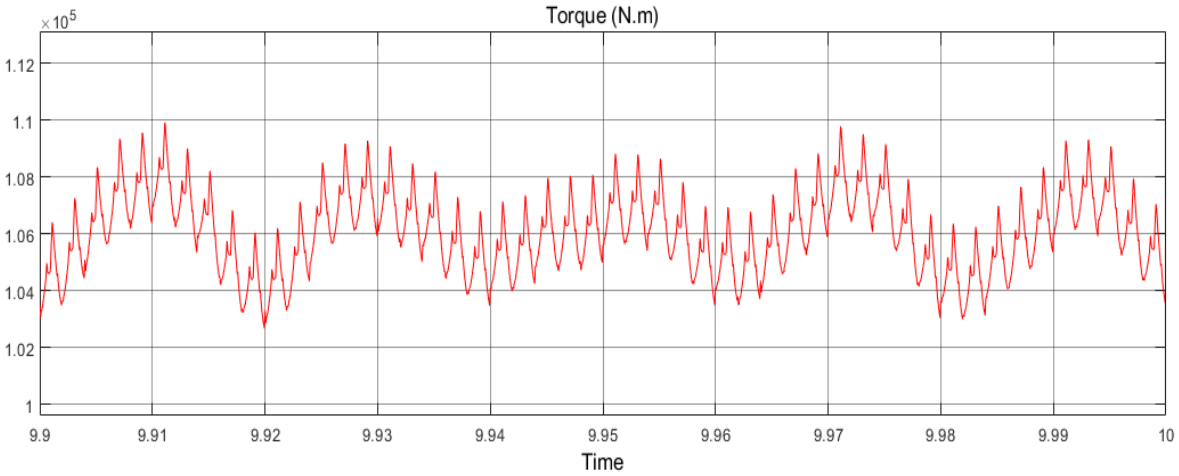

Figure 5-14 Motor torque waveform at full load

It is observed that the torque has a torque ripple components of 0.95%. The torque pulsations are mainly due to the non-sinusoidal voltage waveform resulting from the 5-level NPC inverter's switching. The effect of the inverter's switching over one eighth of a cycle is illustrated in Figure 5-15.

Then, a Fast Fourier Transform (FFT) of the resultant torque has been analyzed and plotted in Figure 5-16. The torque harmonic frequencies depend on the switching frequency and the frequency of the fundamental component of the stator current.

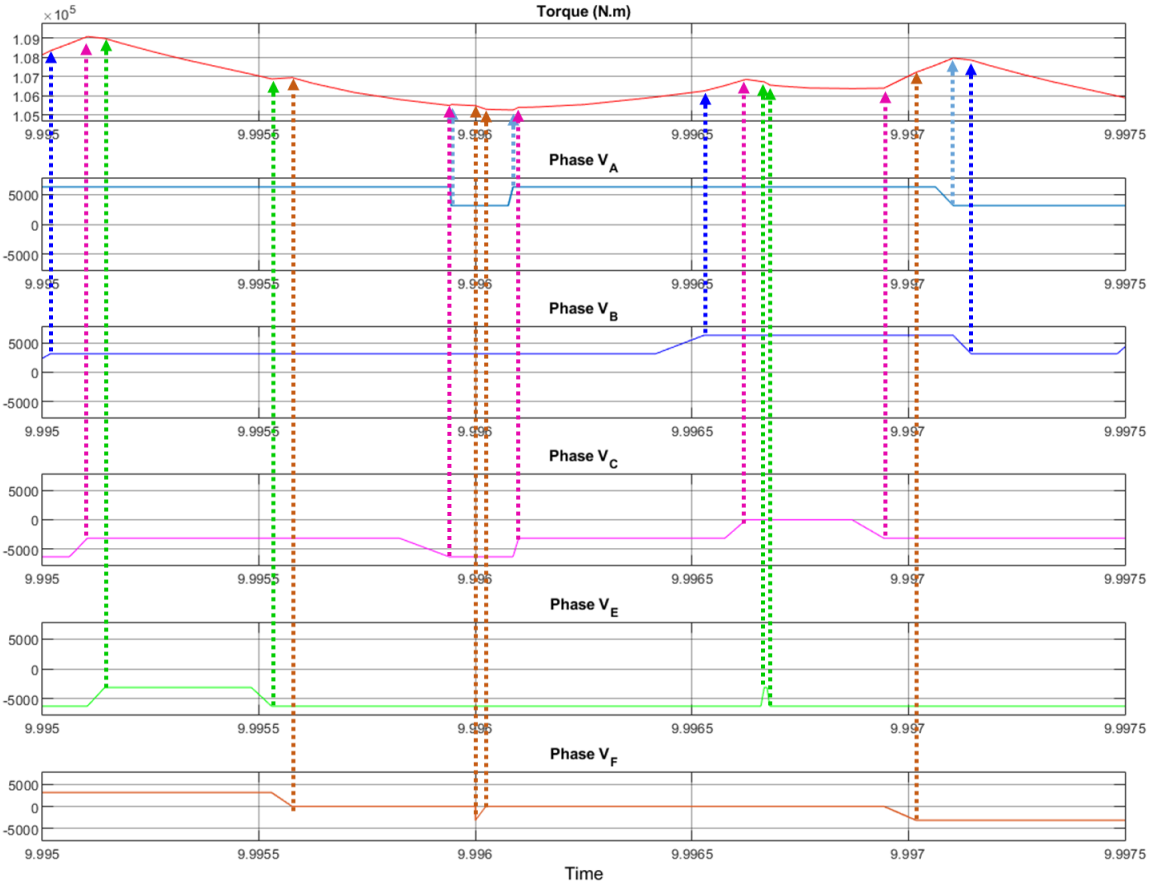

Figure 5-15 Switching effect on torque pulsation

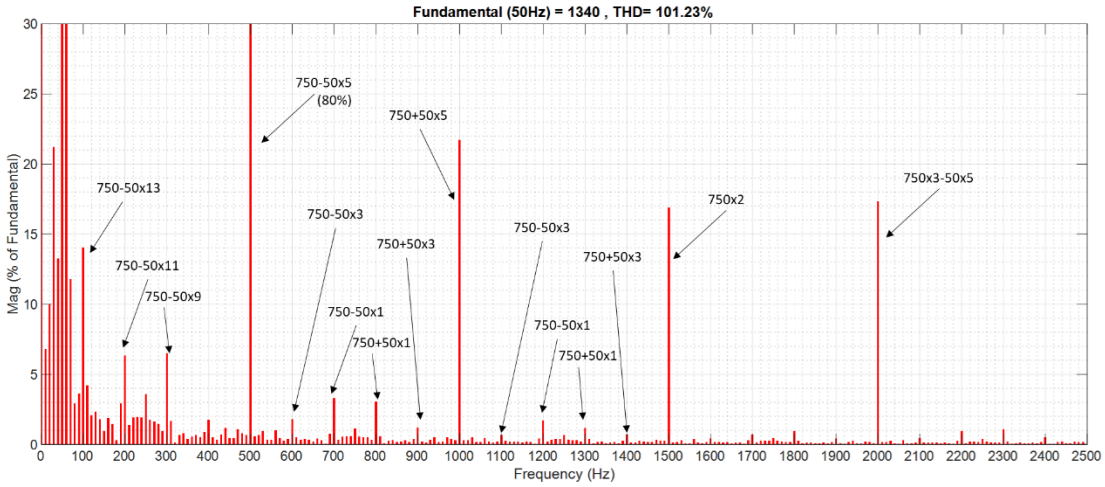

Figure 5-16 Torque waveform harmonic content

5.5 Effect of PWM Technique

The controller used in the previous simulation applied phase disposition PWM to generate the pulses signals. The torque pulsation is heavily affected by the modulation method. Other common modulation techniques have been investigated for their effect on the drive system performance.

5.5.1 Phase Opposition Modulation Technique

In this modulation technique, the carriers on the upper half and on the lower half are phase disposed from each other by 180^{o} as shown in Figure 5-17.

Figure 5-17 Phase opposition PWM for five phase system

The dynamic response of the motor voltage, current and torque at full load and in steady state condition are illustrated in Figure 5-18. The current %THD is 2.79% and voltage

%THD is 26.16%. The torque waveform has peak-to-peak ripples of 9%. Figure 5-19 presents the harmonics contents of the torque.

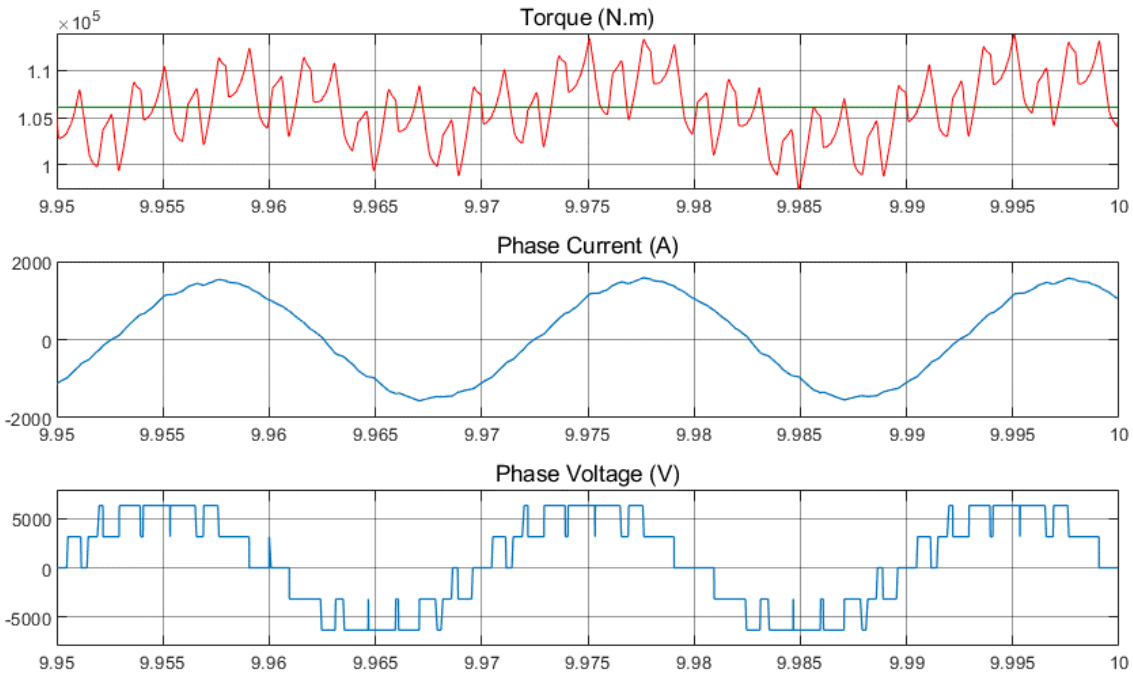

Figure 5-18 Motor dynamics with phase opposition PWM

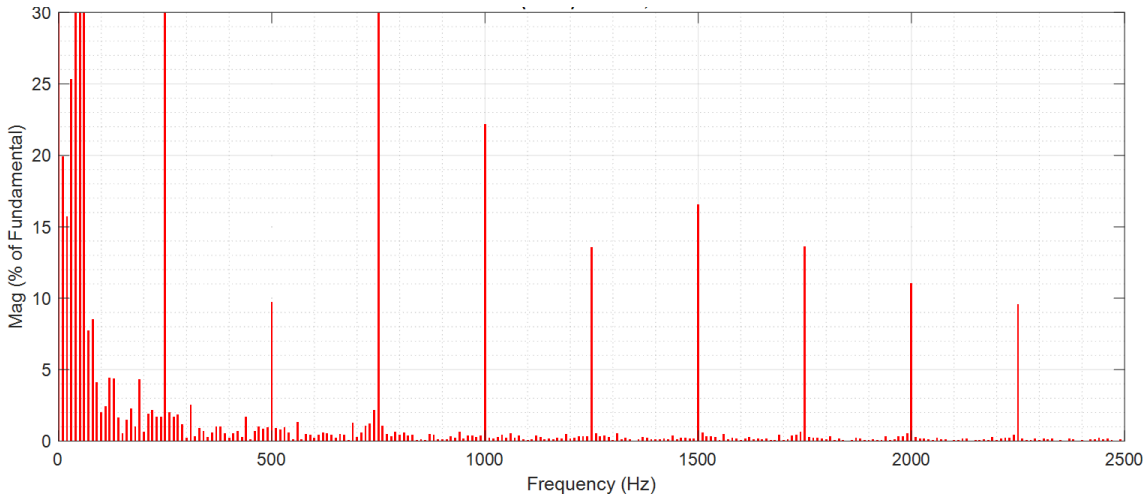

Figure 5-19 Torque waveform harmonic content with phase opposition PWM

5.5.2 Alternative Phase Opposition Modulation Technique

This modulation technique generates the firing pulses by comparing the reference voltage to carrier signals that are out of phase by 180º of the adjacent ones as depicted in Figure 5-20.

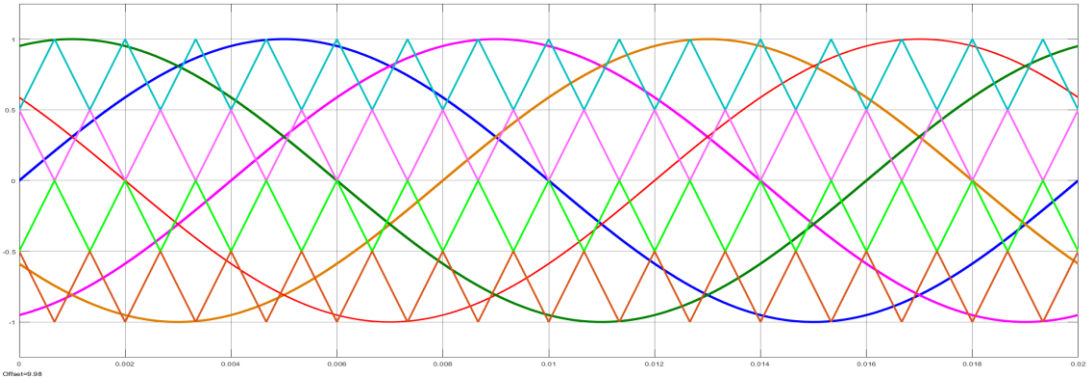

Figure 5-20 Alternative Phase opposition PWM for five phase system

The steady state voltage, current and torque response of motor at full load operation are shown in Figure 5-21.

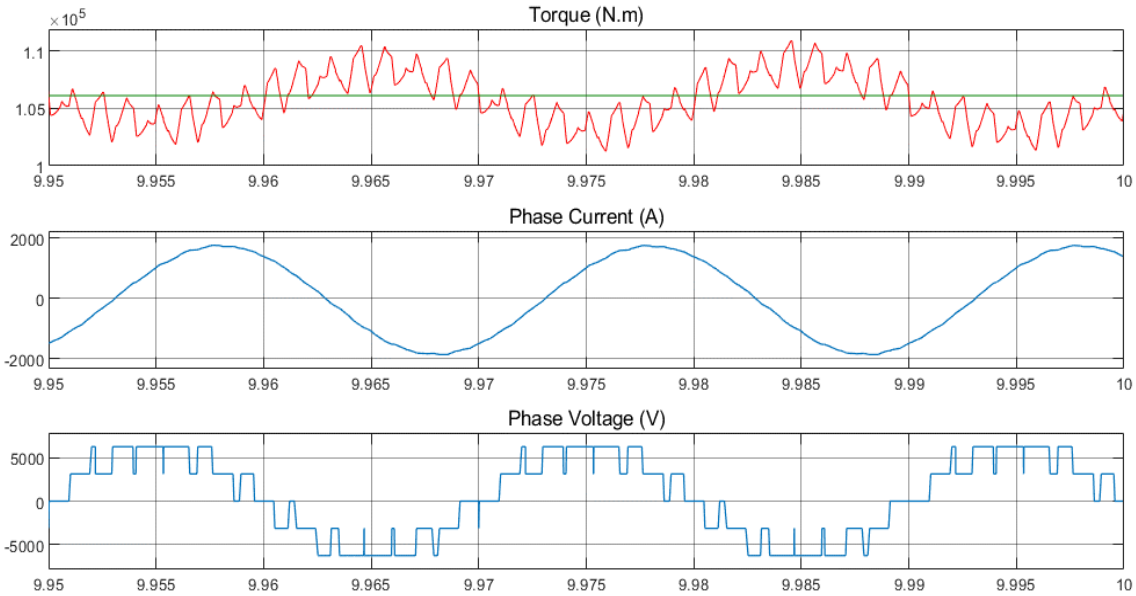

Figure 5-21 Motor dynamics with alternative phase opposition PWM

The current total harmonic distortion is 1.28% and voltage total harmonic distortion is 25.9%. The torque waveform has ripples of 9%. Figure 5-22 shows the harmonics contents of the torque waveform.

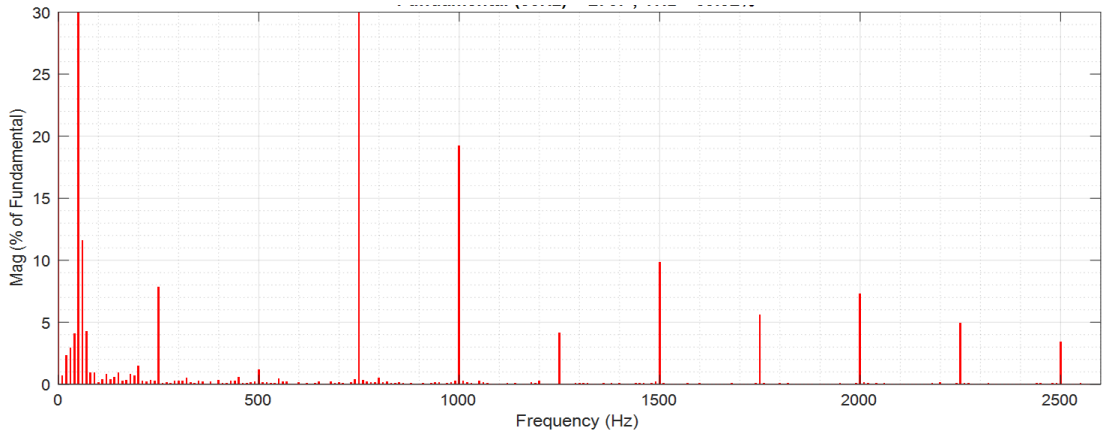

Figure 5-22 Torque waveform content with alternative phase opposition PWM

5.5.3 Phase Shift PWM

The phase shift PWM technique is another type of multicarrier PWM where the carrier signals are of the same amplitude and frequency but shifted by 90 degrees of each other as shown in Figure. 5.23.

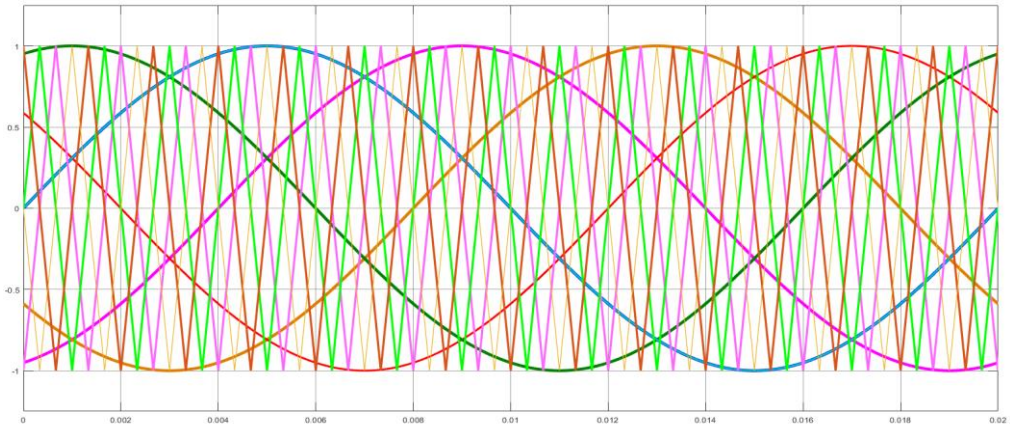

Figure 5-23 Phase shift PWM for five phase system

The plots of full load steady state voltage, current and torque waveforms are shown in Figure 5-24. The current total harmonic distortion with this technique is 0.84% and voltage total harmonic distortion is 25.98%. The torque waveform has ripples are reduced to 1.9%. Figure 5-25 shows the harmonics contents of the torque waveform.

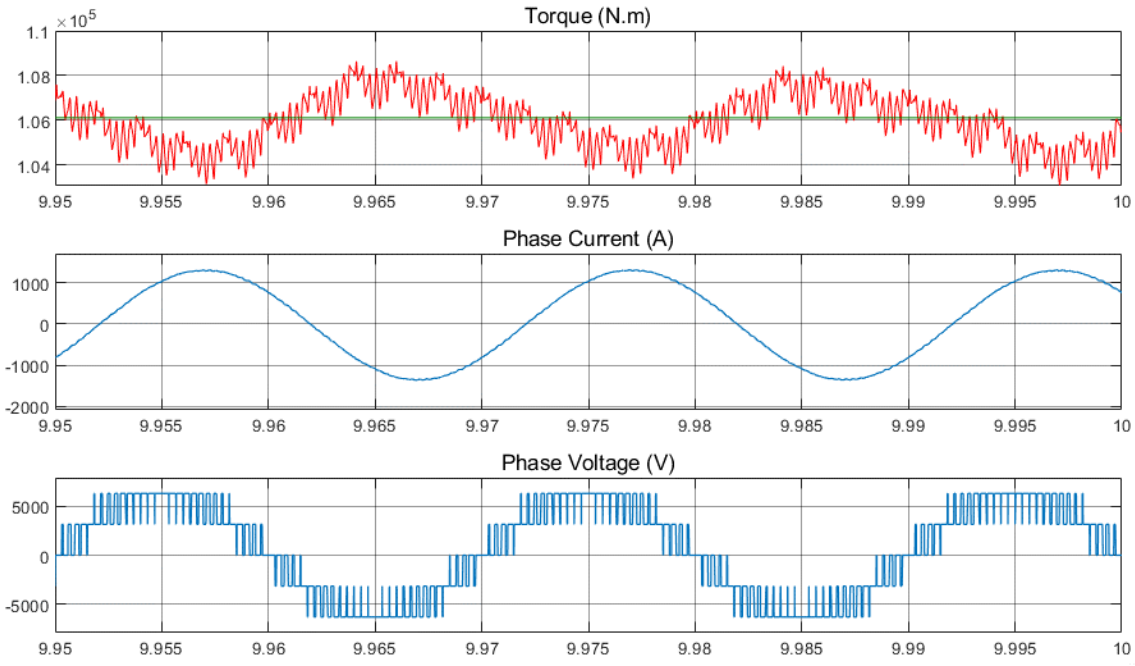

Figure 5-24 Motor dynamics with phase shift PWM

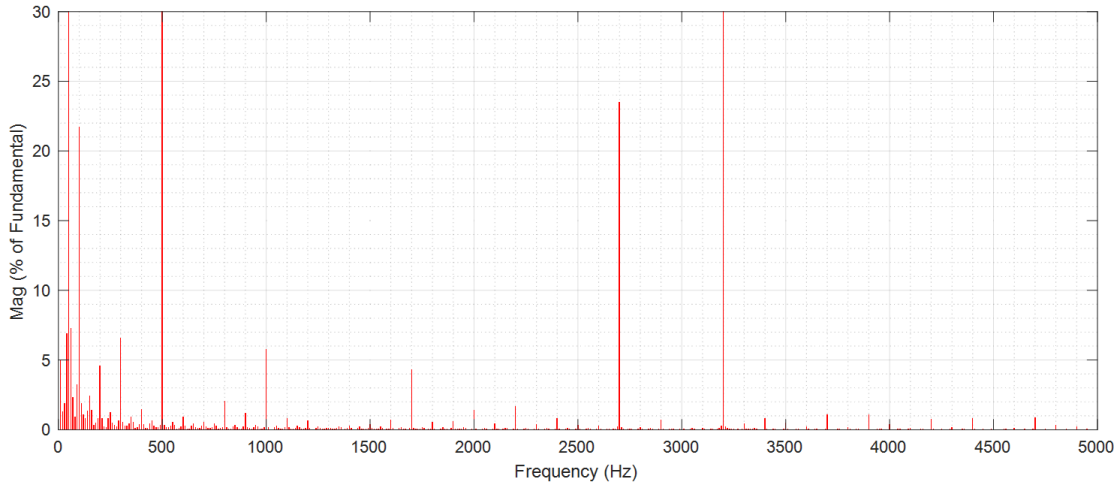

Figure 5-25 Torque waveform harmonic content with phase shift PWM

5.5.4 Phase Disposition PWM with Phase Shifted Carriers

This method is similar to the phase disposition one except that other phase's carrier signals are evenly shifted by 72^{o} as shown in demonstrated in Figure 5-26.

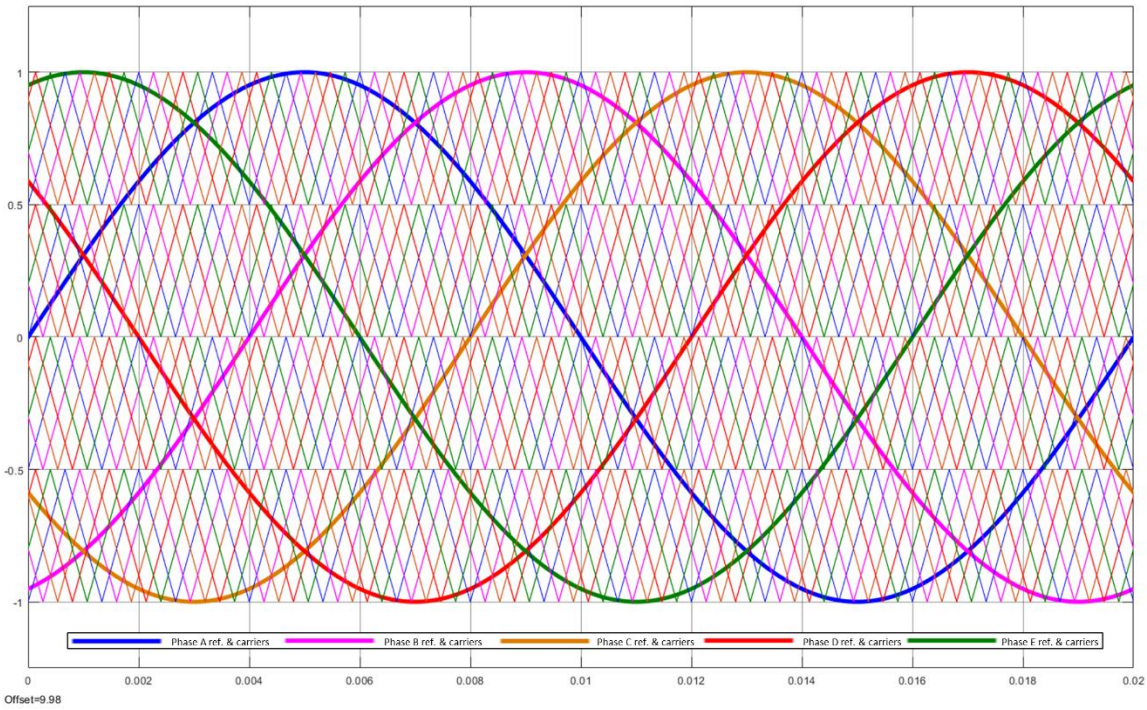

Figure 5-26 Phase disposition shifted carriers PWM for five phase system

The motor dynamic response of the motor is shown Figure 5-27. It can be observed that the overall performance is worsen because of concurrent switching among three adjacent levels at certain intervals. The current total harmonic distortion is 3.60% and voltage total harmonic distortion is 25.49%. The torque waveform has ripples are reduced to 9.5% and torque harmonic contents are very high as presented in Figure 5-28.

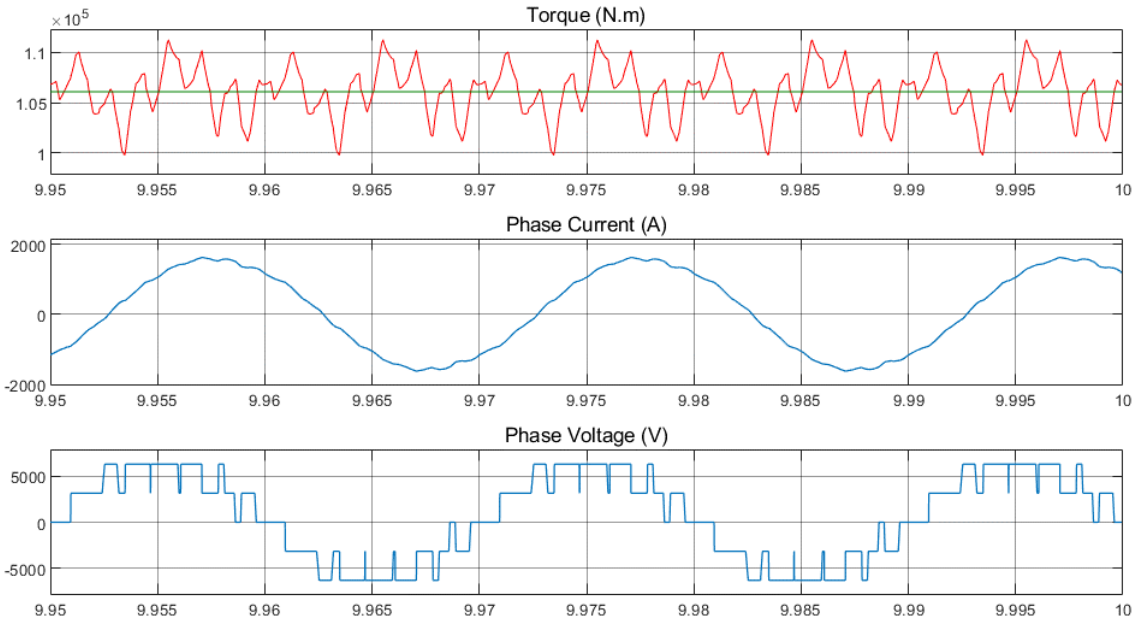

Figure 5-27 Motor dynamics with phase disposition shifted carriers PWM

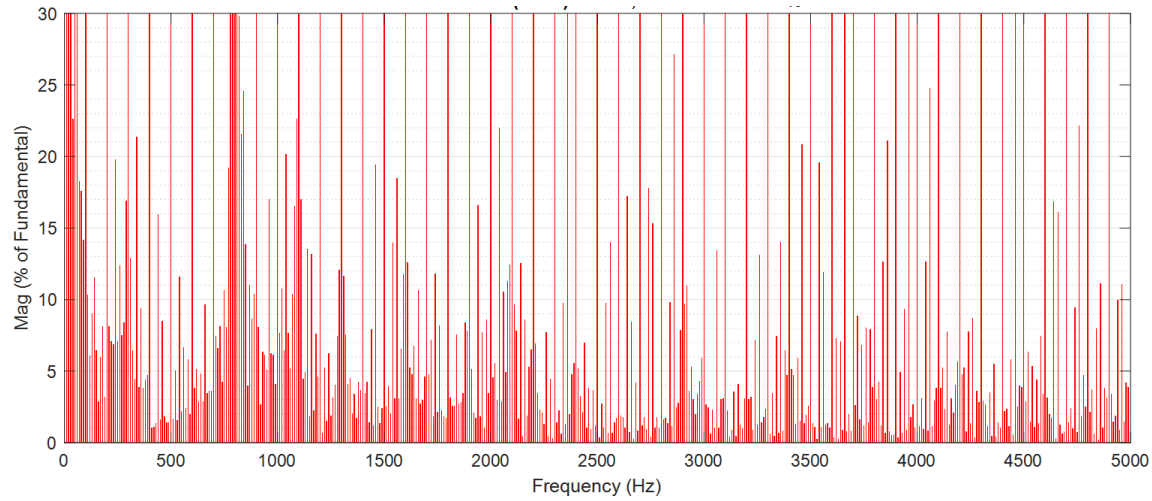

Figure 5-28 Torque harmonic content with phase disposition shifted carriers PWM

5.5.5 Phase Disposition with 5th Harmonic Injection

In this modulation technique, a certain portion of the fifth harmonic is injection into the reference signals sine waveforms to produce saddle like shape waveforms. Then, the new

signal is compared with phase disposition PWM to create the firing pulse as illustrated in Figure 5-29.

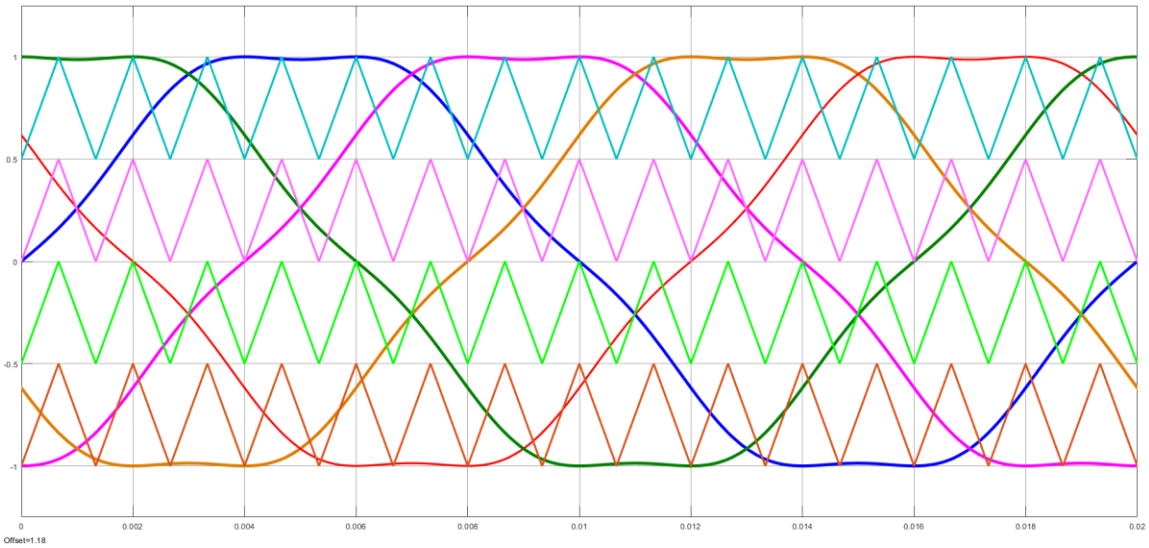

Figure 5-29 Phase disposition with 5th harmonic injection PWM for five phase system

Simulation results of current, voltage and torque show clear improvement (Figure 5-30).

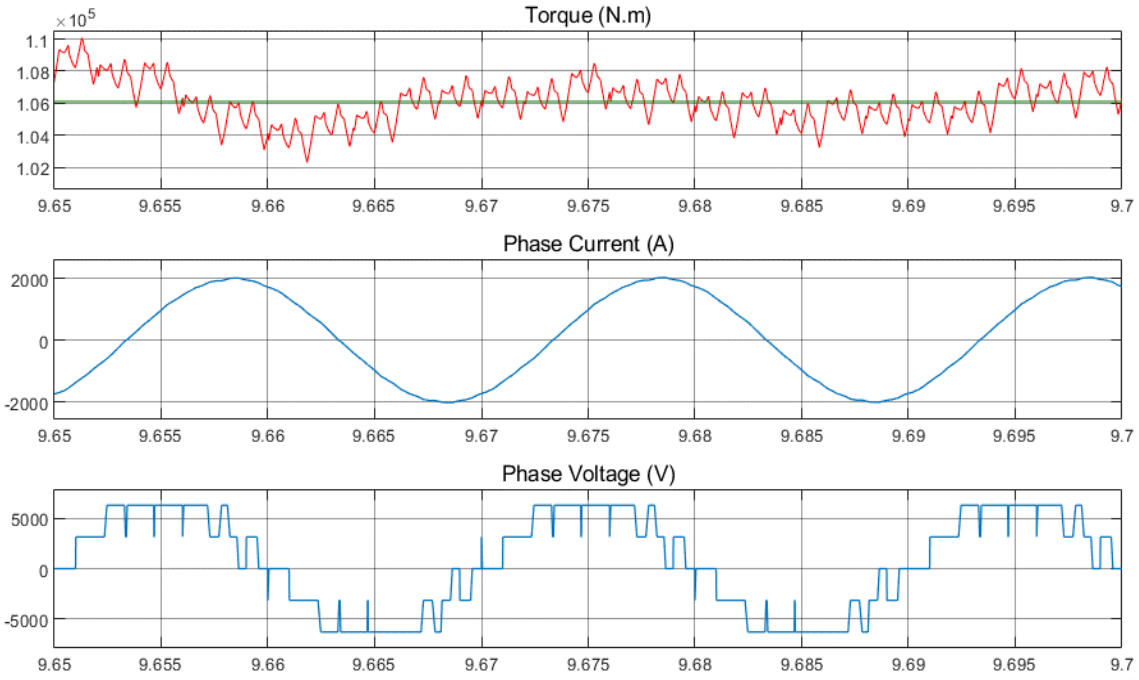

Figure 5-30 Motor dynamics with disposition with 5th harmonic injection PWM

The current total harmonic distortion reduced to 0.95% while voltage total harmonic distortion reduced to 22.7%. The torque ripples go to as low as 0.94%. The torque harmonic contents are presented in Figure 5-31. The 6th harmonic of the carrier has more significant value where the 1st and 2nd harmonics reduced.

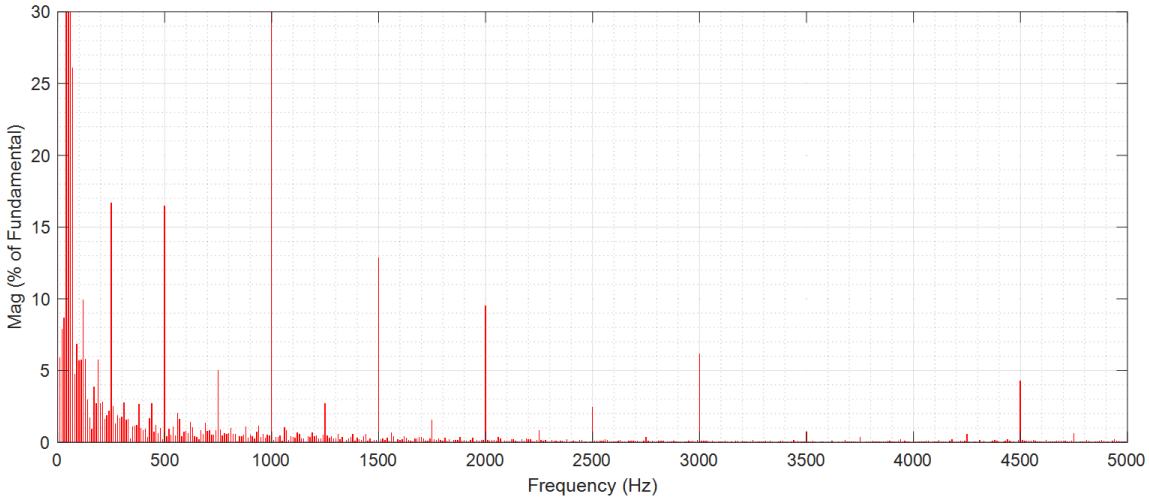

Figure 5-31 Torque harmonics phase disposition with 5th harmonic injection PWM

5.5.6 Phase Shift with 5th Harmonic Injection

This method employs the fifth harmonic injected sine wave with phase shift PWM to produce the firing pulse as illustrated in Figure 5-32.


Figure 5-32 Phase shift with 5th harmonic injection PWM for five phase system

The current, voltage and torque are plotted in Figure 5-33. The current total harmonic distortion went down to 0.83% while voltage total harmonic distortion to 23.15%. The torque ripple went as high as 10%. The torque harmonic contents are presented in Figure 5-34. The fifth harmonic injection increased the torque pulsation by exciting the 3rd carrier harmonics.

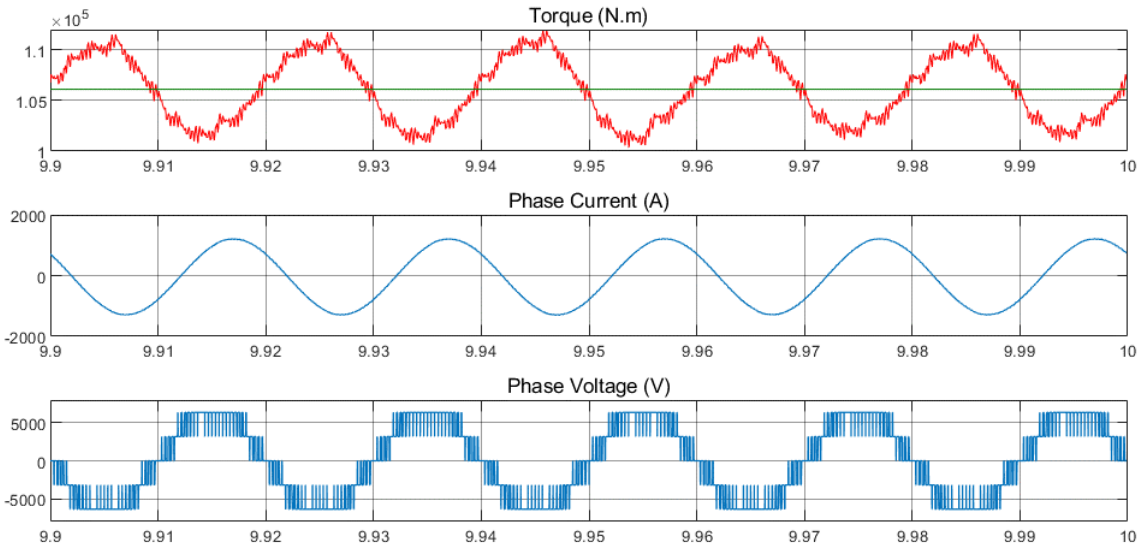

Figure 5-33 Motor dynamics with phase shift with 5th harmonic injection PWM

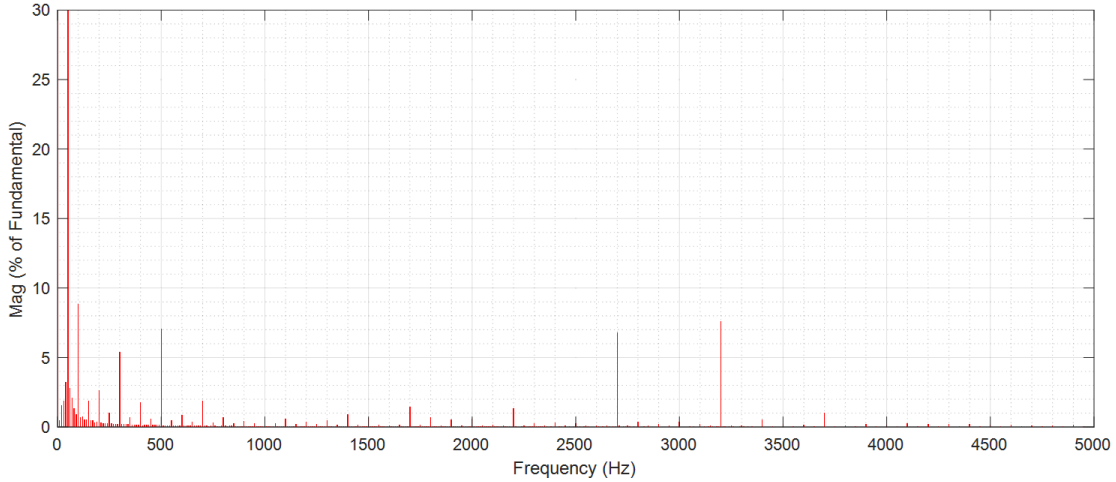

Figure 5-34 Torque harmonics with phase shift with 5th harmonic injection PWM

5.5.7 Comparison of PWM modulation Techniques

Table 5-2 summarizes the observation of the effects of different modulation techniques on the voltage and current harmonics in addition to their effect on the torque ripples. Notice that phase disposition with 5^{th} harmonic injection has the best performance.

Table 5-2 PWM Techniques Comparison

PWM Technique	**V %THD**	**I %THD**	**T_{Ripple}**
Phase Disposition Technique	25.88	1.09	0.95
Phase Opposition Technique	26.16	2.79	9.00
Alternative Phase Opposition Technique	25.90	1.28	9.00
Phase Shift PWM	25.98	0.84	1.90
Phase Disposition PWM with Phase Shifted Carriers	25.49	3.60	9.50
Phase Disposition with 5^{th} Harmonic Injection	22.70	0.95	0.94
Phase Shift with 5^{th} Harmonic Injection	23.15	0.83	10.0

5.6 Modulation Frequency Effect

The high-power and medium-voltage IGCTs can operate safely at switching frequency up to 1000 Hz (depending on the load). The effect of lowering or increasing the IGCTs switching frequency on the motor performance is investigated in this section.

5.6.1 Reduced Switching Frequency

The carriers frequency used in the PWM is reduced to 550 Hz. Simulation of the system at full load (Figure 5-35) shows that the current and voltage %THDs increased to 2.16% and 24.35%, respectively. The torque harmonic content is shown in Figure 5-36.

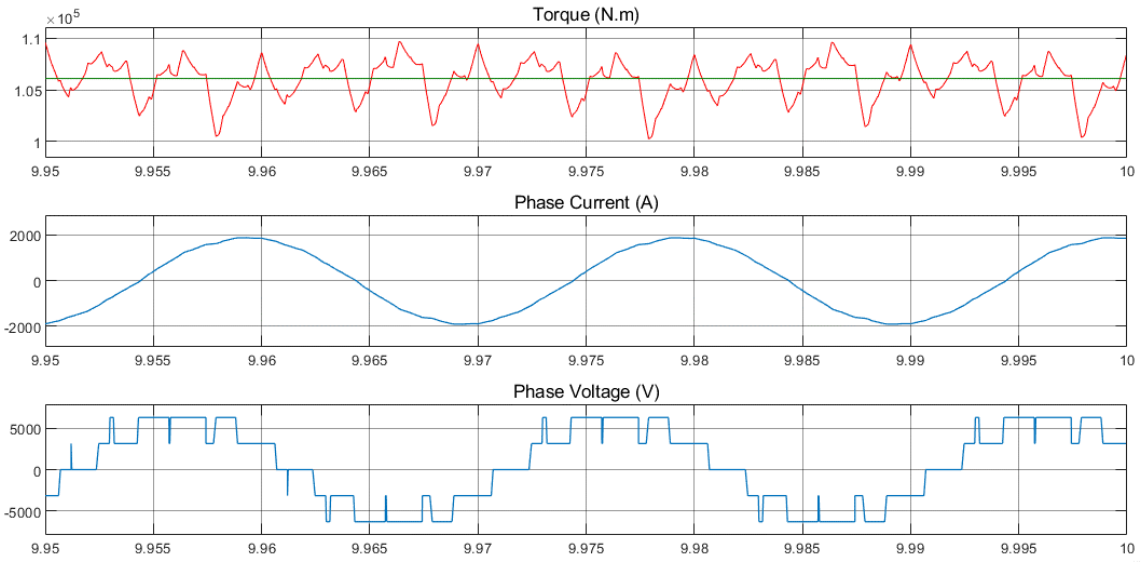

Figure 5-35 Motor dynamics with 550Hz switching frequency

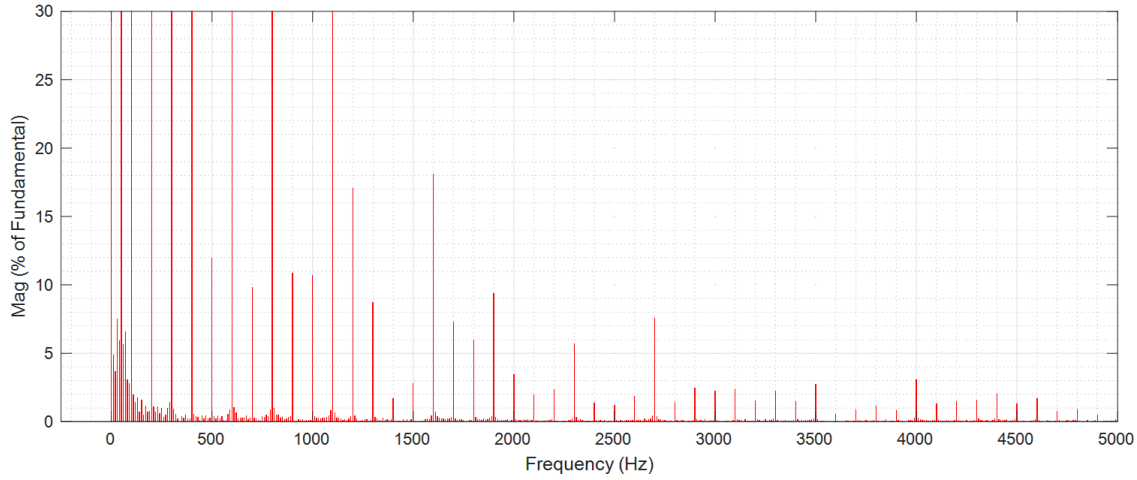

Figure 5-36 Torque harmonics with 550Hz switching frequency

5.6.2 Increased Switching Frequency

The PWM carriers' frequency is increased to 1000 Hz and the system was simulated at full load. The steady state results are shown in Figure 5-37. The current and voltage %THDs improved slightly to 1.07% and 25.93%, respectively. The impact on torque ripples is not very noticeable.

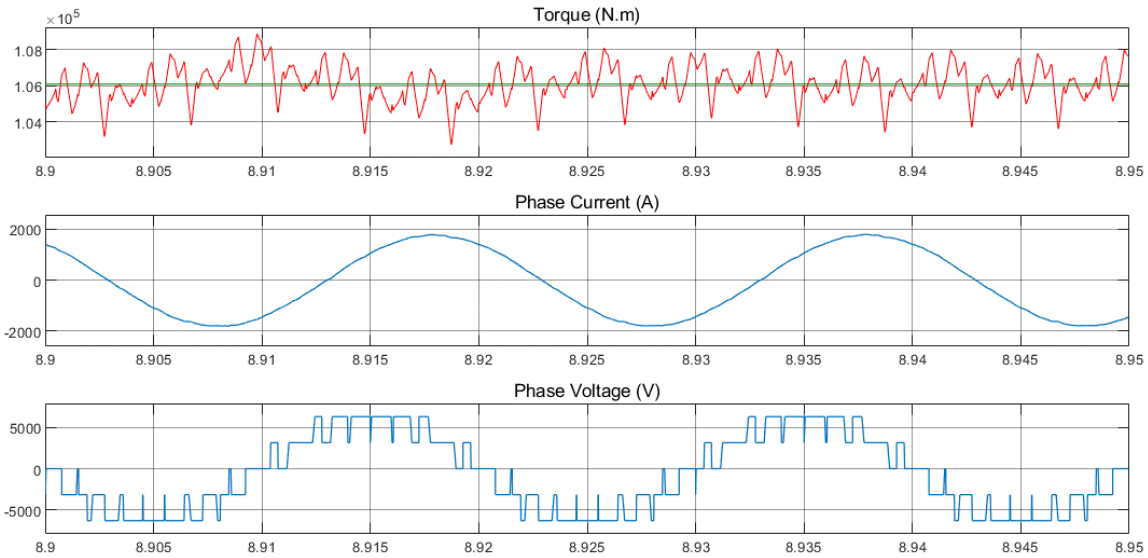

Figure 5-37 Motor dynamics with 1000Hz switching frequency

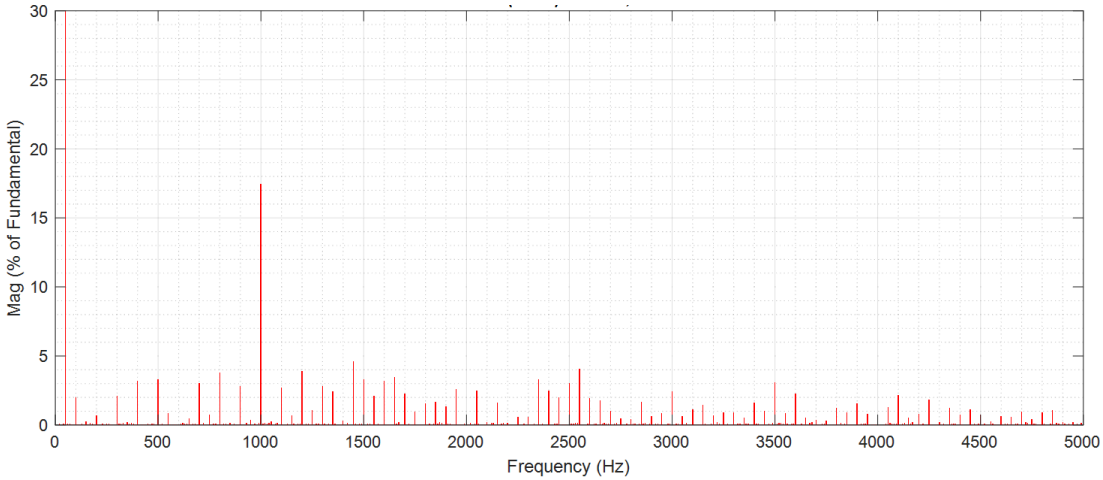

Figure 5-38 Torque harmonics with 1000Hz switching frequency

5.7 Comparison with 2–Level & 3-Level NPC Inverters

To compare the performance of the 5- , 3- and 2-level 5-phase inverter fed motor drive systems have been modeled and simulated. Single-open-loop V/f controller was used to generate the reference signals for the three systems. Phase disposition PWM with carrier frequency of 750Hz is used for all systems. Figure 5-39 shows schematic of simulated drive systems.

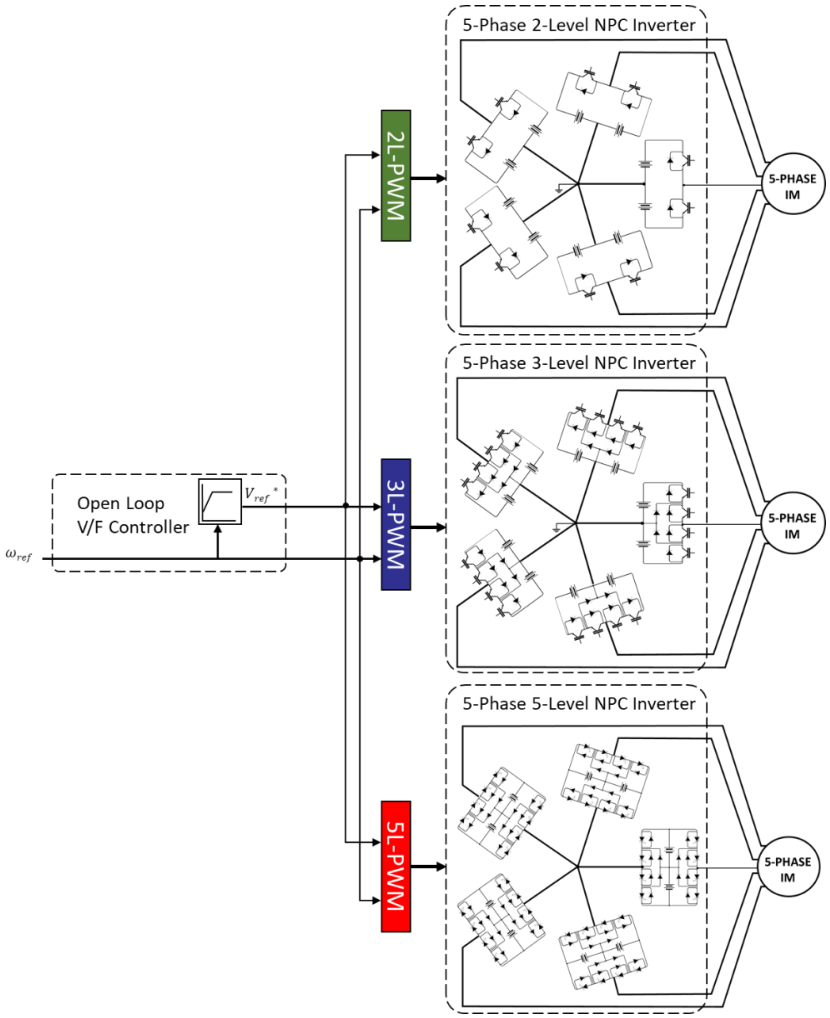

Figure 5-39 Schematic of 2-level, 3-level and 5-level inverter fed motor

The same motor parameters in Table 5-1 have been used in the comparison simulations. The motor performances were observed over a wide range of different speeds and loading conditions to test the functionality of the modeled systems. The speed, torque, current, phase voltage and line voltage responses are plotted in Figures 5.40, 5.41 and 5.42 for the 2-level, 3-level and 5-level systems respectively.

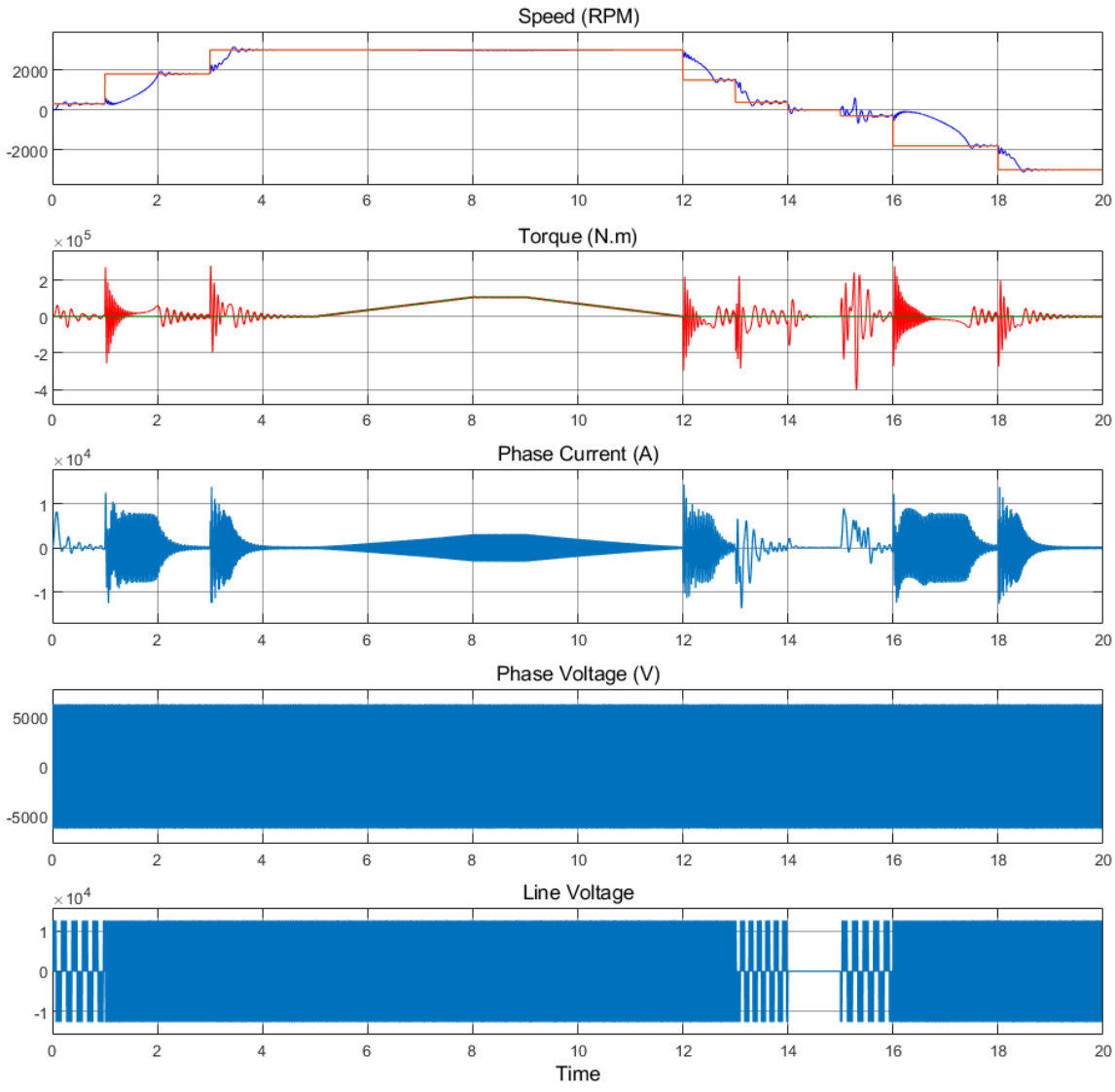

Figure 5-40 Two level inverter fed motor dynamic response

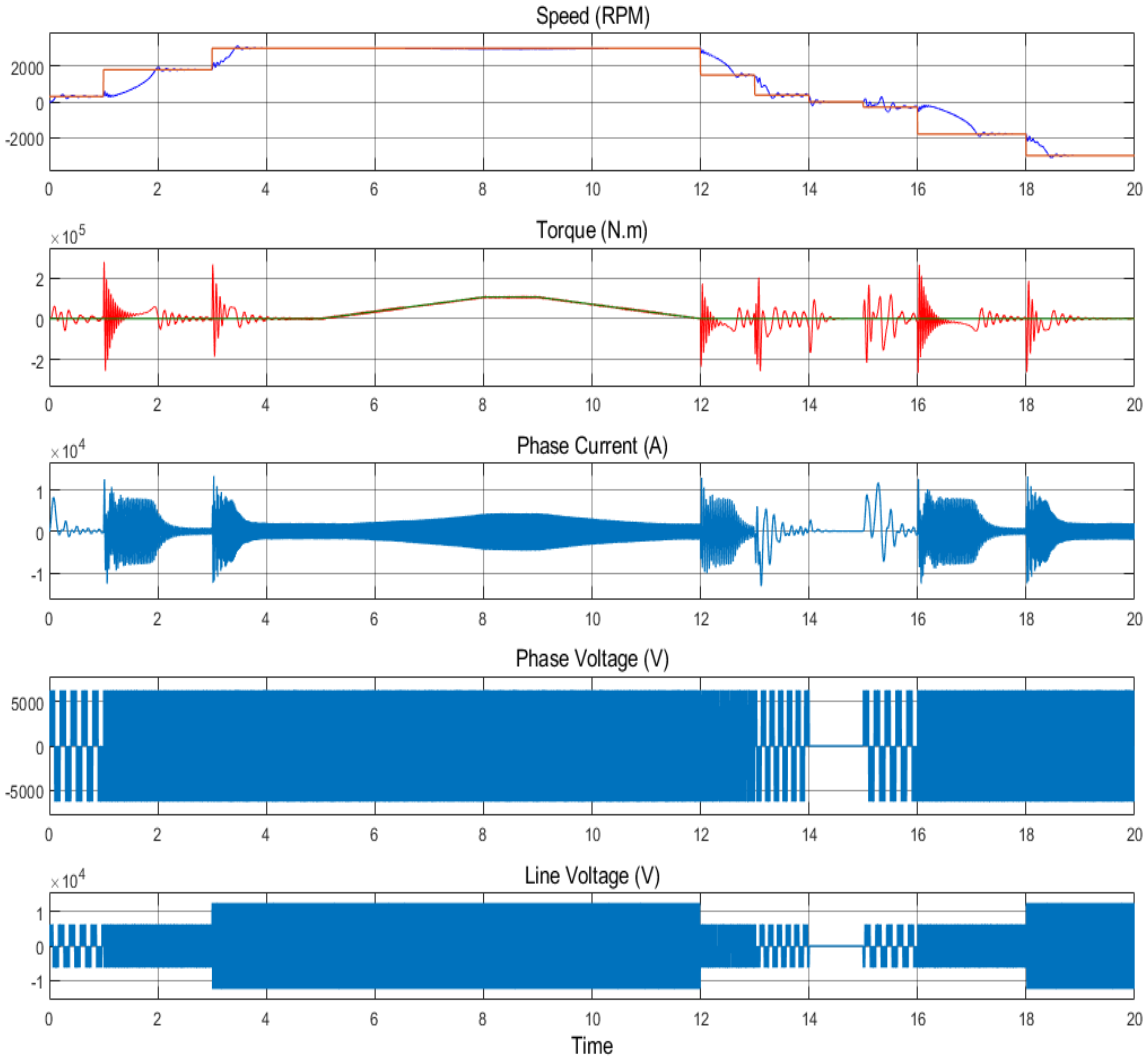

Figure 5-41 Three-level inverter fed motor dynamic response

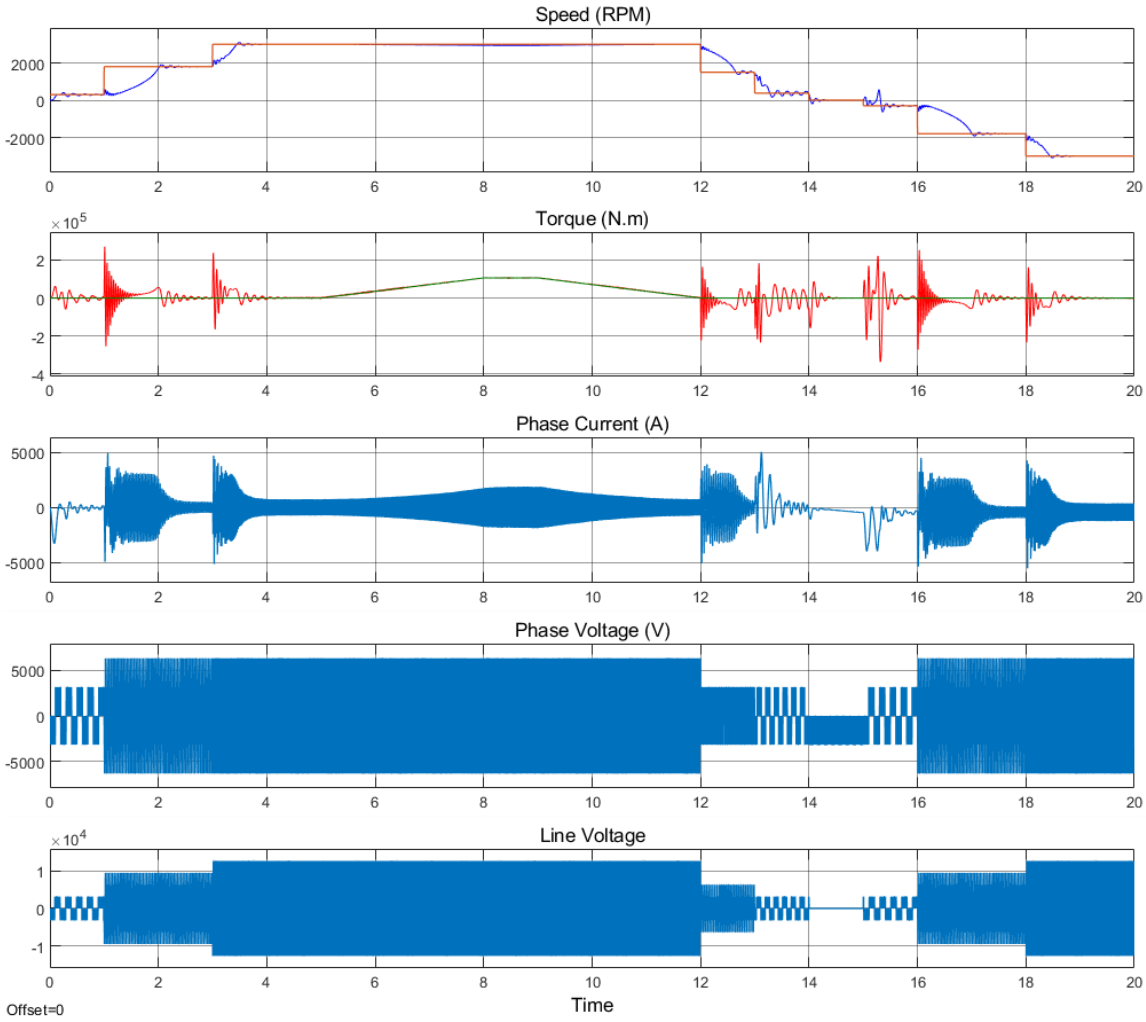

Figure 5-42 Five-level inverter fed motor dynamic response

The comparison between the three different systems are done at steady-state, full-speed and full-load conditions. The voltage waveforms of the phase voltage and line voltages are presented in Figure 5-43 and Figure 5-44. Notice that the inverters output voltage levels appear correctly. The line voltage of the 2-level inverter has three levels and the 3-level inverter shows 5 voltage levels while the 5-level inverter outputs seven levels.

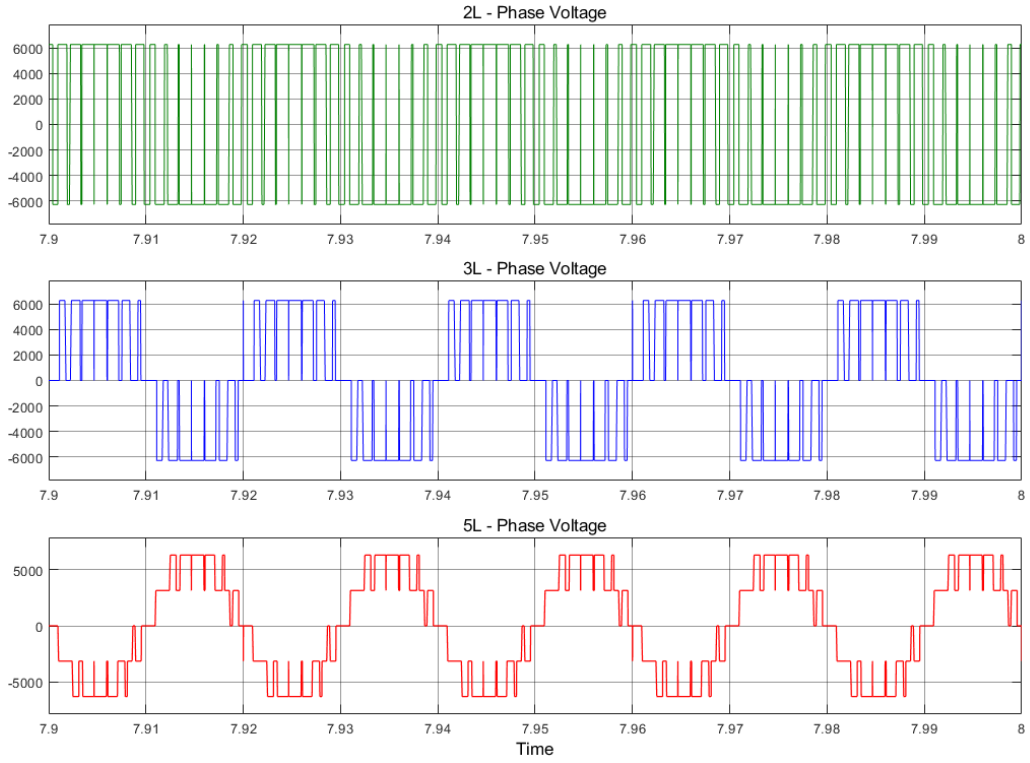

Figure 5-43 Phase voltage of different level inverters.

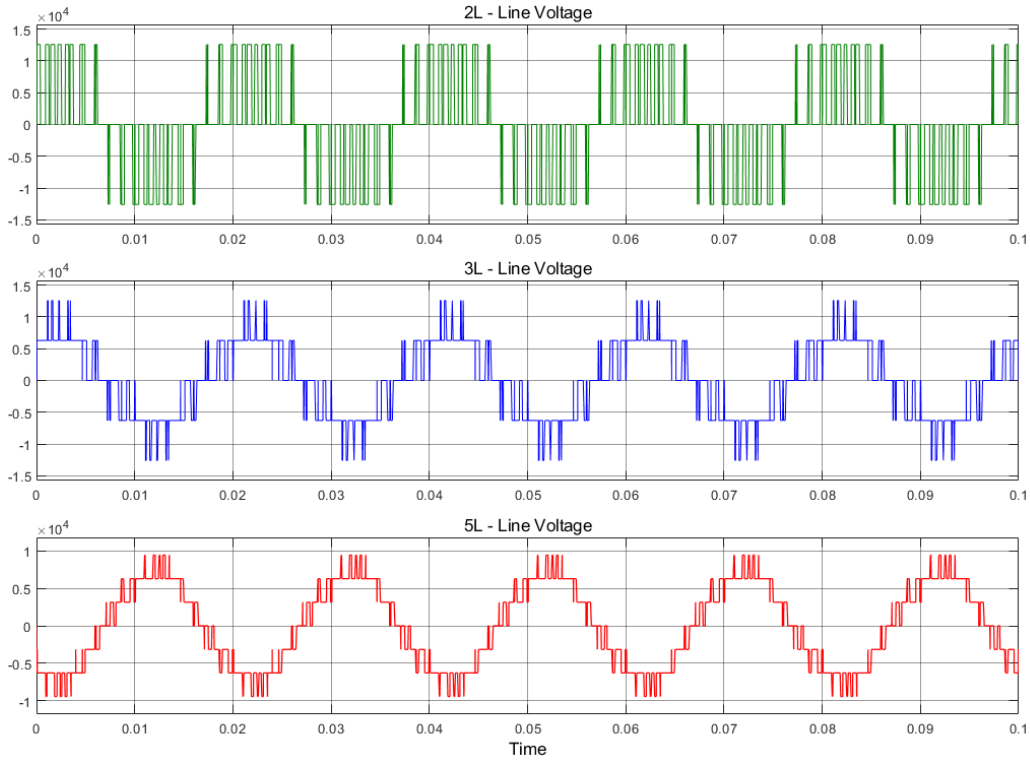

Figure 5-44 Line voltage of different level inverters.

Comparison of the phase current and torque waveforms are shown in Figure 5-45. The current %THD for the 2-level inverter fed motor is 2.46% and torque ripple is %3.33, on full-load steady-state condition. While the 3-level inverter fed motor shows a better performance with 25% less current %THD and 75% less torque ripples. On the other hand, the proposed 5-level double leg NPC inverter demonstrated superior performance with a reduction of 60% of current %THD and more than 70% less torque ripples. Comparison of torque waveform harmonic contents is shown in Figure 5-45. The 5-level inverter has by far less harmonic contents. Table 5-3 summarizes and compares the performance of each of the inverters.

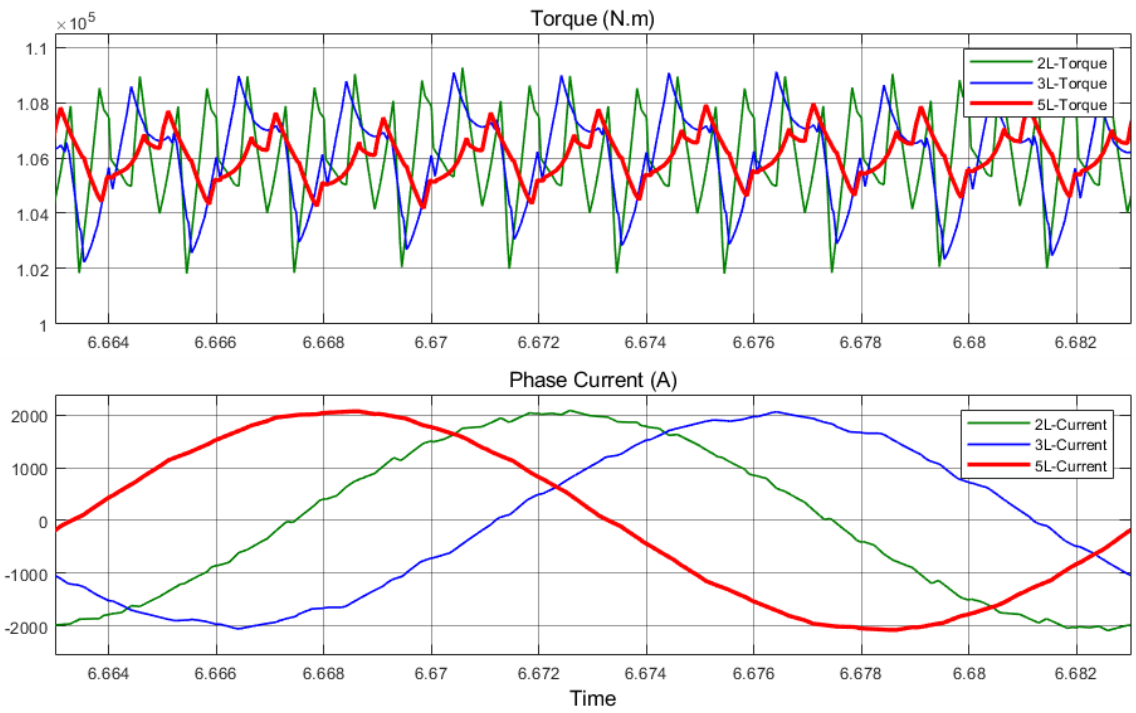

Figure 5-45 Torque and current waveform comparison

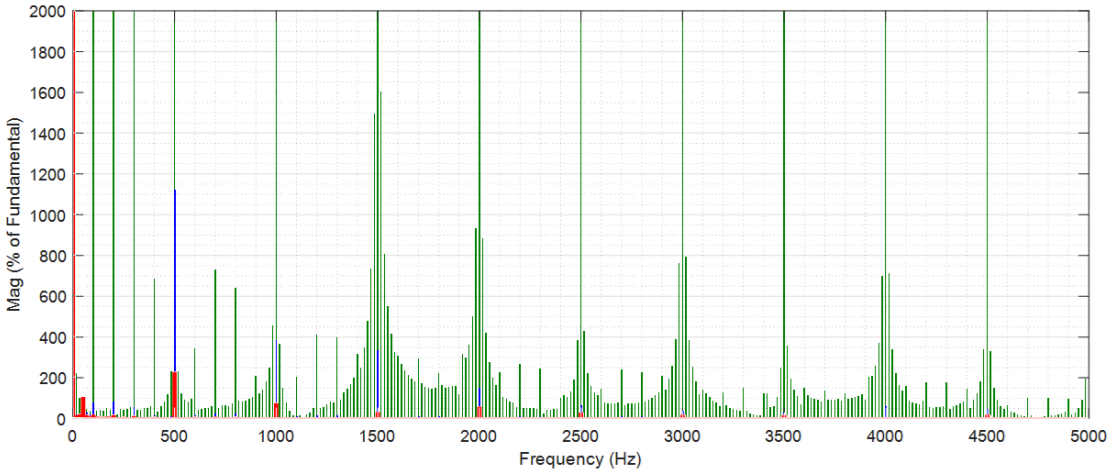

Figure 5-46 Torque harmonics comparison.

Table 5-3 Inverters performance comparison

Inverter Levels	**V %THD**	**V %THD**	**I %THD**	**T_{Ripple}**
Two-Level	99.53	105.81	2.46	3.33
Three-Level	50.42	43.25	1.84	2.38
Five-Level	25.88	23.06	0.98	0.95

Chapter 6: Conclusion and Future Work

6.1 Conclusion

Up scaled LNG trains with large compressors require larger inverter fed motors. Oversizing typical inverters leads to several problems such as the high harmonics and torque pulsation and has several limitation such as cooling requirement and increased components ratings and size. This thesis explored the pros and cons of the common types of VFDs available in the oil and gas industry and presents a solution for large LNG compressors drives, which is a 5-level 5-phase inverter fed motor drive system. The 5-level inverter design is based on NPC type of inverter, which reached a mature state of development and has reliable operating conditions at the required power rating. It utilizes the 3-level NPC in double leg arrangement to have a one-cell 5-level inverter.

MATLAB/SIMULINK was used to develop a model for the proposed 5-level 5-phase inverter fed motor drive system to test and demonstrated its dynamic performance. A 6.3kV 33 MW induction motor parameters were considered in the simulation. The performance was evaluated over a wide range of operating conditions. The results were compared to the common 2- and 3-level NPC inverter driving the same motor. The dynamics response of the proposed system showed much superior performance. Indeed, the current total harmonic distortion of the 5-level inverter was reduced to 0.98% compared to 1.84% when it was driven by 3-level NPC inverter. The produced electromagnetic torque has torque ripples 50% lower of what is produced by the 3-level inverter.

6.2 Future Work

There is plenty of scope for future work. Investigating long cable effects on inverter fed large motors is a field worth exploring as the distance from the VFDs to the motors can be as far as 100 meters. Another area is VSI inverters effect on the torsional vibration excitation and ways to supress it. That is in addition to common mode voltage elimination. The common mode voltage is not new problem but it could intensify in the future with new faster switching devices.

REFERENCES

[1] The National Association of Regulatory Utility Commissioners, “Global Liquefied Natural Gas Supply: An Introduction for Public Utility Commissioners”, 2009.

[2] Exxon Mobil Corporation, “Outlook for Energy: A View to 2040”, 2018.

[3] The international group of liquefied natural importers, “Basic properties of LNG”, LNG ingormation paper No.1, Aug, 2009.

[4] Qatar Petroleum Company. https://www.qp.com.qa, accessed on 20 Dec 2017.

[5] A. Sannino, L. Liljestrand, B. Rothmann, T. Nestli, M. Kjäll-Ohlsson and P.-E. Holsten, “All-electric LNG liquefaction plants,” 42nd IAS Annual Meeting Conference, Sep. 2007.

[6] A. Pelagotti, “LATEST ADVANCES IN LNG COMPRESSORS”, in 17th International Conference and Exhibition on Liquefied Natural Gas 2013, (LNG 17). 2013: Houston, Texas, USA.

[7] Eaton, A., R. Hernandez, A. Risley, P. Hunter, A. Avidan, “Lowering LNG unit costs through large and efficient LNG liquefaction trains-what is the optimal train size” Proceedings of the Spring Meeting, April 25-29, New Orleans, LA., 2004.

[8] B. Wu, “High-power converters and AC drives,” Hoboken, NJ: Wiley, 2006.

[9] A. Tessarolo, G.Zocco, G. Tonello, “Design and testing of a 45-MW 100-Hz quadruple-star synchronous motor for a liquefied natural gas turbo-compressor drive”, International Symposium on Power Electronics, Pisa, Italy.

[10] Mechademy. https://www.mechademy.com access on 01 Jan 2018.

[11] ABB. https://new.abb.com access on 11 Feb 2018.

[12] LNG world news. https://www.lngworldnews.com. Access on 25 Oct 2017.

[13] Gas/Electric Partnership. https://www.gaselectricpartnership.com Accessed on 10 Feb 2018.

[14] A. VanderMeulen, J. Maurin, "Current source inverter vs. voltage source inverter topology", June, 2014.

[15] J. Alves, G. Cunha and P. Torri, “Medium Voltage Industrial Variable Speed Drives”, 2015, static.weg.net, accessed on Jan, 2018.

[16] K. Deacon, S. Lanier, J. Kubik, M. Harshman, “Managing technology step-outs and optimizing process performance of starter-helper-generator VFDs on gas-turbine driven LNG trains”, Petroleum and Chemical Industry Conference Europe, 2014.

[17] F. Kleiner and S. Kauffman, “All Electric Driven Refrigeration Compressors in LNG Plants Offer advantages,” GASTECH2005, Bilbao, Spain 14-17 March 2005.

[18] L. Ben-Brahim, M. Benammar, T. Yoshino, H. Hosoda, R. Kurosawa and Y. Fayyad, “Electric Drives for LNG Plants”, Proceedings of the 3rd Gas Processing Symposium, Qatar, 2012.

[19] G. Marybeth, R. NoredJustin, B. HollingsworthKlaus, “Application Guideline for Electric Motor Drive Equipment for Natural Gas Compressors”, Gas Machinery Council, Release Version 4.0, 2009.

[20] T. Yoshino, H Masuda, Hiromi Hosoda, M. Tsukakoshi, M. Mostafa, L. Ben-Brahim, “High-Reliability Extra-Large Motor Drives for Oil and Gas Industry”, 7th IEEE GCC conference and exhibition 17-20 November 2013, Doha, Qatar.

[21] General Electric Company, https://www.gepowerconversion.com, access on 20 Aug 2018.

[22] T. Holopainen, J. Niiranen, D. Andreo and T. Holopainen, “Electric Motors and Drives in Torsional Vibration Analysis and Design”, Proceedings of the 40th Turbomachinery Symposium, 2013.

[23] Toshiba Mitsubishi-Electric Industrial Systems Corporation, “Synchronous Motors Empowering the Future", D-0036-1303-A, 2013.

[24] G. Oscarson, J. Imbertson, B. Imbertson and S. Moll, “The ABC’s of Synchronous Motors”, Electric Machinery, WEG Group, Minnesota, USA, 2012.

[25] H. Abu-Rub, H. Malinowski and M. Al-Haddad, K., “Power Electronics for Renewable Energy Systems”, Transportation and Industrial Applications, Chichester, UK: John Wiley & Sons, 2014.

[26] P. Blaiklock, M. Verma, S. Bondy, “When should an Electric Adjustable Speed Drive be used instead of a Gas or Steam Turbine”, TMEIC Corporation, Roanoke, VA, 2013.

[27] T. Miyashita, S. Koichi, K. Murata and M. Sakai, “Multi-winding motor”, US patent 20060220486, 30 Mar., 2005.

[28] C. Thangaraj, S. Srivastava and P. Agarwal, “Energy Efficient Control of ThreePhase Induction Motor - A Review”, International Journal of Computer and Electrical Engineering, Vol. 1,No.1, pp.60-70, 2009.

[29] L. Parsa, “On advantages of multi-phase machines”, in Industrial Electronics Society, 2005. IECON 2005. 31st Annual Conference of IEEE, Nov 2005, pp. 6.

[30] F. Barrero and M. J. Duran, "Recent Advances in the Design, Modeling, and Control of Multiphase Machines—Part I," in IEEE Transactions on Industrial Electronics, vol. 63, no. 1, pp. 449-458, Jan. 2016.

[31] J. Rodrigues, J. Lai, F. Peng, “Multilevel Inverters: A Survey of Topologies, Controls, and Applications", IEEE Transactions on Industrial Electronics, vol. 49, no. 4, August 2002.

[32] B. Bose, “Power Electronics and Variable Frequency Drives - Technology and Application”, IEEE Press, 1997.

[33] J. Apsley, S. Williamson, A. Smith, and M. Barnes, “Induction motor performance as a function of phase number” IEE Proc. Electr. Power Appl., vol. 153, no. 6, pp. 898–904, Nov. 2006.

[34] A. Tessarolo, “On the modeling of poly-phase electric machines through vector-space decomposition: theoretical considerations”, International Conference on Power Engineering, Energy and Electrical Drives, POWERENG 2009, pp. 519-523.

[35] E. Levi, M. Jones, S. Vukosavic, and H. Tolyiat, “A novel concept of a multiphase, multimotor vector controlled drive system supplied from a single voltage source inverter,” IEEE Trans. Ind. Applicat., vol. 19, pp. 320–335, Mar. 2004.

[36] L.Ben Brahim, A. Gastli, T. Yoshino, T. Yokoyama, A. Kawamura, “Review of Medium Voltage High Power Electric Drives”, IEEJ Journal of Industry Applications. Vol.8 No.1 pp.1–11, 2018.

[37] M. Rashid, *power electronics handbook, third edition*. San Diego: Academic Press, 2011.

[38] L. Ben-Brahim, and T. Yoshino, “High-Power Drive Systems for Industrial Applications: Practical Examples,” in Power Electronics for Renewable Energy Systems, Transportation and Industrial Applications (eds H. Abu-Rub, M. Malinowski and K. Al-Haddad).

[39] B. P. Mcgrath and D. G. Holmes, “Natural capacitor voltage balancing for a flying capacitor converter induction motor drive,” IEEE Trans. Power Electron., vol. 24, no. 6, pp. 1554–1561, Jun. 2009.

[40] X. Liang, and J. He. “Load Model for Medium Voltage Cascaded H-Bridge Multi-Level Inverter Drive Systems,” IEEE Power Energy Tech. Sys. Jour., vol. 3, no. 1, pp. 13–23, March 2016

[41] L.Ben-Brahim, “A Discontinuous PWM Method for Balancing the Neutral Point Voltage in Three-Level Invereter-Fed Variable Frequency Drives (VFDs)”, IEEE Transactions on Energy Conversion, Vol. 23, No. 4, pp. 1057-1063, 2008.

[42] M. Irfan, P. Prasad, and P. V. Rao, “Simulation of five-level five-phase SVPWM voltage source inverter” in Proc. Int. Conf. Power Control Embedded Syst., Nov. 2010.

[43] A. Prayag and S. Bodkhe, “A comparative analysis of classical three phase multilevel (five level) inverter topologies”, Intelligent Control and Energy Systems (ICPEICES), July 2016.

[44] S. Busse, M. Hiller, K. Kahlen, and P. Himmelmann, “MTBF Comparison of Cutting Edge Medium Voltage Drive Topologies for Oil and Gas Applications,” in Proc. of the Petroleum and Chemical Industry Conference Europe (PCIC Europe 2015), London, UK, 2015.

[45] H. A. Toliyat, M.M. Rahimian, and T.A. Lipo, ”dq Modeling of Five Phase Synchronous Reluctance Machines Including Third Harmonic of Air-Gap MMF” Proceedings of the IEEE-IAS Annual Meeting Conference, October 1991.

[46] A. Tessarolo, G. Zocco, C. Tonello, "Design and testing of a 45-MW 100-Hz quadruple-star synchronous motor for a liquefied natural gas turbo-compressor drive", IEEE Trans. Ind. Appl., vol. 47, no. 3, pp. 1210-1219, May/Jun. 2011.

[47] X. Zhang and G. H. B. Foo, "A Constant Switching Frequency-Based Direct Torque Control Method for Interior Permanent-Magnet Synchronous Motor Drives," IEEE/ASME Transactions on Mechatronics, vol. 21, no. 3, pp. 1445-1456, June 2016.

[48] C. Ong, Dynamic Simulation of Electric Machinery Using MATLAB/Simulink, Indiana: Prentice Hall PTR, 1998.

[49] F. Niu, K. Li, B. Wang and E. G. Strangas, "Comparative evaluation of direct torque control strategies for permanent magnet synchronous machines", 2014 IEEE Applied Power Electronics Conference and Exposition - APEC 2014, Fort Worth, TX, 2014.

[50] G. Renukadevi, K. Rajambal, “Generalized model of multi-phase induction motor drive using matlab/simulink”, in Innovative Smart Grid Technologies - India (ISGT India), 2011 IEEE PES, pp. 114 –119, Dec. 2011.

[51] L.Ben-Brahim, T. Yoshino, High Power Drive Systems For Industrial Applications – Practical Examples, Power Electronics for Renewable Energy Systems, Transportation and Industrial Applications, Willey, 2014.

[52] L.Ben-Brahim, and S. Tadakuma, , "A Novel Multilevel Carrier-Based PWM Control Method for GTO Inverter in Low Index Modulation Region", IEEE Transactions On Industry Applications, Vol. 42, No. 1, 2006.

[53] L. Ben-Brahim, and A. Kawamura, "Digital Current Regulation of Field Oriented Controlled Induction Motor Based on Predictive Flux Observer. IEEE Transactions on Industry Applications, VOL. 27, NO.5, pp. 956-961, 1991.